

SOL-783

Comp

8450 FILE COPY

COO-2839-3(Vol. 1)

HEAT PIPE CENTRAL SOLAR RECEIVER

Volume 1

By
Walter B. Bienert
David A. Wolf

April, 1979

Work Performed Under Contract No. EY-76-C-02-2839

Dynatherm Corporation
One Industry Lane
Cockeysville, Maryland



U.S. Department of Energy

No: 23, 2431



Solar Energy

9

NOTICE

This report was prepared as an account of work sponsored by the United States Government. Neither the United States nor the United States Department of Energy, nor any of their employees, nor any of their contractors, subcontractors, or their employees, makes any warranty, express or implied, or assumes any legal liability or responsibility for the accuracy, completeness or usefulness of any information, apparatus, product or process disclosed, or represents that its use would not infringe privately owned rights.

This report has been reproduced directly from the best available copy.

Available from the National Technical Information Service, U. S. Department of Commerce, Springfield, Virginia 22161.

DTM-79-6

FINAL TECHNICAL REPORT

for

**HEAT PIPE CENTRAL SOLAR RECEIVER
VOLUME I**

**Walter B. Bienert
David A. Wolf**

April 1979

Prepared under Contract No. EY-76-C-02-2839

**Period of Performance
March 1, 1976 through September 30, 1978**

by

**Dynatherm Corporation
One Industry Lane
Cockeysville, Maryland**

for

**U. S. Department of Energy
Chicago Operations Office**

ABSTRACT

The objective of this project was the conceptual design of a Central Solar Receiver Gas Turbine Plant which utilizes a high temperature heat pipe receiver. Technical and economic feasibility of such a plant was to be determined and preliminary overall cost estimates obtained. The second objective was the development of the necessary heat pipe technology to meet the requirements of this receiver.

A heat pipe receiver is ideally suited for heating gases to high temperatures. The heat pipes are essentially loss free "thermal diffusers" which accept a high solar flux and transform it to a lower flux which is compatible with heat transferred to gases. The high flux capability reduces receiver heating surface, thereby reducing receiver heat losses.

An open recuperative air cycle with a turbine inlet temperature of 816°C (1500°F) was chosen as the baseline design. This results in peak metal temperatures of about 870°C (1600°F). The receiver consists of nine modular panels which form the semicircular backwall of a cavity. Gas enters the panels at the bottom and exits from the top. Each panel carries 637 liquid metal heat pipes which are mounted at right angle to the gas flow. The evaporators of the heat pipes protrude from the flux absorbing front surface of the panels, and the finned condensers traverse the gas stream.

The maximum heat load required of any heat pipe in the solar receiver is about 13 kW. This maximum heat load occurs at 750°C ; at lower and higher temperatures the requirement is considerably less. Three liquid metal heat pipes which meet these requirements were successfully developed. They had a diameter of 60 mm (2.375 inches), a length of 1100 mm (43 inches), and were fabricated from Inconel 601. The heat pipes were tested at power levels up to 16 kW and over the full temperature range.

Capital cost estimates were made for a 10 MW(e) pilot plant. The total projected costs, in mid-1978 dollars, range from \$1,947 to \$2,002 per electrical kilowatt. On the same basis, the cost of a water/steam solar plant is approximately 50% higher.

FOREWORD

This is the Final Technical Report under Contract EY-76-C-02-2839. The technical work was performed by Dynatherm Corporation as prime contractor to DOE and Foster Wheeler Corporation as subcontractor to Dynatherm. Foster Wheeler's input is referenced in the summary and reproduced in toto as Volume II. Dynatherm's section of the report was prepared by W. B. Bienert and D. A. Wolf and Foster Wheeler's section by Giovanni Carli.

TABLE OF CONTENTS

	<u>Page</u>
1. INTRODUCTION	1
2. SUMMARY	3
3. HEAT PIPE DEVELOPMENT	22
3.1 Heat Pipe Requirements	22
3.2 Theoretical Heat Pipe Performance Capability	34
3.2.1 Axial Transport Capability	37
3.2.2 Radial Heat Flux Limits	54
3.2.3 Heat Pipe Structural Requirements	57
3.3 Experimental Heat Pipe Development	63
3.3.1 Objectives and Approach	63
3.3.2 Heat Pipe Fabrication	67
3.3.3 Description of Test Setup	68
3.3.4 Testing Considerations and Data Interpretation	70
3.3.5 Heat Pipe Testing	74
4. HEAT PIPE TECHNOLOGY ASSESSMENT	90
5. POWER CONVERSION CYCLES FOR THE HEAT PIPE CENTRAL SOLAR RECEIVER	93
6. COMPARATIVE COST ANALYSIS	100
7. RECOMMENDED FUTURE WORK	108
8. REFERENCES	112

1. INTRODUCTION

This Final Technical Report describes the work and the results of a development program entitled "Heat Pipe Central Solar Receiver". The work was performed by Dynatherm Corporation as the prime contractor and Foster Wheeler Development Corporation as the major subcontractor. The program was started under ERDA sponsorship and completed under DOE Contract EY-76-C-02-2839. The period of performance was March 1, 1976 through September 30, 1978.

At the present time, DOE is engaged in the development of solar thermal power plants capable of supplying substantial quantities of the United States' electric power needs during the late 1980's. A major milestone in this program is the completion of a 10 megawatt solar electric power plant which is currently being constructed at Barstow, California. This pilot plant utilizes first generation solar technology which can be implemented with a minimum of technical risk. At the same time, DOE is proceeding with the development of advanced technology that will produce electricity at a cost substantially lower than that possible with the current water-steam central receiver system. One of the advanced concepts utilizes a Brayton conversion system in conjunction with a hot gas receiver. The Brayton system has the potential of high efficiency, good response during transient conditions, and easy adaptation to hybrid plants. This report describes the initial development of a hot gas receiver which utilizes heat pipes as heat transfer elements between the solar flux and the gas stream. The heat pipes function as "thermal diffusers" which accept the concentrated heat input and transform it nearly loss free to a lower flux which is compatible with gas heating. Heat pipes minimize the thermal stresses in the receiver tubing, permit the design of a low pressure drop receiver, and provide for redundancy.

The initial phase of the program consisted of the evaluation of various receiver concepts and conversion cycles. A baseline system was then selected and a semi-detailed design of the receiver was generated. The capital cost of a 10 MW(e) solar plant of this type was estimated. A major portion of the program effort was devoted to the development of the necessary heat pipe technology. As a result of the present work, the basic feasibility and cost effectiveness of a central solar gas turbine plant

with a heat pipe receiver was established. Those areas where additional development effort is needed were identified and are included as recommendations in the report.

The concept evaluation, systems analysis, and cost estimating were a joint effort between Dynatherm and Foster Wheeler. Dynatherm performed all the heat pipe development and Foster Wheeler was responsible for the receiver design.

This Final Technical Report consists of two volumes. An executive summary of the entire program is given in Volume I. This volume also described in detail the heat pipe development effort and the comparative cycle and cost analysis. Volume II, which was prepared by Foster Wheeler, deals with the cycle selection, the overall plant layout, and the receiver design. Additional details of the work can be found in two Semiannual Progress Reports. ⁽¹⁾ ⁽²⁾

2. SUMMARY

The objective of this project was the conceptual design of a central solar-receiver gas turbine plant which utilizes a high temperature heat pipe receiver. The technical and economic feasibility of such a plant was determined and preliminary overall cost estimates were obtained. A second objective was the development of the necessary heat pipe technology to meet the requirement of this receiver.

A heat pipe receiver is ideally suited for heating gases to high temperatures. The heat pipes are essentially loss-free "thermal diffusers" which accept a high solar flux and transform it to a lower flux which is compatible with heat transfer to gases. The high flux capability reduces receiver heating surface, thereby reducing receiver heat losses.

Toward meeting the program objectives, several open and closed Brayton cycles were analyzed. Parametric data were developed to enable selection of a baselinedesign concept. The selected size of the power plant intentionally paralleled the 10 MW(e) water/steam solar pilot plant to permit direct cost and performance comparisons. However, unlike in the design of the steam pilot plant, thermal storage was not included in the gas turbine plant. This choice was made solely because of the limited scope of the study.

The open recuperative air cycle with a conventional utility-type turbine was selected as the baseline design. The overall plant efficiency does not vary significantly in the turbine inlet temperature range of 816 to 980°C (1500 to 1800°F). For this reason and because conservative values are desirable in a prototype plant, a turbine inlet temperature of 816°C (1500°F) was chosen. This results in heat pipe metal temperatures of about 870°C (1600°F) which are compatible with nickel based super alloys.

The pertinent parameters of the selected cycle are shown in Figure 2.1. The cycle utilizes a standard heavy duty gas turbine with a conversion efficiency of 33%. After accounting for the losses associated with the heliostat field and the receiver, the baseline system will yield an overall solar-to-electric efficiency of approximately 20%.

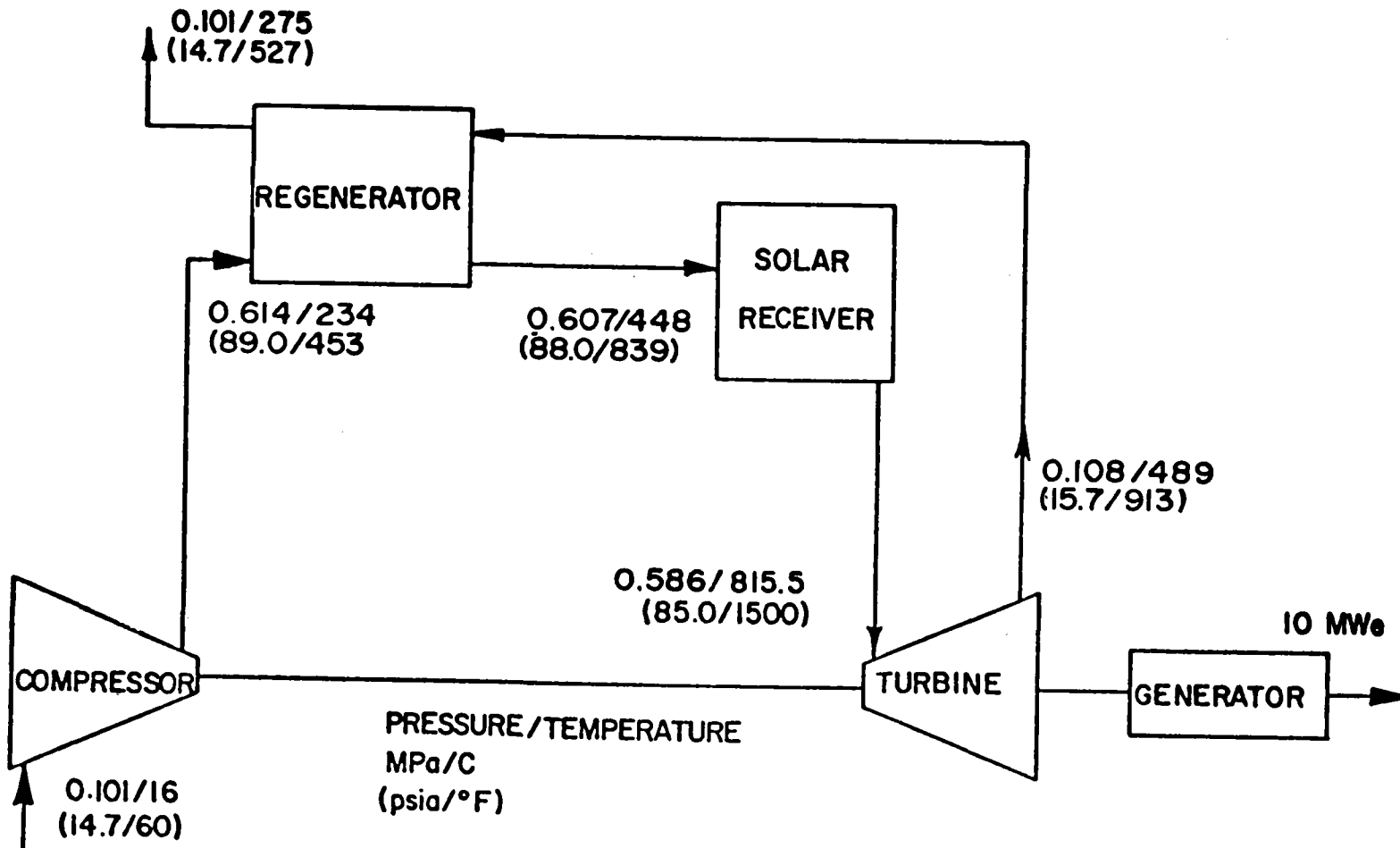


FIGURE 2.1
SELECTED REGENERATIVE OPEN AIR CYCLE

One feature of a solar gas turbine plant is its potential for higher efficiency. The selected prime mover can be upgraded to achieve a conversion efficiency of 38% (23% overall) through the use of higher efficiency components (turbine, compressor, regenerator). Another available area for improving the overall plant efficiency is to utilize the high exhaust temperature of the gas turbine engine in a bottoming cycle. Organic Rankine Cycles are currently being developed under DOE sponsorship which, when combined with the gas turbine system, can yield conversion efficiencies of 41% (25% overall). Finally, the plant can be modified to allow hybrid operation where the turbine operates by solar energy alone, by combustion of fossil fuel alone, or by a combination of both, so that the power generation is not subject to fluctuations in insolation. Hybrid operation, which is unique to the open-cycle gas turbine system, represents a practical alternative to the use of thermal storage.

After an initial screening process, preliminary design of the three most promising receiver candidates were developed. These candidates included one open (exposed) cylindrical configuration, one cavity cylindrical configuration, and one box configuration. Heat loss calculation showed that an exposed receiver operating at the high outlet gas temperature of 816°C (1500°F) resulted in prohibitive heat losses. For this reason, a cavity configuration was selected since this yielded the maximum receiver efficiency. Further evaluation based on solar flux, thermal/hydraulic, structural, and cost analysis led to the receiver geometry shown in Figures 2.2 and 2.3. It consists of nine modular panels which form the semicircular backwall of the cavity. Each panel carries 637 liquid metal heat pipes which are mounted at right angle to the gas flow. The evaporators of the heat pipes protrude from the flux absorbing front surface of the panels and the finned condensers traverse the gas stream. The chosen configuration provides:

- Maximum receiver efficiency by minimizing heat losses caused by reradiation, reflection, and convection
- Minimum pressure drop between compressor and turbine
- Maximum use of existing hardware and manufacturing techniques

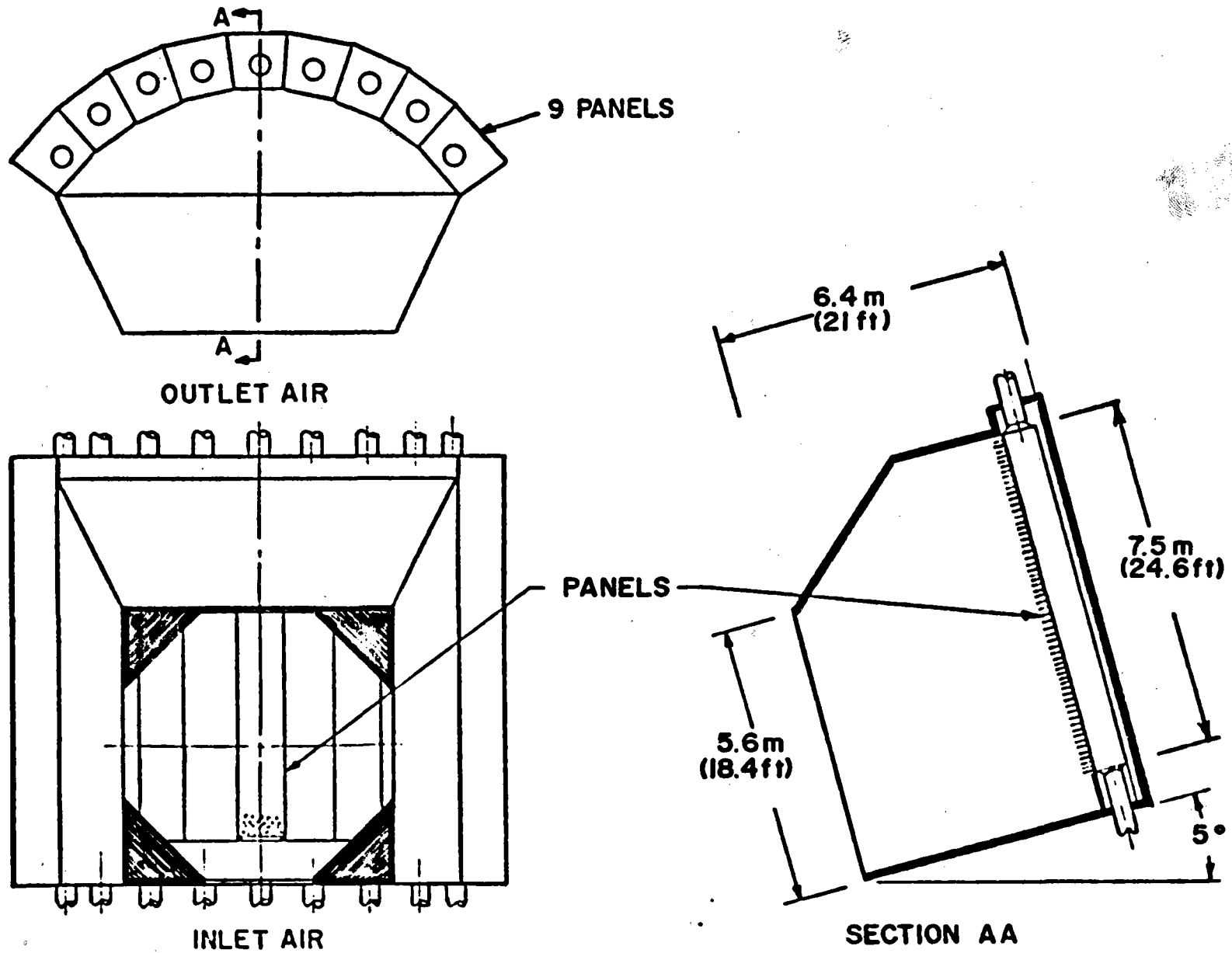


FIGURE 2.2

CAVITY RECEIVER CONFIGURATION

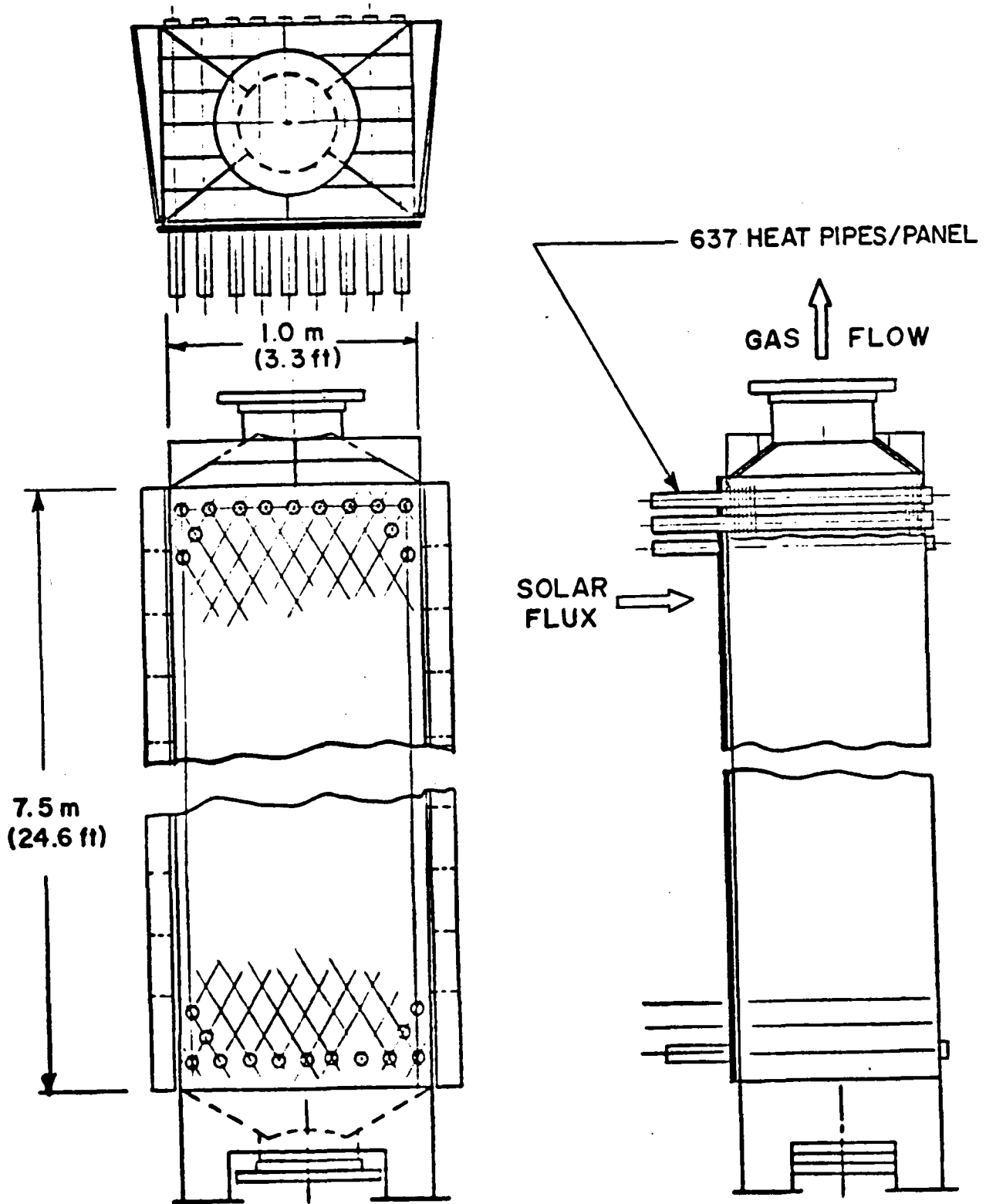


FIGURE 2.3
 PANEL CONFIGURATION

- Modular design that enhances reliability, flexibility, and maintenance since each panel is designed to be removable as a unit should replacement be necessary
- Optimum performance, since the airflow to each panel can be made proportional to the energy received by each panel
- Minimum cost

The incident solar radiation from the heliostat field enters the cavity through an octagonal aperture. The requirement of a high receiver efficiency necessitates that the receiver aperture be large enough to collect a high percentage of the solar flux, yet small enough to prevent excessive heat losses by reradiation and reflection. To accomplish this, an octagonal receiver aperture was selected. The receiver is tilted five degrees in order to optimize the solar flux distribution on the heat pipes and the panel walls.

Each of the nine panels which form the internal-energy absorbing surfaces in the back of the receiver is 7.5 m (24.6 feet) high by 1.0 m (3.3 feet) wide. The depth of the panel varies as a function of the amount of air passing through it, which in turn is proportional to the amount of heat flux impinging upon and being absorbed by its surface. The panel depth is such that each panel has approximately the same pressure drop of 0.007 MPa (1.0 psia). The average panel weight is approximately 10,000 kg (22,000 lb). Each panel consists of 637 sodium-filled heat pipes, inlet and outlet plenums, insulation, and support structure. A summary of the pertinent receiver parameters is given in Table 2.1.

A schematic of the heat pipes and their installation is shown in Figure 2.4. The heat pipes, 60 mm (2.375 inches) OD, are located in an 11.5 mm (4.5 inches) triangular pitch pattern and are attached to the front and back plates so that they can be removed from the back of the panel in case of failure. The evaporator surfaces of the heat pipes, which protrude 300 mm (12 inches) from the front panel plate absorb the incident solar flux. The tips of the evaporators are conical in order to reduce the flux at the end caps to approximately the same value as on the cylindrical evaporator surfaces. The heat pipes transport the energy nearly isothermally to the finned condenser section. Since each heat pipe is a self-contained heat transfer system, a

TABLE 2.1. RECEIVER PARAMETERS

Type of Receiver	:	North Facing Cavity
Total Weight	:	108,295 kg (238,250 lbs)
Number of Panels	:	Nine (9)
Number of Heat Pipes	:	5,733
Incident Solar Radiation	:	30 to 35 MW(th)*
Heat Losses	:	3 to 4 MW(th)
Peak Aperture Flux	:	5.71 to 5.94 MW/m ² * (1.81 x 10 ⁶ to 1.88 x 10 ⁶ Btu/hr-ft ²)
Peak Flux on Receiver Walls	:	1.16 to 1.32 MW/m ² * (367,500 to 419,000 Btu/hr-ft ²)
Air Inlet/Outlet Temperature	:	448/816 ^o C (839/1500 ^o F)
Receiver Pressure Loss (Including Headers & Piping)	:	3 psia (0.02 MPa)

*Depending on Conversion Efficiency of Power Generation System

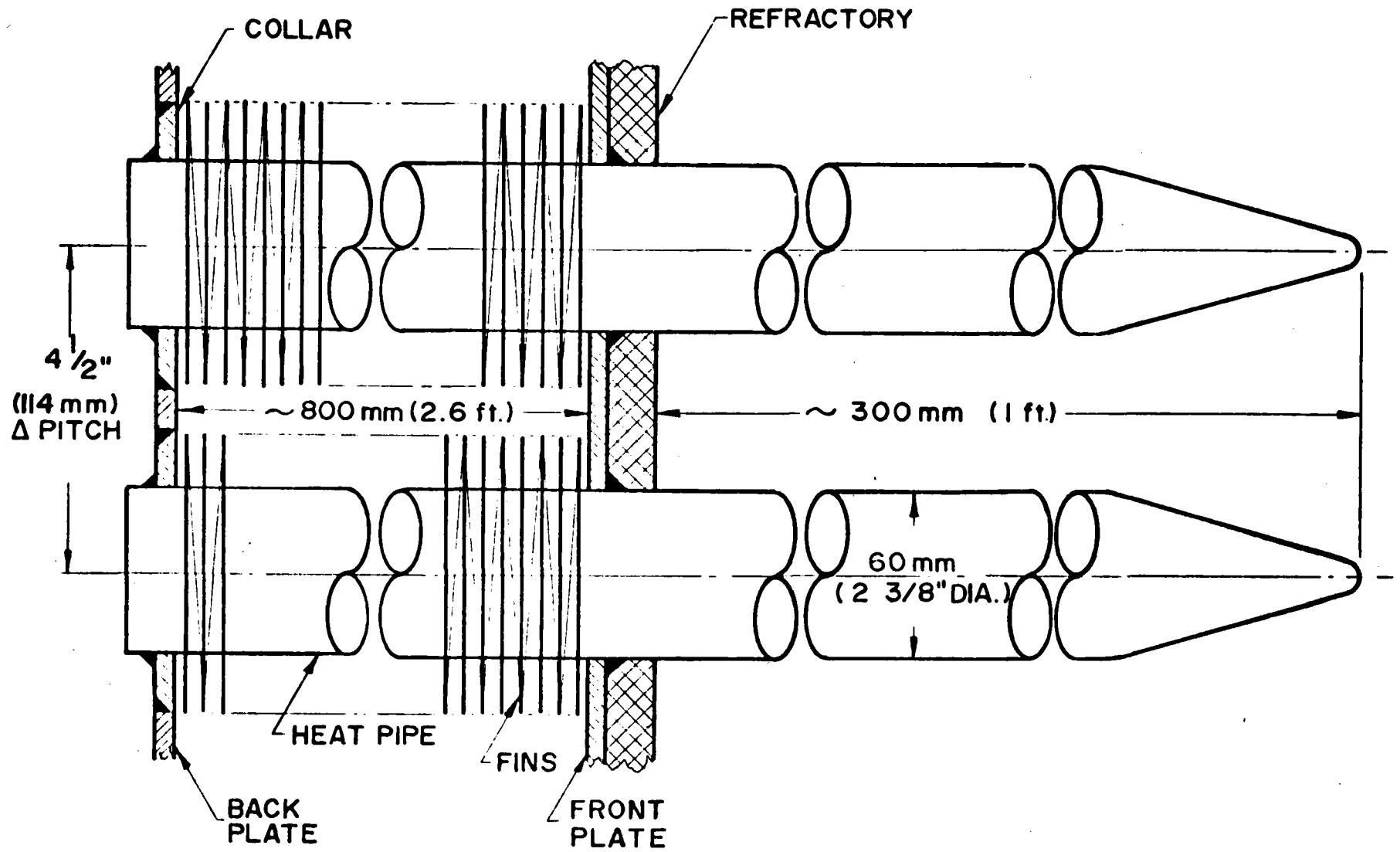


FIGURE 2.4
HEAT PIPE SCHEMATIC

failure of a single heat pipe will not affect the system catastrophically. The design parameters of the heat pipes are given in Table 2. 2.

The collector subsystem is based on the heliostat field designed by the Martin Marietta Corporation for their water/steam pilot plant. It is a north field arrangement with focusing heliostats symmetrically distributed about a north-south line from the tower, which is erected at the south edge of the collector field. The north field geometry provides the maximum optical collector efficiency. The focused heliostats enable the use of a smaller aperture for the cavity receiver, thus minimizing receiver losses. Each heliostat carries 41 m^2 (441 feet^2) of reflective surface. The number of heliostats required ranges from 1164 to 1344.

The electric power generation subsystem consists of conventional utility-type power plant components. For the pilot plant, the General Electric gas turbine-generator package G3132R regenerative-cycle, two shaft heavy-duty gas turbine was selected. The nominal rated capacity is 10.4 MW(e) and the gross weight is 69,000 kg (152,000 lb). The regenerator, which comes with the gas turbine generator package, is a Harrison Regenerator Model TR-105. The basic conversion efficiency of this gas turbine set is 33%. Preliminary discussions with GE personnel indicated that the efficiency can be upgraded to 38% by increasing component efficiencies; i. e., turbine efficiency from 85 to 92%, compressor efficiency from 80 to 88%, and recuperator effectiveness from 85 to 94%.

The heat pipe receiver, the electric power generation subsystem, and the interconnecting piping are all located on top of the tower. This location minimizes the airflow path among components and thus reduces thermal and pressure losses. This is particularly important in a Brayton cycle because, to reduce pressure losses, large diameter pipes are needed to transport large volumes of air. The structural-steel tower is similar in design to the one designed by McDonnell Douglas Astronautics Company for the water/steam pilot plant. The tower, which is approximately 90 m (295 feet) high, supports on its top a weight of approximately 360 metric tons (396 short tons).

The key components of this solar-thermal conversion system are the liquid metal heat pipes. Since the requirements for the heat pipes exceeded current state-

TABLE 2.2. HEAT PIPE DESIGN PARAMETERS

Dimensions	:	60 mm OD x 2.4 mm wall x 1100 mm long (2.375 inch x 0.093 inch x 43 inch)
Orientation	:	5° Gravity Assist
Material	:	Inconel 601
Working Fluid	:	Sodium
Wick Structure	:	Parallel Tent Arteries
Max./Min. Vapor Temperature	:	821/445°C (1510/833°F)
Max./Average Heat Load	:	13.1/5.2 kW
Max./Average Evaporator Flux	:	0.34/0.067 MW/m² (108,000/21,200 Btu/hr-ft²)

of-the-art technology, a substantial portion of the program was devoted to the development of the needed heat pipe technology.

Historically, liquid metal heat pipes date back to the early stages of heat pipe development during the mid-sixties. Although high heat fluxes and heat transport rates were achieved in laboratory experiments, little actual hardware capability was developed because of a lack of applications. Furthermore, most experimental heat pipes were much smaller than needed for the present application. The closest analog to the solar heat pipes are probably the Isothermal Furnace Liners developed and marketed by Dynatherm. They consist of annular liquid metal heat pipes ranging in diameters from 60 to 168 mm (2.375 to 6.63 inches) and in lengths from 150 to 914 mm (6 to 36 inches). They are fabricated from Inconel 601 and the working fluid is sodium. The operating temperature ranges from 400 to 1100°C. To date, over 450 of these heat pipes are in use by over a hundred industrial, government, and university laboratories. Since many of the devices have been in operation for over six years, their long life capability is well established. There is one important difference, however, between the solar receiver heat pipes and the commercial Isothermal Furnace Liners. The latter are basically low flux and low transport devices since their main function is to isothermize furnaces. Thus, the need existed to develop heat pipes which combine the performance capabilities of laboratory devices with the size and reliability of the commercial products.

Typical theoretical and experimental performance capabilities of a solar receiver heat pipe are shown in Figure 2.5. At the low end of the useful temperature range the heat transport capability is limited by the gas dynamics of the vapor flow. At higher temperatures (550 to 800°C), the performance is dominated by the wick and is relatively independent of temperature. Above 800°C, nucleate boiling near the heat input surfaces limits the heat fluxes that can be applied.

The maximum heat load required of any heat pipe in the solar receiver is about 13 kW. This maximum heat load occurs at about 750°C; at lower and higher temperatures the requirement is considerably less (under one kilowatt at 450 and 820°C). As seen from Figure 2.5, the measured performance matches well with the requirements.

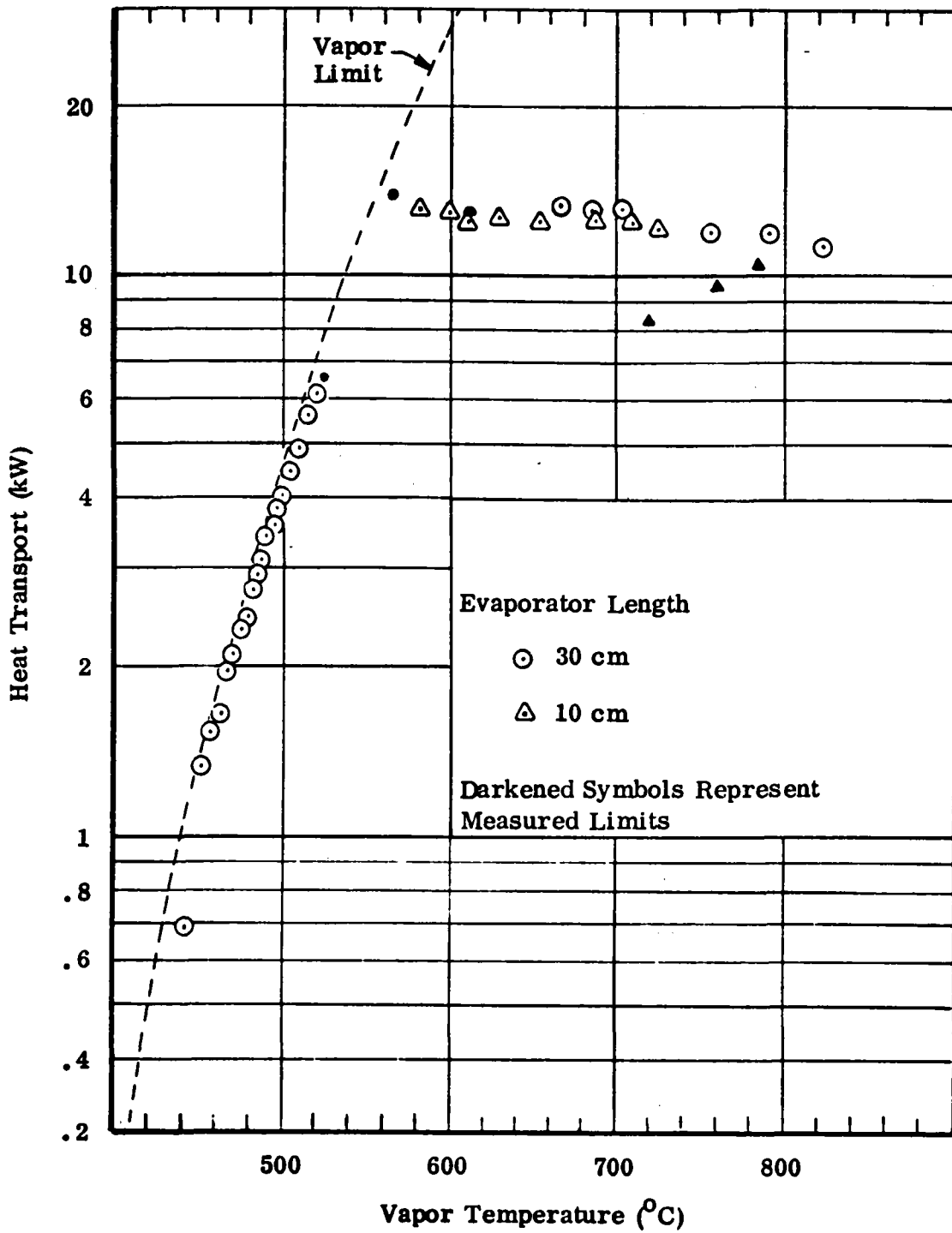


FIGURE 2.5
 PERFORMANCE CAPABILITY OF
 CENTRAL SOLAR RECEIVER HEAT PIPE

During the early stages of the development program, several subscale sodium heat pipes (2.5 cm diameter) were fabricated and tested. The design goal for these heat pipes was to achieve an axial heat flux of 10 MW/m^2 ($3.16 \text{ MBtu/hr-ft}^2$) and an evaporator flux of 1 MW/m^2 ($0.316 \text{ MBtu/hr-ft}^2$). These fluxes exceed the current receiver requirements but were representative of earlier receiver concepts. A total of eight subscale heat pipes were tested; one of them, SN 1-5, is shown in the photograph of Figure 2.6.

One purpose of the experimental program was the development of a suitable wick. Of all the wicks tested, the most successful one proved to be the "tent artery" which is shown in Figure 2.7. It consists of several semicircular arteries which are fabricated from fine wire mesh and are attached to the heat pipe wall. They provide the main axial flow path for the liquid. At the evaporator, the liquid is distributed by capillary forces in a secondary wick.

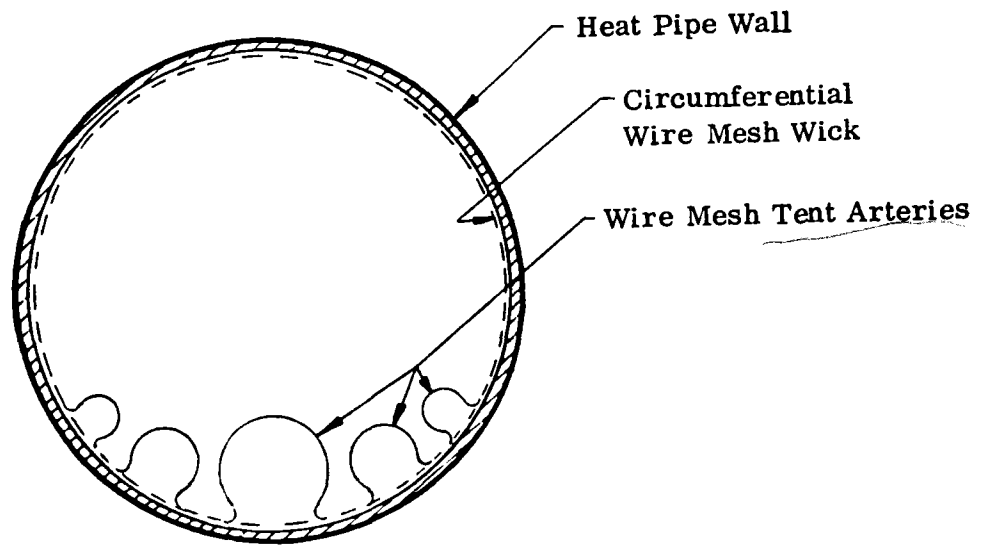


FIGURE 2.7
WICK DESIGN OF CENTRAL SOLAR RECEIVER HEAT PIPE



FIGURE 2.6
PHOTOGRAPH OF SUBSCALE THERMAL DIFFUSER HEAT PIPE

Following the successful development of the subscale heat pipes, three full-scale solar receiver heat pipes were tested. One of them was equipped with a conical end cap as a means for reducing the peak flux on that surface. A photograph of this heat pipe during test is shown in Figure 2.8. Typical performance data of these heat pipes were shown in Figure 2.5.

The overall conductance of the heat pipes is approximately $420 \text{ Watts}/^{\circ}\text{C}$. For the average loaded heat pipe, this corresponds to a temperature difference of 12°C (22°F). Virtually all of this temperature drop occurs across the walls of the evaporator and of the condenser. By comparison, the temperature gradient along the heat pipe is almost negligible. In order to achieve high conductances and small temperature drops, it is therefore desirable to minimize the wall thickness. This has the added advantage of reducing the stresses in the wall at the evaporator which result from through-the-thickness temperature gradients. A cyclic thermal analysis of the heat pipes was conducted to determine the allowable heat fluxes for various values of the sodium temperature. For the selected wall thickness of 2.4 mm (0.093 inch) the permissible evaporator flux is compatible with the receiver design.

The projected cost of a heat pipe central receiver gas turbine plant compares favorably with an equivalent water/steam plant. Capital cost estimates were made for the 10 MW(e) pilot plant. The costs of the receiver including the heat pipes and the mounting platform were developed from the design drawings generated during this project. Tower assembly, foundation, and site preparation costs were scaled from the costs developed for the water/steam system. The cost of the power generation system, which is a standard GE product, was obtained from the manufacturer. Following DOE ground rules, the cost of the collector field was estimated at \$65 per square meter of heliostat surface. Since details of a master control system have not been developed during this program, its cost was assumed to be the same as for the water/steam plant. Finally, miscellaneous items such as buildings, facilities, electric plant equipment, etc., were estimated by Foster Wheeler based on experience with conventional plants of similar nature and size.

The total projected costs, in mid-1978 dollars, are shown in Table 2.3 for the two assumed cycle efficiencies of 33 and 38%. These costs range from \$1,947

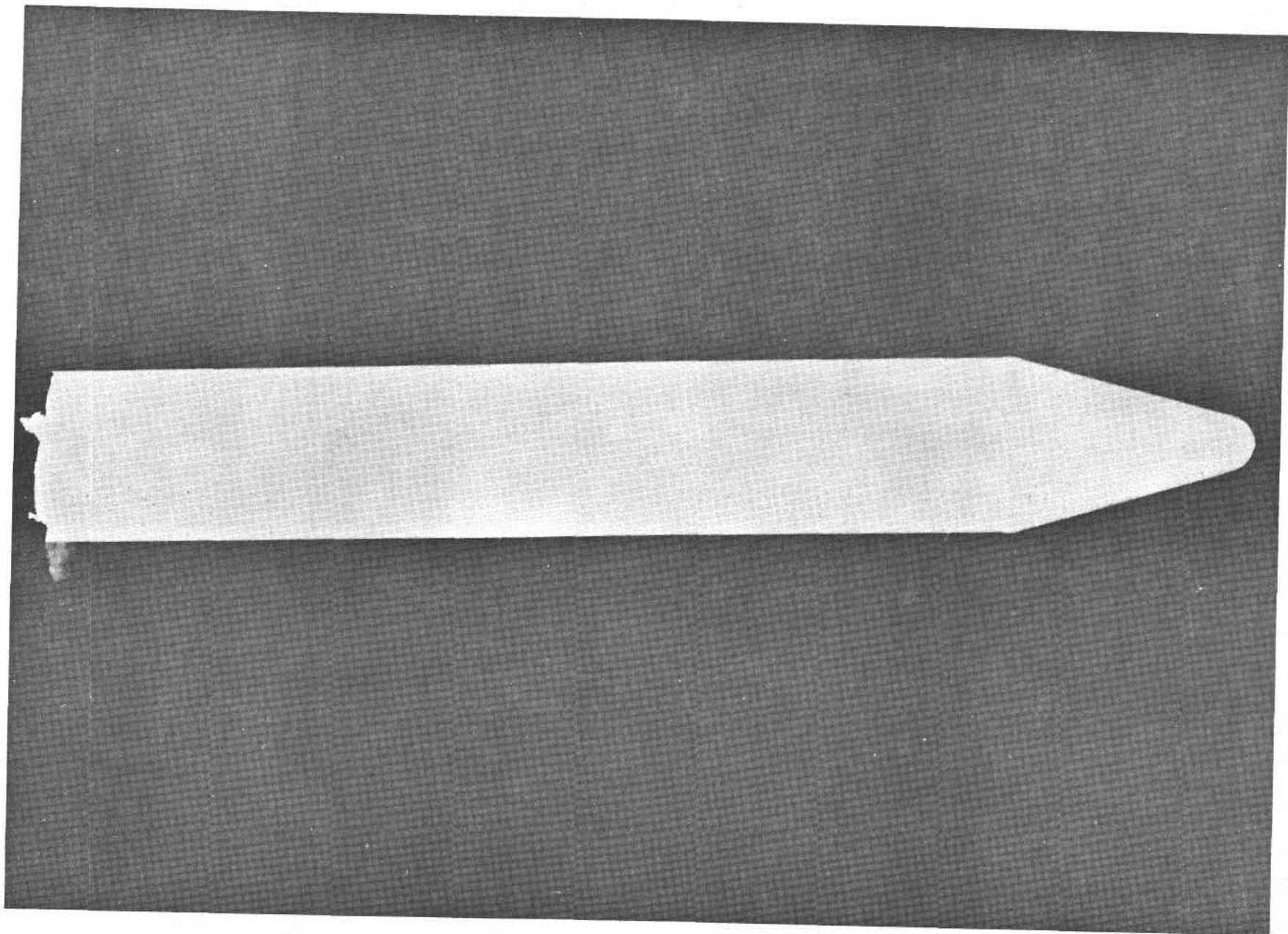


FIGURE 2.8
FULL SCALE THERMAL DIFFUSER HEAT PIPE

**TABLE 2.3. CAPITAL COST OF HEAT PIPE
SOLAR GAS TURBINE PLANT**

<u>Cost Item</u>	<u>\$ Millions</u>
Receiver and Platform	3.51
Transportation and Installation	0.88
Tower Assembly	1.50
Tower Foundation and Site Preparation	0.54
Collector Field (Heliostats)	3.10 - 3.58
Buildings and Facilities	0.50
Turbine-Generator Unit	2.97
Master Control	2.24
Miscellaneous	<u>1.60</u>
Total Direct Costs	16.93 - 17.41
Contingency Allowance and Indirect Costs (15%)	<u>2.54 - 2.61</u>
Total Capital Costs	19.47 - 20.02

Note: Costs based on mid-1978 dollars

\$2,002 per electrical kilowatt.

In order to compare the cost of the heat pipe gas turbine system with that of the 10 MW(e) steam/water pilot plant, a slightly different analysis was used. The costs were broken down into the WBS items used for the steam/water plant. Each item was then evaluated and adjustments were made to eliminate costs associated with thermal storage and those costs which do not apply to the gas turbine plant. The results which are given in Table 2.4 show that the total capital costs of the gas turbine plant are only 67% of those of the equivalent steam/water plant. This cost reduction is considerably better than the 85-90% projected by a recent study by the Aerospace Corporation.

The above analysis does not take credit for utilizing the high exhaust temperature of the gas turbine in a bottoming plant. Only a rough estimate of the cost of such a combined plant was made. Assuming an Organic Rankine Bottoming Cycle (ORC) which will boost the overall plant efficiency from 33 to about 41%, the capital cost per kilowatt will be reduced from the above \$2000 (see Table 2.3) to about \$1830.

As a result of the present study, the heat pipe solar receiver has emerged as a viable and cost-effective contender for a central receiver solar power plant. In order to develop this system in a timely fashion, a three task program has been suggested. As a first task, a small scale model of a heat pipe receiver (250 kW(th)) would be tested at one of the existing DOE solar test facilities. Concomitantly with this task, long-term performance tests of the solar receiver heat pipes under simulated actual conditions must be conducted. Finally, a more detailed study and optimization of the overall plant need to be performed. This study will define the most economical plant with regard to size, storage requirement, and bottoming or hybrid operation.

**TABLE 2.4. COST COMPARISON OF HEAT PIPE AIR BRAYTON
AND STEAM RANKINE 10 MW(e) POWER PLANT**

<u>Cost Item</u>	<u>Heat Pipe Gas Turbine Plant</u> <u>\$ Millions</u>	<u>Steam Rankine Plant</u> <u>\$ Millions</u>
Receiver	4.39	10.74
Tower & Foundation	2.04	0.67
Collectors ⁽¹⁾	3.63	4.35
Turbine Equipment	2.97	5.40
Buildings ⁽²⁾	1.10	2.47
Misc. Electric Equipment ⁽³⁾	1.13	1.13
Misc. Plant Equipment ⁽²⁾	1.24	2.85
Master Control ⁽³⁾	2.26	2.26
Distributables ⁽³⁾	3.05	3.05
Yard Work	<u>0.70</u>	<u>0.70</u>
Total Direct Cost	22.51	33.62
Contingency Allowance and Indirect Costs (15%)	<u>3.38</u>	<u>5.04</u>
Total Capital Costs	25.89	38.66

(1) Based on \$65/m²

(2) Adjusted to reflect savings in gas turbine plant

(3) Assumed identical in gas turbine and steam plant

Note: Costs based on mid-1978 dollars

Percentage Cost of Heat Pipe Gas Turbine Plant: 67%

3. HEAT PIPE DEVELOPMENT

This section of the report describes the analytical and experimental work which was performed by Dynatherm toward the development of the heat pipe technology for the central solar receiver.

3.1 Heat Pipe Requirements

The receiver design which resulted from the present work utilizes 5733 liquid metal heat pipes. The heat pipes absorb the concentrated solar flux, transport the collected thermal energy nearly loss-free to a gas stream, and dissipate it into the gas stream with a minimum pressure loss in the gas. Details of the receiver and heat pipe geometry are given in the attached Foster Wheeler report. For ease of reference, several pertinent figures of that report are reproduced here.

Figures 3.1 and 3.2 show the selected receiver. It consists of nine modular panels which form the semicircular back-wall of the cavity. Incident solar radiation from the heliostat field enters the cavity through an octagonal aperture. The receiver is tilted five degrees in order to optimize the solar flux distribution on the absorber wall. Each of the modular panels carries 637 liquid metal heat pipes which are mounted at right angles to the gas flow. The evaporators of the heat pipes protrude from the flux absorbing front surface of the panels, the finned condensers traverse the gas stream.

A schematic of the heat pipes and their installation is shown in Figure 3.3. The heat pipes, 60 mm (2.375 inches) OD, are located in an 11.5 mm (4.5 inches) triangular pitch pattern and are attached to the front and back plates so that they can be removed from the back in case of failure. The tips of the evaporators are conical in order to reduce the flux at the endcaps to approximately the same value as on the cylindrical evaporator surfaces. In order to provide maximum commonality for all receiver components, all heat pipes in the receiver are identical with the exception of the condenser length which varies from panel to panel.

The design and performance parameters of the heat pipes are given in Table 3.1.

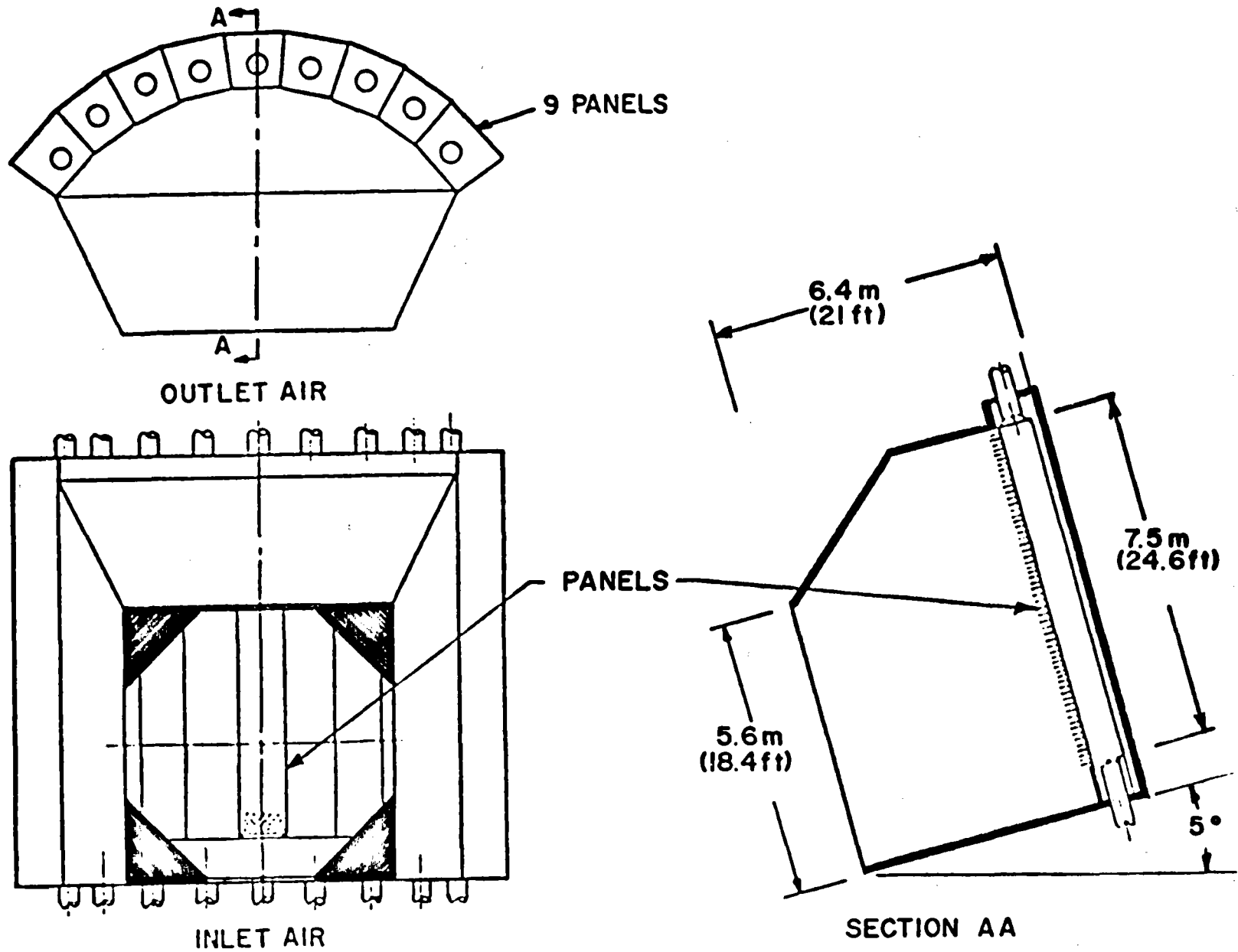


FIGURE 3.1
CAVITY RECEIVER CONFIGURATION

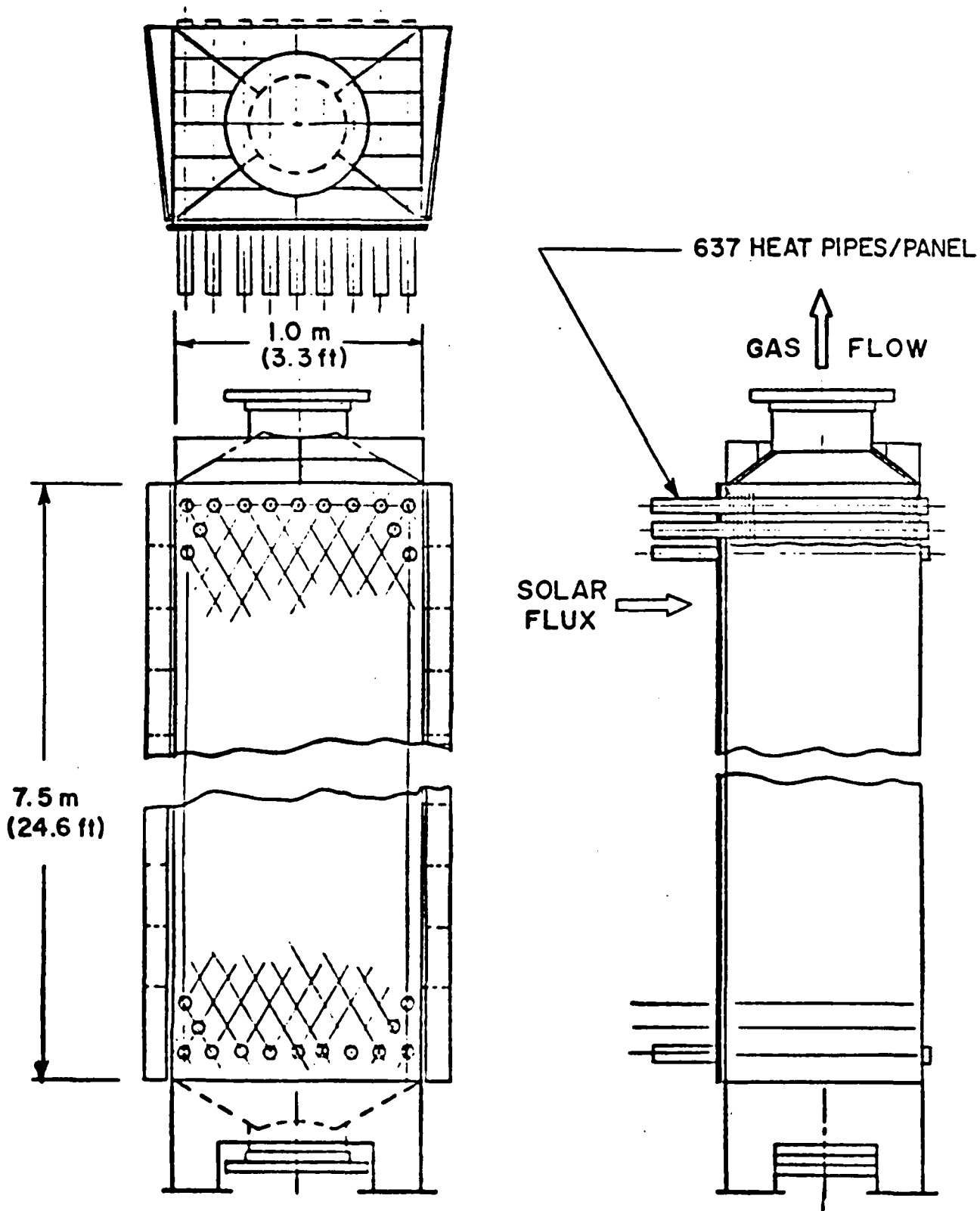


FIGURE 3.2
 PANEL CONFIGURATION

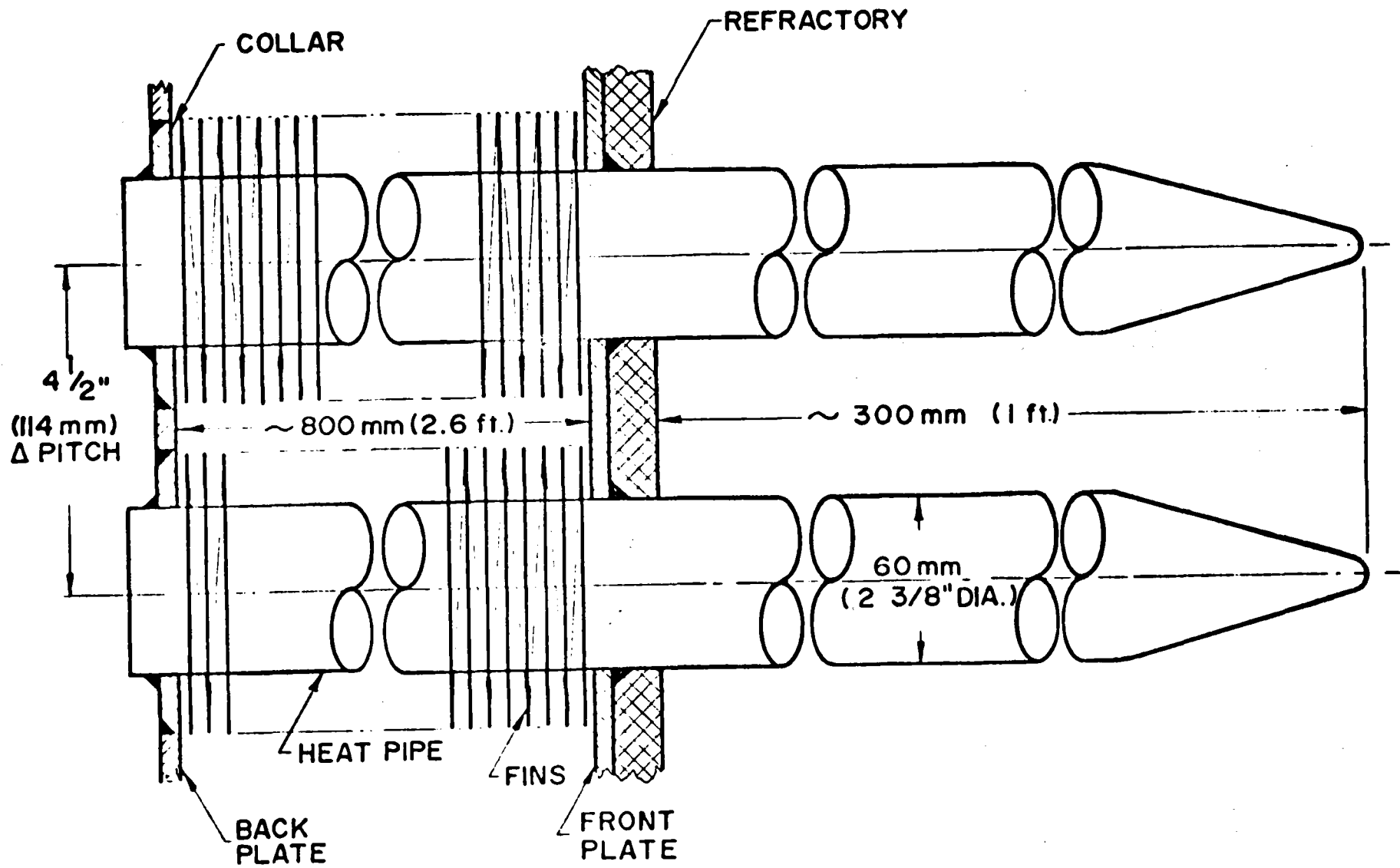


FIGURE 3.3
 HEAT PIPE SCHEMATIC

TABLE 3.1 HEAT PIPE DESIGN PARAMETERS

Dimensions	:	60 mm OD x 2.4 mm wall x 1100 mm long (2.375 inch x 0.093 inch x 43 inch)
Orientation	:	5° Gravity Assist
Material	:	Inconel 601
Working Fluid	:	Sodium
Wicking Structure	:	Parallel Tent Arteries
Max./Min. Vapor Temperature	:	821/445° C (1510/833° F)
Max./Average Heat Load	:	13.1/5.2 kW
Max./Average Evaporator Flux	:	0.34/0.067 MW/m² (108,000/21,200 Btu/hr-ft²)

The dimensions of the heat pipes were selected on the basis of a trade-off study between the total number of pipes, their weight, evaporator temperature gradients, and reasonable values for radial and axial heat fluxes. Details of the study were reported in the First Semiannual Progress Report.⁽¹⁾ The initial optimization of the heat pipes was based on an average axial heat flux of 10 MW/m^2 which appeared achievable with current heat pipe technology. This selection led to an optimum heat pipe diameter of approximately 5 cm and a total of 1640 heat pipes for a 30 MW(th) receiver. The same optimization also yielded an optimum evaporator length of 30 cm with an attendant evaporator flux of 0.5 MW/m^2 .

Subsequent computer studies of the solar flux distribution on the heat pipes and on the absorber wall yielded more detailed information of the evaporator fluxes. These, combined with a better definition of the flux limits imposed by the heat pipe material, resulted in an increase of the number of heat pipes from 1640 to the present 5733. Correspondingly, the required axial flux has dropped from 10 MW/m^2 to a maximum of 5.4 MW/m^2 . The maximum evaporator flux of any heat pipe is now 0.34 MW/m^2 .

The aforementioned solar flux model was specifically developed for this project. Initially it had been hoped that computer models which were generated for the water/steam receivers could be adapted. However, those models all predict only the total flux on a given receiver surface without distinguishing as to the direction of the impinging radiation. Since the heat pipes protrude at right angles from the absorber surface, a knowledge of the directional intensity distribution is required in order to predict the flux distribution on the cylindrical heat pipe surfaces. Thus it became necessary to develop a new solar flux model for the heat pipe receiver. A map of the heat flux density on the absorber walls (the semicircular back of the cavity) is shown in Figure 3.4. Note that the peak flux near the center of the cavity is 1.16 MW/m^2 . By comparison, the peak flux at the aperture is 5.25 MW/m^2 .

Since the axes of the heat pipes are oriented perpendicular to the absorber wall, the flux on the cylindrical heat pipe surfaces is substantially lower. But it is also highly nonuniform around the circumference. This is shown in Figure 3.5.

Distance From Bottom of Panel (Z)	Heat-Flux Density, MW/m ² (10 ³ Btu/h·ft ²)				
	Panel No.				
	5	4 and 6	3 and 7	2 and 8	1 and 9
90 - 100	0.0698 (22.126)	0.0711 (22.531)	0.0650 (20.601)	0.0422 (13.371)	0.0048 (1.522)
80 - 90	0.0655 (20.760)	0.0861 (27.283)	0.1000 (31.698)	0.0908 (28.786)	0.0262 (8.315)
70 - 80	0.1157 (36.671)	0.1633 (51.759)	0.1569 (49.746)	0.1501 (47.575)	0.0704 (22.307)
60 - 70	0.2646 (83.866)	0.3182 (100.865)	0.3172 (100.545)	0.3705 (117.432)	0.1601 (50.760)
50 - 60	0.9108 (288.684)	0.9570 (303.331)	1.0857 (344.120)	1.0890 (345.166)	0.7023 (222.589)
40 - 50	1.0180 (322.662)	1.0602 (336.037)	1.1589 (367.321)	1.0763 (341.140)	0.8750 (277.332)
30 - 40	0.8151 (258.351)	0.8573 (271.733)	0.9170 (290.665)	0.8612 (272.979)	0.7446 (236.013)
20 - 30	0.5257 (166.624)	0.5582 (176.915)	0.6122 (194.044)	0.5613 (177.914)	0.5036 (159.606)
10 - 20	0.2063 (65.388)	0.2454 (77.768)	0.2960 (93.819)	0.2893 (91.711)	0.2367 (75.031)
0 - 10	0.0106 (3.369)	0.0259 (8.195)	0.0674 (21.362)	0.0787 (24.938)	0.0479 (15.193)

FIGURE 3.4

INCIDENT HEAT FLUX DENSITY ON ABSORBER WALL

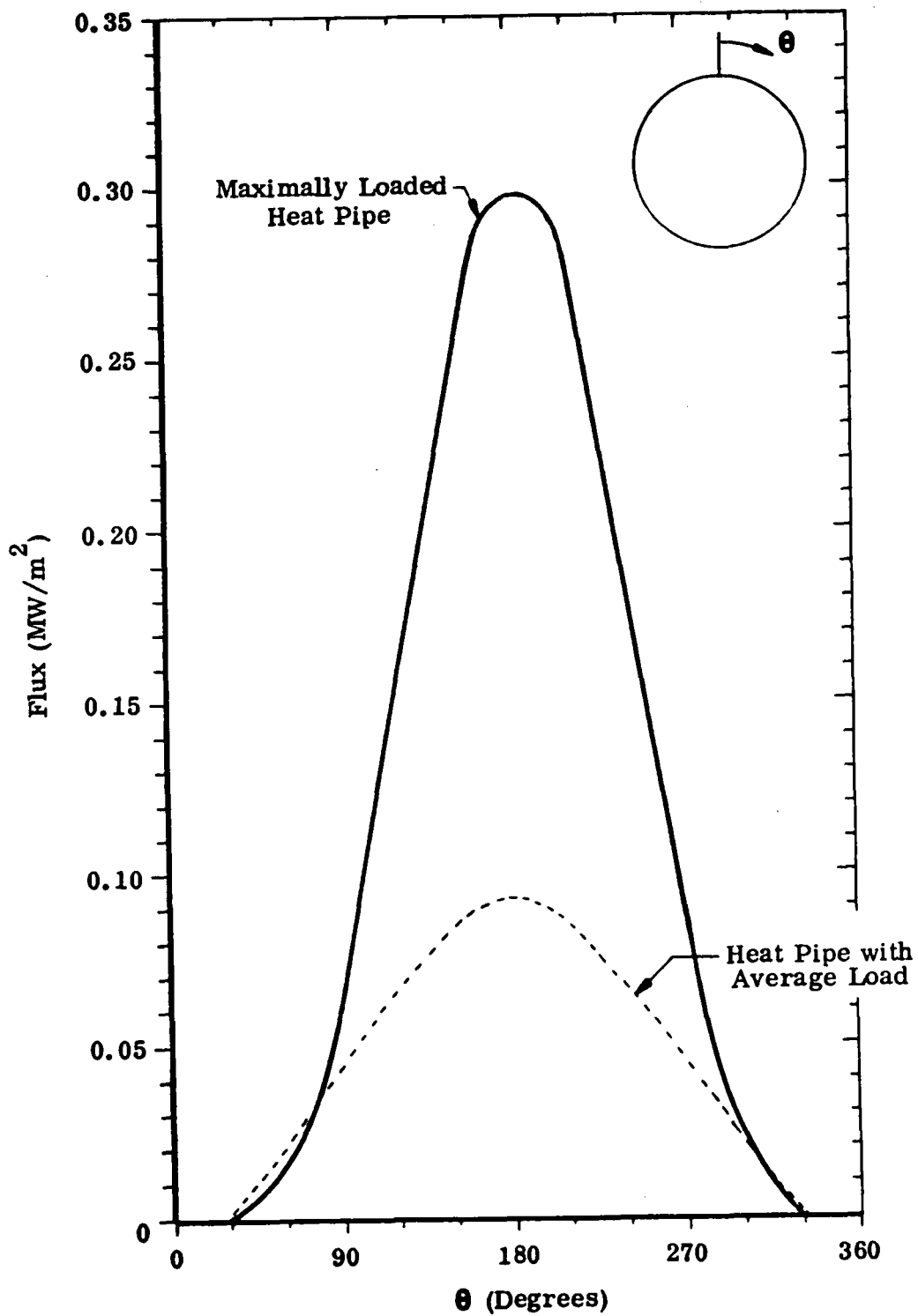


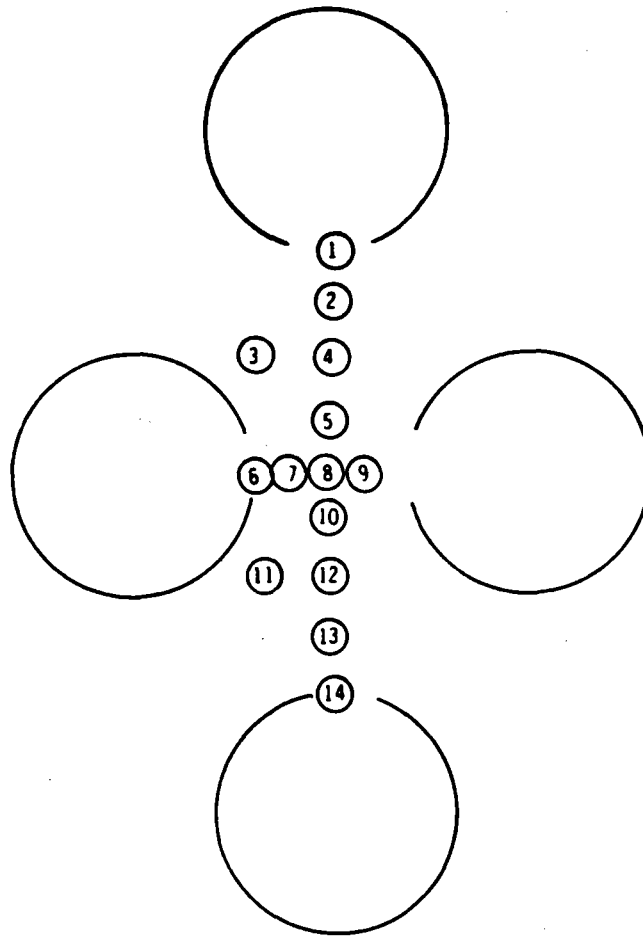
FIGURE 3.5
CIRCUMFERENTIAL FLUX DISTRIBUTION
ON HEAT PIPE EVAPORATOR

The maximum flux occurs at the bottom of the heat pipe because of the chosen orientation of the receiver and the layout of the heliostat field. The end caps of the heat pipes are of course exposed to the full normal flux of more than 1 MW/m^2 . Because of material limitations which are discussed in another section of this report, it was deemed necessary to reduce the end cap flux. Therefore, the conical end cap design shown in Figure 3.3 was selected. The cone angle was chosen such that the maximum end cap flux approximately equals the maximum flux on the cylindrical surfaces of the heat pipes. Finally, the solar flux impinging directly on the receiver wall has to be considered. Although somewhat shielded by the heat pipes, the remaining flux on the wall is nevertheless substantial as shown in Figure 3.6. Only a small amount of this energy is transmitted directly to the gas stream behind the panel wall. In order to avoid damage to the wall, it is covered with a high temperature refractory material. This will cause the surface which is exposed to the solar flux to become nearly adiabatic and reach a peak temperature of about 1620°C (2950°F). Most of the reradiated energy is intercepted by the heat pipes. Because of the homogeneous nature of this secondary radiation, it is uniformly distributed around the circumference of the heat pipes and adds little to the peak evaporator flux. In summary, the maximum evaporator flux is about 0.34 MW/m^2 ($1.08 \times 10^5 \text{ Btu/hr-ft}^2$).

Unlike the evaporator flux, the axial heat transport requirement and the axial heat flux is easier to evaluate. From the flux pattern on the absorber panel (Figure 3.4) and the given heat pipe spacing, the maximum and average heat loads per pipe are calculated to be 13.1 and 5.3 kW, respectively. The corresponding axial heat fluxes for the pipes with an OD of 6.03 cm (2.375 inches) and an ID of 5.58 cm (2.195 inches) are 5.4 and 2.1 MW/m^2 (1.7×10^6 and $6.6 \times 10^5 \text{ Btu/hr-ft}^2$).

The evaporator and the axial heat flux are the two most important heat pipe performance parameters. The condenser flux is much lower because the condensers are from two to three times longer than the evaporators. Furthermore, condenser fluxes are not limited by the same hydrodynamic phenomena (such as boiling) as are evaporator fluxes. Only material limits need to be considered but the design fluxes are too low to cause any concern.

The temperature range over which the heat pipes must operate is determined



<u>Point</u>	<u>Flux at Location of Maximally Loaded Heat Pipe</u>	<u>Flux at Location of Average Loaded Heat Pipe</u>
1	.543	.272
2	.647	.271
3	.432	.153
4	.485	.168
5	.633	.245
6	.278	.210
7	.600	.312
8	.678	.327
9	.668	.312
10	.694	.384
11	.539	.310
12	.480	.276
13	.194	.128
14	.000	.000

FIGURE 3.6
FLUX ON ABSORBER WALL

by the gas inlet and outlet temperatures and the heat transport rate. Gas enters the receiver at 448°C (839°F) at the bottom of the panels and leaves at 816°C (1500°F) at the top of the panels. From the known flux distribution, the vapor temperature of each heat pipe along with the required heat transport rate can be calculated. Figure 3.7 shows a plot of this heat transport requirement versus vapor temperature. Note that the requirement is highest near the middle of the temperature range which occurs near the center of the panel where the highest solar flux is absorbed. The requirements are much lower at both ends of the range. This is fortunate since the theoretical capability shows a similar pattern as the requirements. The theoretical performance capability of liquid metal heat pipes will be discussed in the next section.

✓ In addition to performing under steady state conditions, the heat pipes must also function during transient start-up and shutdown. The nature of the transients depend on the operating strategy of the power plant. The worst case during start-up is represented by the hypothetical condition where the system is initially cold (no gas flow) and the heliostats are instantaneously focused on the receiver. In this case, the vapor temperature of the heat pipes with the highest loading would rise at a rate of $2.8^{\circ}\text{C}/\text{sec}$ ($18,200^{\circ}\text{F}/\text{hr}$). The same rate would apply during shutdown when the solar flux is instantly removed but the cooling by the gas stream continues. The shutdown scenario could be real, for instance, when clouds suddenly obscure the sun. But the above instantaneous start-up is unlikely to occur because the compressor and the turbine will always be spun up before the heliostats are focused. The gas which is heated during compression will in turn preheat the heat pipes by several hundred degrees. By the same mechanism, the heat pipes will always be preheated if the full solar flux is suddenly reapplied after a solar outage. The effect of preheating on the start-up characteristics will be discussed in a later section.

Other required characteristics of the thermal diffuser heat pipes are high thermal conductance and life expectancy of 30 years. The conductance is determined mostly by the heat transfer through the walls, by comparison of which the internal axial conductance is almost infinite. In order to maximize the overall

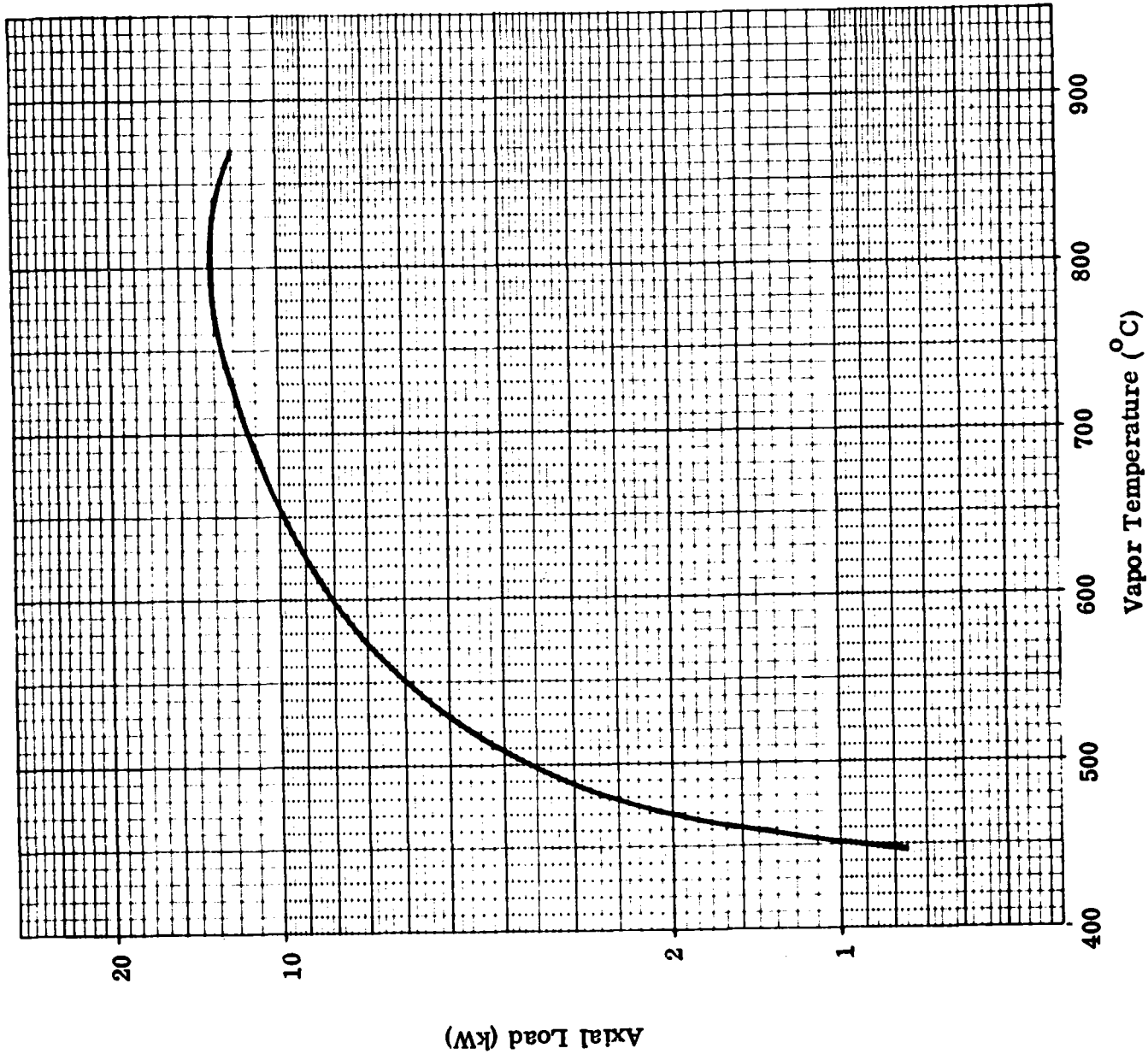


FIGURE 3.7
HEAT TRANSPORT REQUIREMENTS

conductance, the thinnest possible wall consistent with pressure containment and reliability needs to be selected. A life expectancy of 30 years is consistent with the requirement of the overall system. Such a lifetime is difficult, if not impossible, to prove on the basis of past experience. No liquid metal system of a similar nature has been in operation for anywhere near that period of time. Since life expectancy is an important concern in the selection of a heat pipe receiver, a review of the technology and of past experience is presented in a later section.

3.2 Theoretical Heat Pipe Performance Capability

The temperature range over which the heat pipes in the solar receiver must operate extends from 450°C (840°F) to approximately 850°C (1560°F). For this range, the alkali metals potassium and sodium are the obvious choices for working fluids. Some of their pertinent thermodynamic properties, namely, the vapor pressure p_v , the vapor transport limits q_s , the Liquid Transport Factors N_1 , and the Wicking Height Factors H are shown in Figures 3.8 and 3.9. The significance of p_v , q_s , N_1 , and H are discussed in detail in Reference 8; only a brief summary is given here. The vapor pressure has a dual significance. Since the heat pipe is a sealed pressure vessel operating at a very high temperature, the internal pressure (whether below or above atmospheric) determines the stresses in the wall material and therefore its required thickness. Indirectly, the vapor pressure also defines the vapor density and, with it, the vapor velocity for a given heat throughput. In general, the higher the saturation vapor pressure of a heat pipe working fluid, the less important are gas dynamic effects. In the other extreme, at very low vapor pressures, the dynamics of the vapor flow may dominate the heat pipe's performance. The maximum achievable axial heat flux in a vapor dominated heat pipe is given by the vapor transport limit q_s . It is the flux that can be transported when the vapor flow reaches sonic velocity.

The Liquid Transport Factor N_1 is a grouping of transport properties of the liquid (surface tension, heat of evaporation, density, and viscosity). It is frequently referred to as the Figure of Merit of the fluid and is a measure of the amount of condensate which a wick of a given design can circulate. Finally, the

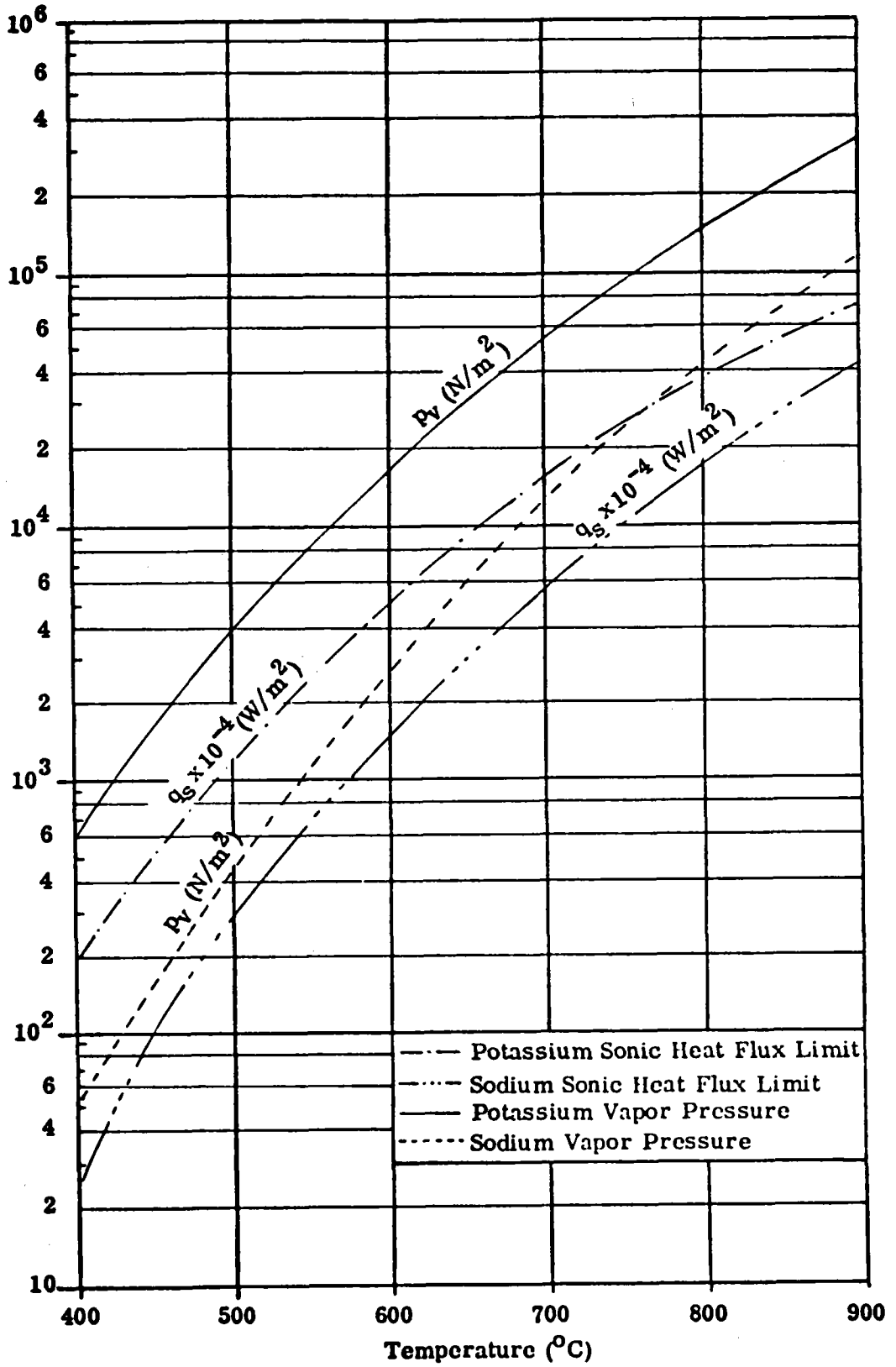


FIGURE 3.8
 VAPOR PRESSURE AND SONIC HEAT FLUX LIMIT
 OF SODIUM AND POTASSIUM

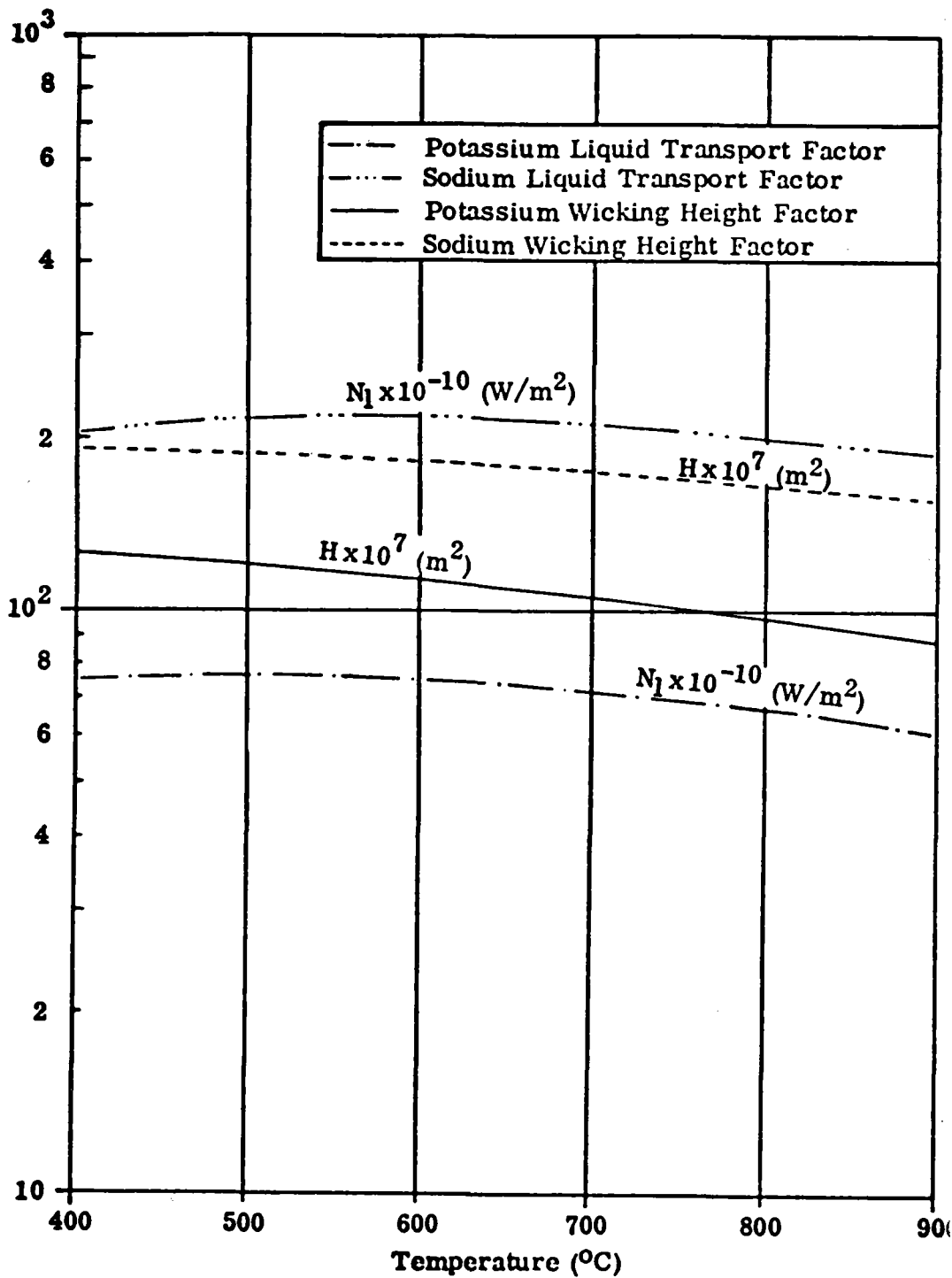


FIGURE 3.9
 LIQUID TRANSPORT FACTOR AND WICKING HEIGHT FACTOR
 OF SODIUM AND POTASSIUM

Wicking Height Factor H defines the wicking capability of a fluid under the influence of gravity. It is directly proportional to the static wicking height of the fluid in a specified wick.

Of the two fluids under consideration, potassium has a higher vapor transport limit than sodium over the entire temperature range. This advantage is offset, however, by the poorer liquid properties of potassium. Since initial calculations showed that it will be difficult to design a wick for a potassium heat pipe (for the requirements of the solar receiver), sodium was selected as the first choice working fluid. But, since the vapor transport limit of sodium may preclude operation of all heat pipes at their optimum temperature, potassium is retained as a backup working fluid.

In the remainder of this section, performance and limits of liquid metal heat pipes are evaluated in three areas:

- (1) Axial heat transport capability
- (2) Evaporator fluxes
- (3) Pressure containment

3.2.1 Axial Transport Capability

Heat pipes transport thermal energy through the circulation of a two-phase working fluid. Capillary pumping provides the driving force for the flow of vapor and liquid. The upper limit of the heat transport capability is reached when the available capillary pumping is balanced by the hydrodynamic losses due to dynamic effects and friction. This axial transport limit is the topic of the present subsection.

In liquid metal heat pipes, the losses associated with the vapor flow are frequently dominating. The hydrodynamics of the vapor flow is therefore examined first and independently of the liquid flow. This approach assumes that, given sufficient cross-sectional area, a wick can always be designed to meet the transport requirements for the liquid. Wick designs will be considered later.

The hydrodynamics of the vapor flow in liquid metal heat pipes has been

analyzed by several investigators (see bibliography at end of Section 2 of Reference 3). The vapor flowing from the evaporator to the condenser experiences a pressure drop because of two effects: frictional drag forces and acceleration in the evaporator region. The latter effect can actually lead to sonic flow conditions at the exit of the evaporator. The mass transport associated with sonic vapor velocity (also referred to as choking) represents an upper limit for the axial heat transport capability of a heat pipe. The analyses in the past have considered one or the other of these effects; i. e., limits were determined for the cases of either predominantly viscous flow or for a regime where acceleration (inertial) effects are dominating (Ref. 4). Levy (Ref. 5) considered the combined effects of acceleration and drag, but his model does not permit a closed form analytical evaluation. Reference 1 presents a simplified analysis of the rather complicated vapor flow processes in a heat pipe. It yields consistent expressions for the pressure gradients in the vapor. In the limit of either purely inertial or purely viscous flow, the analysis gives the proper expressions reported in the literature.

This new model was employed in this study to calculate the maximum axial heat flux in a sodium pipe over the temperature range of interest. One result is shown in Figure 3.10. It gives the maximum achievable heat flux for different heat pipe diameters as a function of evaporator temperature. The upper curve in this figure represents the gas dynamic limit associated with sonic flow at the exit of the evaporator. It is the true upper limit of heat transport at each temperature regardless of the capillary pumping provided by the wick. The other curves show the effects of viscous drag for finite heat pipe diameters. Again, these are true upper limits and are independent of the wick design. It can be seen from these curves that viscous effects are negligible above about 480°C , as long as the heat pipe diameter is at least 5 cm. This result was one reason why this heat pipe diameter was chosen as a baseline design.

The effects of capillary pumping on the maximum axial heat flux are shown in Figure 3.11. In this set of curves, only inertial effects are considered; i. e., the results are applicable for heat pipe diameters exceeding approximately 5 cm. The upper curve is again the gas dynamic vapor limit which is identical to that of

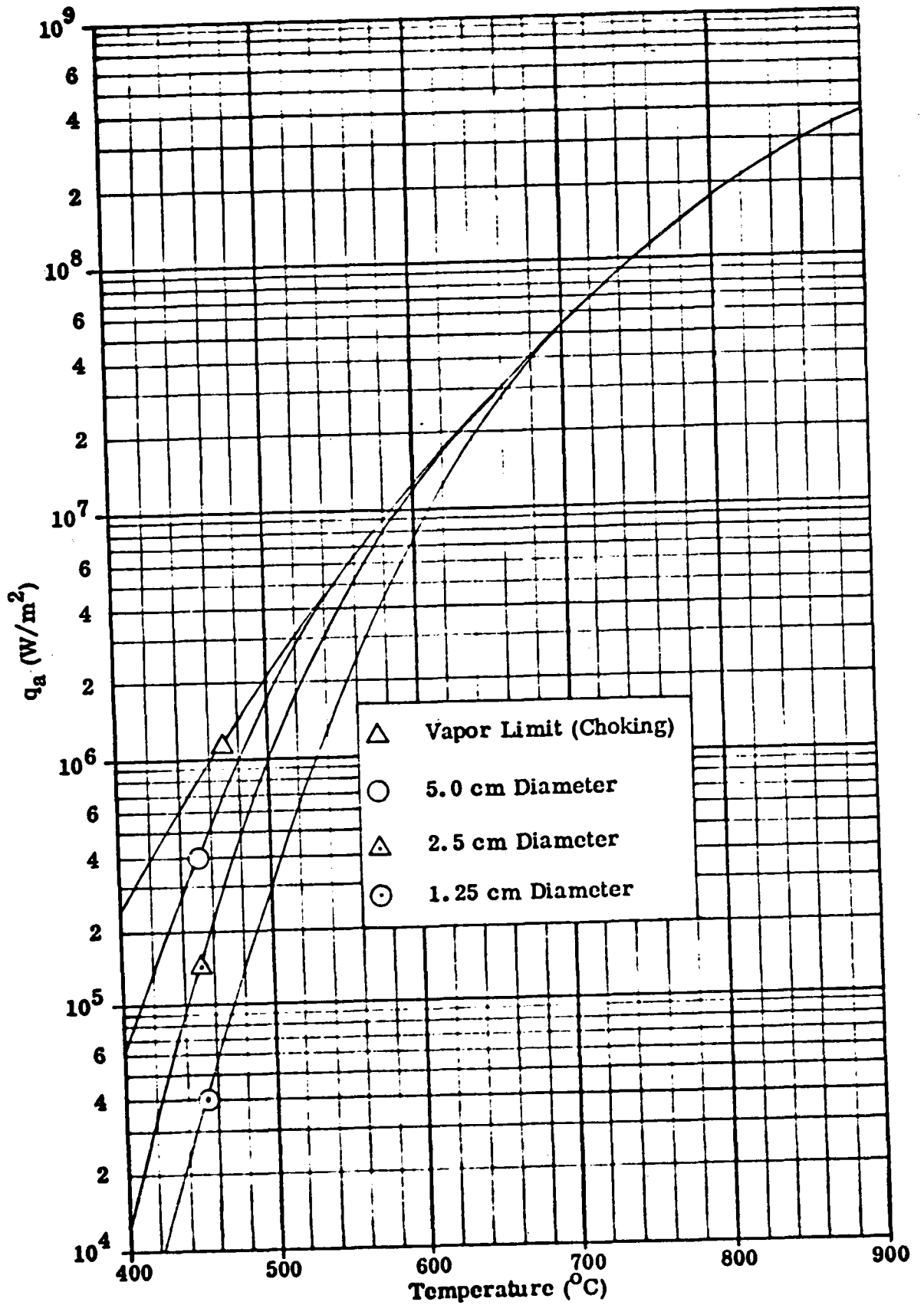


FIGURE 3.10
 LIMITING AXIAL FLUX (NOT LIMITED BY CAPILLARY PUMPING)
 WITH SODIUM FOR VARIOUS HEAT PIPE DIAMETERS

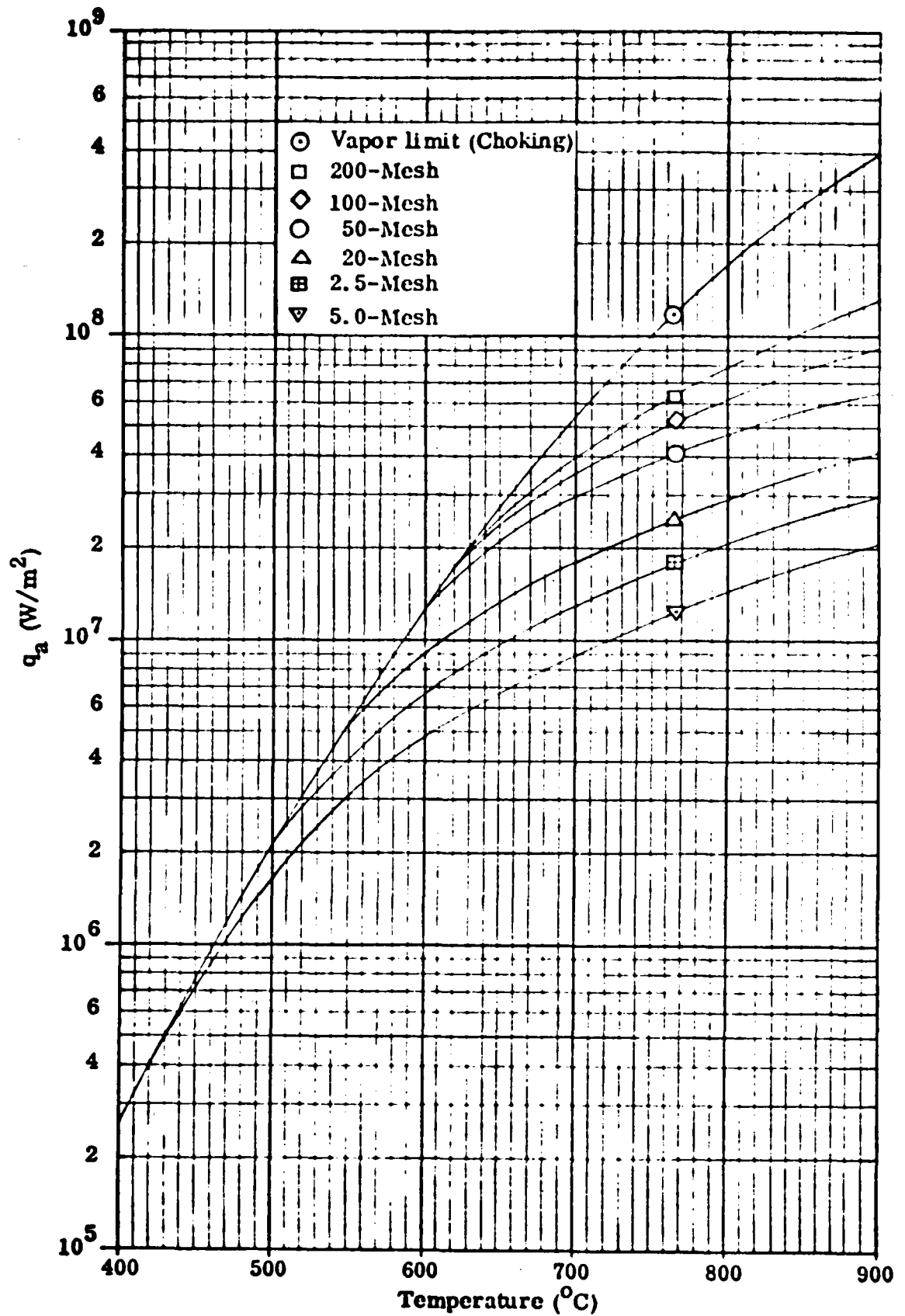


FIGURE 3.11

LIMITING AXIAL HEAT FLUX (VISCOUS LOSSES NEGLECTED)
WITH SODIUM FOR VARIOUS CAPILLARY PUMPING PRESSURES

Figure 3.10. The pressure gradient associated with this limiting heat flux is approximately one-half of the absolute vapor pressure. The other curves show the reduction of the ultimate heat flux due to the pumping limitations of various mesh size wicks and open arteries. For the baseline heat flux of 10^7 watts/m², a 50-mesh wick appears to be sufficient to provide the necessary capillary pumping at all temperatures where the vapor flow is not limited by gas dynamic choking (above approximately 590°C). The actual wick must, of course, provide somewhat more pumping, since pressure gradients in the liquid constitute additional requirements.

According to Figures 3.10 and 3.11, the design heat flux of 10^7 watts/m² cannot be achieved below 590°C. Some of the heat pipes in the solar receiver will be exposed to gas temperatures as low as 448°C. If the same heat pipes receive solar input corresponding to an axial flux of 10^7 watts/m², their heat transfer capability is clearly exceeded. Deverall, et al., (Ref. 6) calculated that the temperature gradient along the evaporator of a choked sodium heat pipe at 590°C is about 50°C. If we allow 55°C between the gas of the Brayton cycle and the vapor of the heat pipe, and assume no pressure recovery in the condenser, then the evaporator temperature of the coolest heat pipe will be $448 + 55 + 50 = 553$ °C. According to Figure 3.11, which gives the limiting flux versus evaporator temperature, the heat pipe can transport about 6×10^6 watts/m² under this condition. In reality, the temperature gradient along the evaporator may be larger than the calculated value of 50°C because supersonic flow with ensuing larger pressure and temperature gradients have been observed in liquid metal heat pipes. But a better engineering solution will be to increase the heat transfer resistance to the gas of the lower temperature heat pipes in order to achieve vapor temperatures which do not require choked flow at the design heat load.

The purpose of the wick in the heat pipe is to: (1) generate the capillary pumping necessary to overcome flow losses in liquid and vapor, (2) provide a return path for the condensate from the condenser to the evaporator, and (3) distribute the liquid over the entire evaporator surface. The capillary pumping may be augmented with gravity through proper orientation of the heat pipe. Figure 3.12 shows the height equivalent to capillary pumping for Na and K and for three representative tempera-

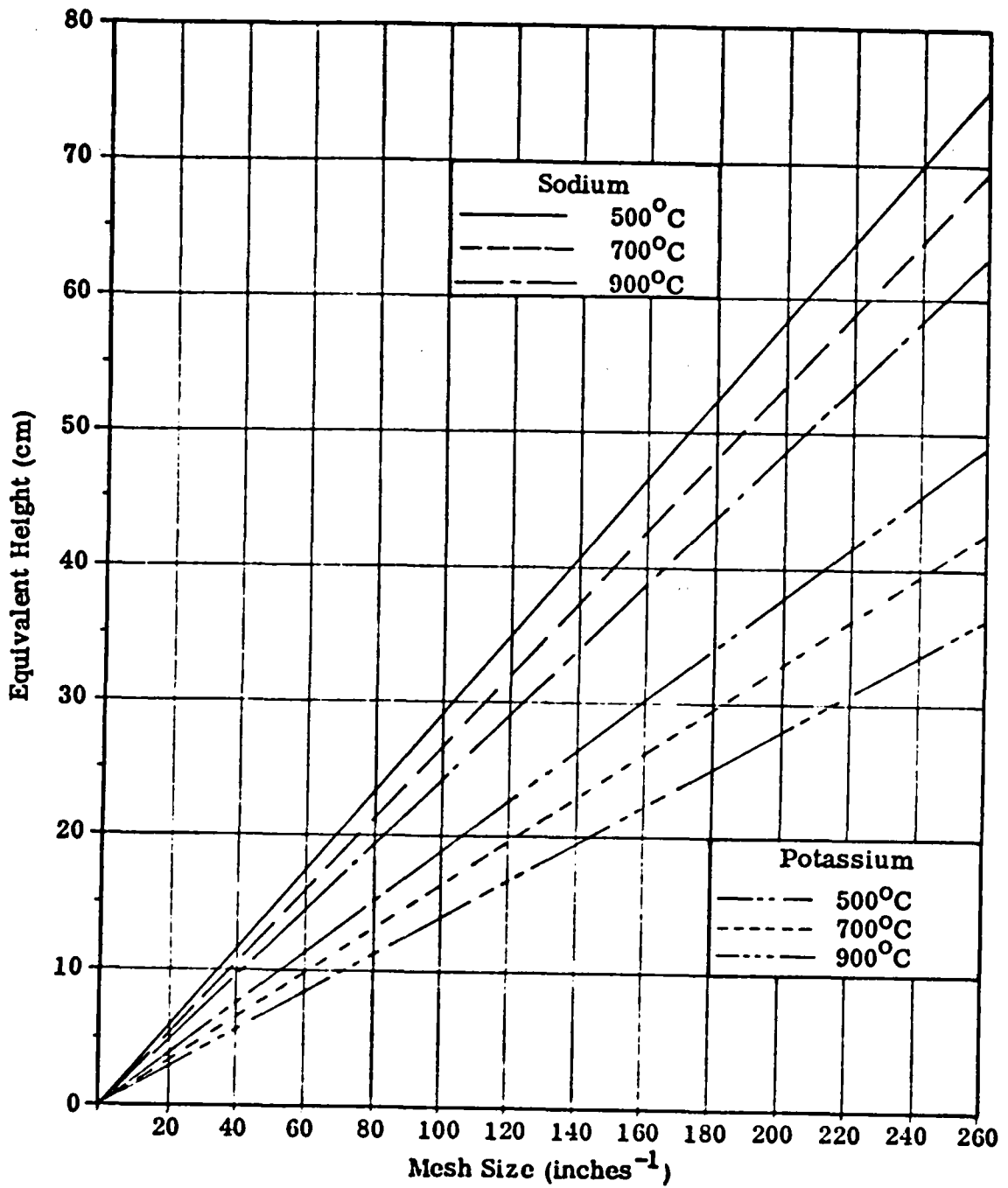


FIGURE 3.12
HEIGHT EQUIVALENTS TO CAPILLARY PUMPING

tures. If flow losses were distributed uniformly over the length of the heat pipe, then tilting the pipe favorably would be equivalent to capillary pumping of a certain mesh size wick as shown in the figure. However, when inertial flow losses in the vapor are dominating (as is the case in liquid metal heat pipes), most of the losses occur in the evaporator. Thus, the equivalent height applies almost entirely to the evaporator and very large overall tilts may result. So, while it appears impractical to utilize gravity alone as a pumping mechanism, it certainly can be employed as a means of augmentation.

In addition to pumping, the wick also provides a shielded return path for the liquid. If the latter would flow as a free puddle in a gravity-assisted heat pipe, shear stresses exerted by the countercurrent vapor flow would impede the liquid flow. Another effect of shear is entrainment of liquid droplets by the vapor. The onset of entrainment can be expressed in terms of a Weber number (Ref. 7):

$$\frac{\rho_v v^2 \sigma}{l} = 1 \quad (1)$$

The characteristic length l is related to the wavelength of perturbation of the liquid surface. As a first approximation, it may be set equal to the wire spacing of the wick. Recognizing that

$$q = \rho_v v \lambda \quad (2)$$

the entrainment limit may be expressed as:

$$q_{ent} = \lambda (\rho_v \sigma M)^{\frac{1}{2}} \quad (3)$$

Where M is the mesh size of the wick (dimension m^{-1}). The entrainment limit for sodium and potassium is shown in Figures 3.13 and 3.14 for four typical screen meshes. Because of its higher vapor density, potassium has a higher limit at lower temperatures than sodium. But, at the high temperature end of the range, sodium is superior because of its higher latent heat. Also shown in Figures 3.13 and 3.14

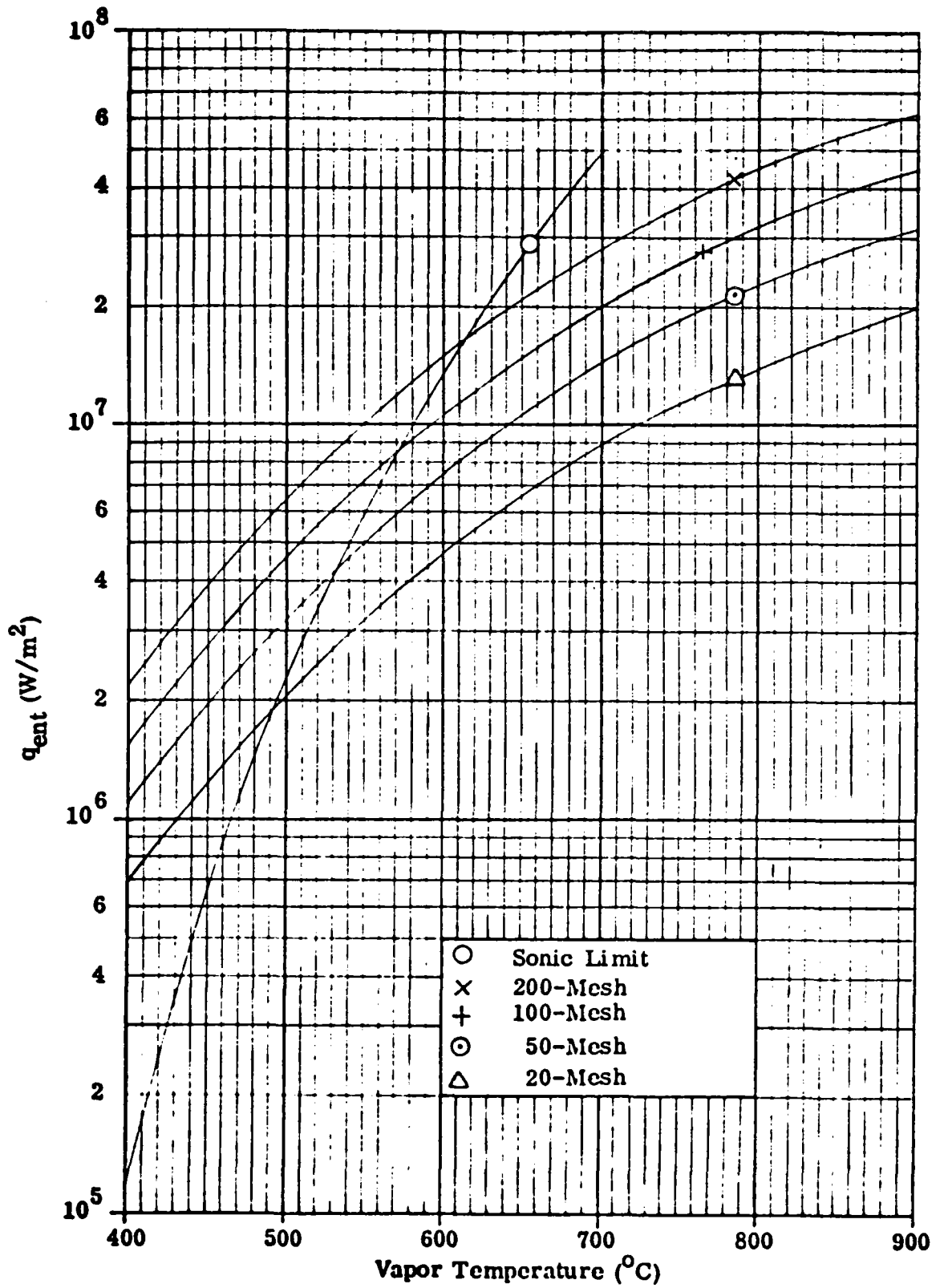


FIGURE 3.13
ENTRAINMENT LIMIT FOR SODIUM

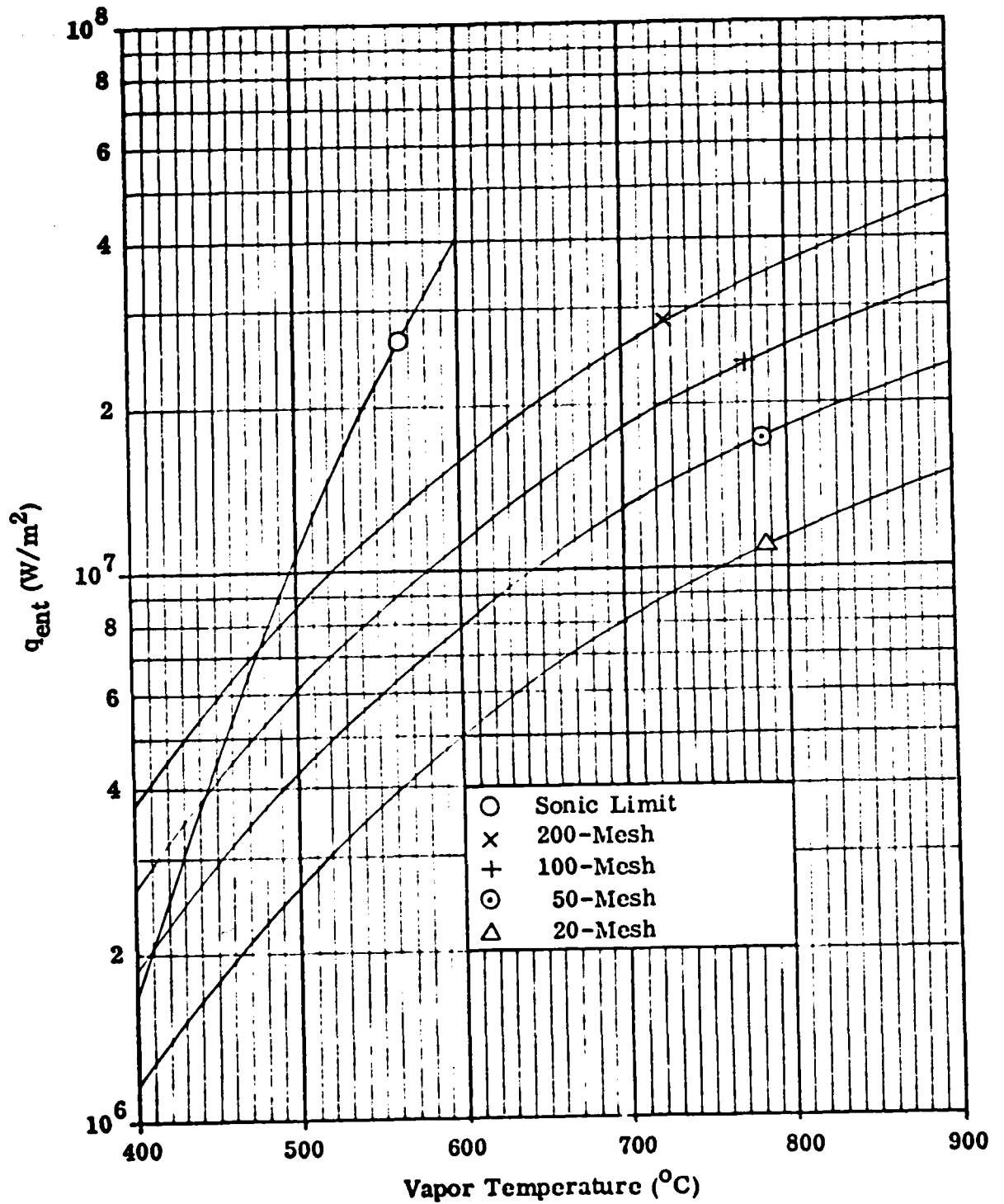


FIGURE 3.14
ENTRAINMENT LIMIT FOR POTASSIUM

are the sonic limits. In order not to be limited by entrainment at the design heat flux of 1×10^7 watts/m², the mesh size of the wick must be at least 100 for sodium and more than 200 for potassium.

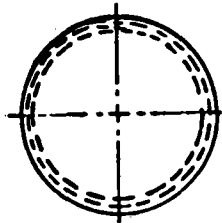
The third function of the wick is to distribute the liquid over the entire evaporator. Some wicks, such as the historical multilayer screen wick, cover the entire evaporator and perform this function automatically. Other wicks are located remote from the wall and then a "secondary" or "circumferential" wick is required in the evaporator.

Several candidate wick designs which were considered for this application are shown in Figure 3.15. These wicks can be classified as either homogeneous or arterial. A homogeneous wick is one in which the flow passages for the liquid have the same pore size as the pores responsible for capillary pumping. In an arterial wick, the flow channels are large and relatively unobstructed while capillary pumping is obtained with a fine wick surrounding the liquid passages. The homogeneous wick is simple and very reliable, but its performance capability is very limited. Arterial wicks have nearly unlimited liquid transport capability; but they are more complicated, less reliable, and need to be primed.

The wicks can also be classified as to whether or not they are communicating. In communicating wicks, the static pressure in the liquid is referenced to the bottom of the heat pipe. It can be shown (Ref. 8) that communication is equivalent to operating the heat pipe with an adverse tilt equal to one pipe diameter.

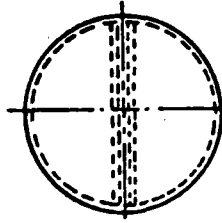
Referring to Figure 3.15, the wicks a, b, and c are variations of the simple homogeneous wick. The designs d, e, and f have the same basic configuration but they are formed of alternating layers of fine and coarse screen. If only the fine screen is exposed to the vapor, these designs act as arterial wicks with the coarse screen providing the main flow channels. Axial grooves formed as an integral part of the heat pipe wall can be a homogeneous wick when open (g), or they can be of the arterial type when covered with screen (h).

The wick structures i, j, and k are of the arterial type. Capillary pumping is achieved by the fine screen while the liquid flows unobstructedly in the annulus (i),



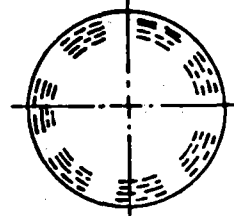
a

Notes 1, 3, & 6



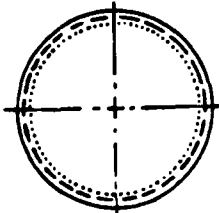
b

Notes 1, 3, & 5



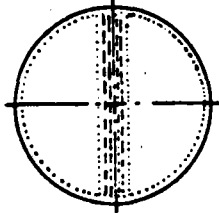
c

Notes 1, 4, & 6



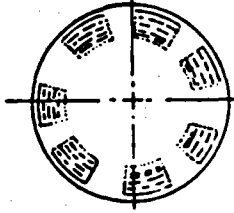
d

Notes 2, 3, & 6



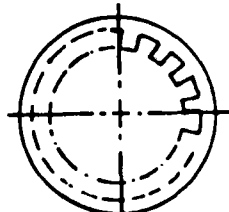
e

Notes 2, 3, & 5



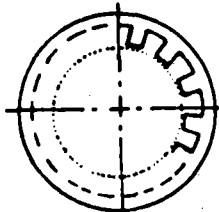
f

Notes 2, 4, & 6



g

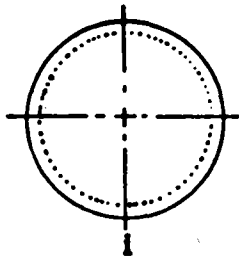
Notes 1, 4, & 6



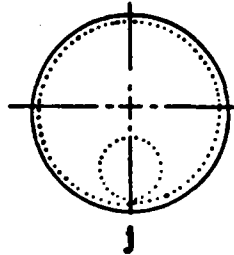
h

Notes 2, 3, & 6

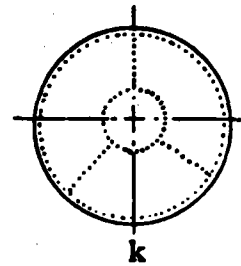
FIGURE 3.15
WICK GEOMETRIES



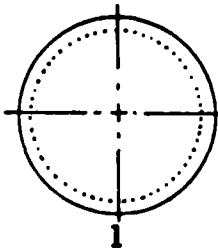
Notes 2, 3, & 6



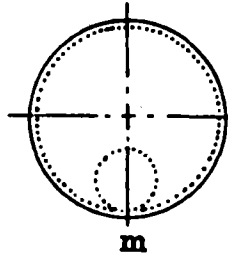
Notes 2 & 5



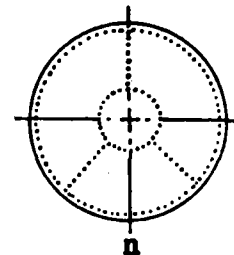
Notes 2 & 5



Notes 1, 3, & 6



Notes 1, 7, & 5



Notes 1, 7, & 5

NOTES

1. Homogeneous
2. Arterial
3. Communicating
4. Noncommunicating
5. Circumferential wick required
6. Circumferential wick not required
7. Communication not applicable

FIGURE 3.15 (Continued)

WICK GEOMETRIES

the pedestal artery (j), or the centrally located artery (k). The final three wick designs l, m, and n are identical in appearance to i, j, and k except that the arteries are not sealed. Thus, they are homogeneous wicks with the artery or the annulus themselves providing the pumping.

Most of the homogeneous wick designs will not meet the present requirements of 10^7 watts/m² in a heat pipe of 5 cm in diameter. The simple homogeneous screen wicks a, b, and c require an excessive cross-sectional area. This can be shown by the following analysis. From the basic equation for the pressure gradient in a wick (Ref. 8):

$$\frac{dp_1}{dx} = - \frac{\mu_1 \dot{m}_1}{K A_w \rho_1} \quad (4)$$

the required wick area can be calculated by integration.

$$A_w = - \frac{\pi \mu (L_e + L_c) q D_v^2}{8 K \lambda \rho_1 \Delta p_1} \quad (5)$$

In Equation 5, Δp_1 is the pressure difference available for overcoming the viscous flow losses in the wick. In order to estimate the minimum required wick area, we neglect the pressure losses in the vapor. Δp_1 then becomes:

$$\Delta p_1 = \frac{2 \sigma}{r_p} \quad \text{for noncommunicating wicks} \quad (6)$$

$$\Delta p_1 = \frac{2 \sigma}{r_p} - \rho_1 q D_v \quad \text{for communicating wicks} \quad (7)$$

In typical homogeneous wicks such as screen and fibers, the permeability K is related to the pore radius r_p through:

$$K = b r_p^2 \quad (8)$$

The dimensionless constant b has a value of about 1.1×10^{-2} . Combining Equations

5, 6, or 7 and 8 and normalizing with respect to the heat pipe area, yields the following expressions for the minimum required wick area:

$$\frac{A_w}{A_v} = \frac{(L_e + L_c) q}{4 N_1 b r_p} \quad \text{for noncommunicating wicks} \quad (9)$$

and

$$\frac{A_w}{A_v} = \frac{(L_e + L_c) q}{4 N_1 b r_p} \left(1 - \frac{D_v r_p}{2H} \right)^{-1} \quad \text{for communicating wicks} \quad (10)$$

Equations 9 and 10 are plotted in Figure 3.16 for the design heat flux of 10^7 watts/m², a heat pipe diameter of 5 cm, and for sodium at 680°C (approximately the center of the temperature range of interest). It is obvious from this figure that communicating homogeneous wicks (a, b) require too much wick material ($A_w/A_v > 2$). Homogeneous but noncommunicating wicks (c, g, m) could utilize very coarse meshes and then the amount of wick would be reasonable (e.g., $A_w/A_v < 0.5$). But coarse wicks do not provide sufficient capillary pumping to overcome the vapor losses at lower temperatures (minimum of 50 mesh required). In the case of the open grooves (g), entrainment would pose an additional problem.

All arterial wicks meet the requirements, at least in principle. The selection among them was based on fabricability and priming considerations. Axial grooves (h) are difficult to fabricate in large diameter stainless steel or Inconel tubes. Arterial wicks, in which the artery consists of an annulus near the wall (i) or of a coarse, porous screen matrix (d, e) are difficult to prime. Since the liquid must initially fill the entire coarse wick or annulus in order to establish a primed artery, the large diameter of the heat pipe poses severe restrictions on the selection of the effective artery permeability. Priming problems also exist for the centrally located artery (h).

The best chance of reliable priming exists for an artery located near the bottom of the heat pipe (j). (A variation of this design, the "tent artery", actually proved to be the most suitable wick during the development program.) The associated circum-

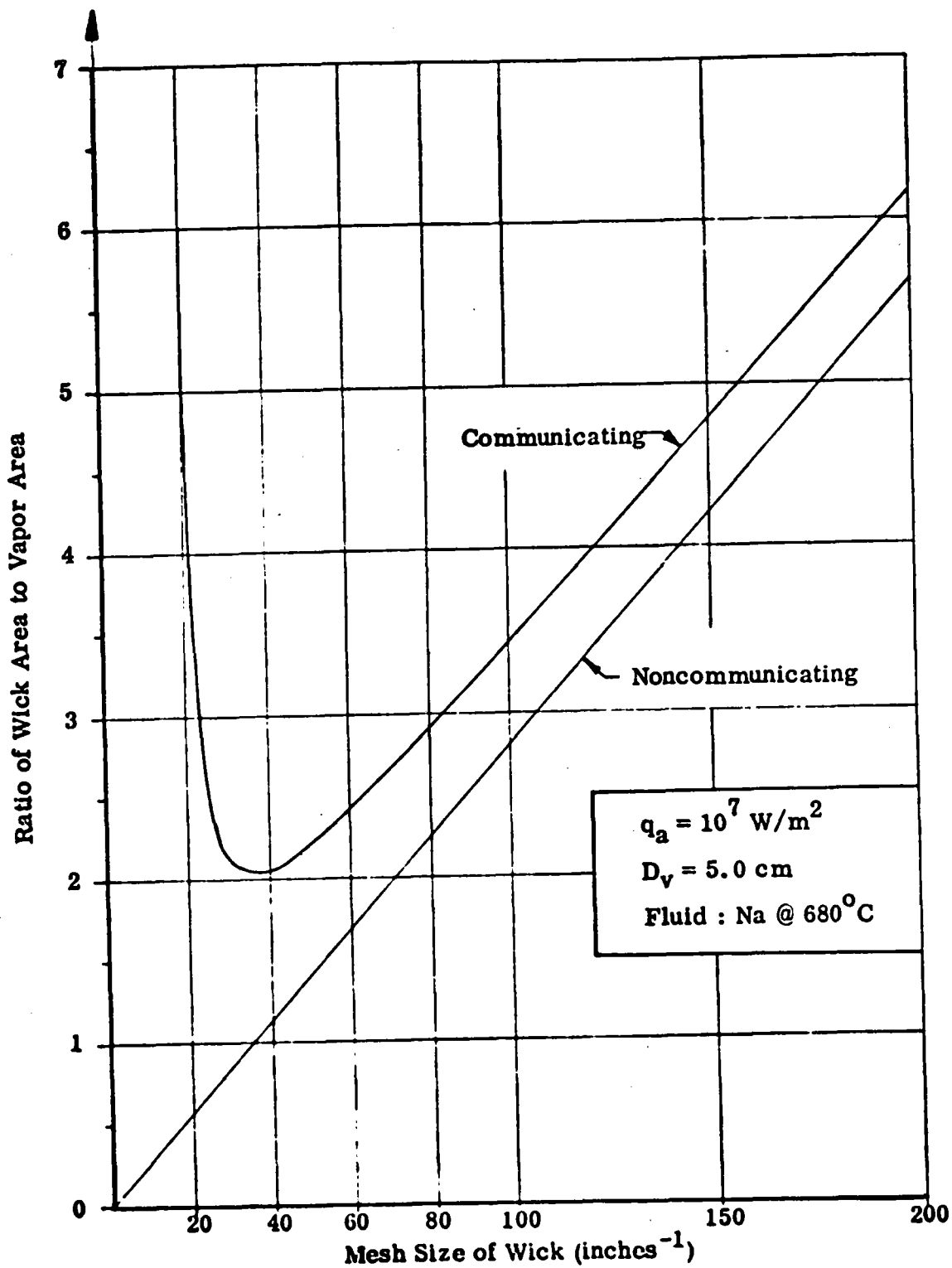


FIGURE 3.16
 AREA REQUIREMENT FOR HOMOGENEOUS WICK

ferential wick could be a thin, porous wick such as a single or multilayer of screen. Another type of circumferential wick consists of fine screw threads cut into the wall. Calculations were performed and have shown that such grooves are marginal for a 5 cm diameter heat pipe and a radial flux of 10^6 W/m^2 .

The preceding discussion does not give credit to the additional pumping resulting from properly orienting the heat pipe with respect to gravity. As shown in Figure 3.12, a tilt of 15 cm (about 5° in a 200 cm long pipe) provides the equivalent pumping of a 60 mesh wick in a sodium heat pipe. For a gravity-assisted heat pipe, the restrictions of Figure 3.16 for wick selection in a homogeneous wick heat pipe therefore do not apply. This makes it possible to use, for example, a simple open artery (m) whenever the heat pipe can be suitably oriented.

In summary, arterial wicks such as the one shown in Figure 3.15 (j) will provide sufficient transport capability over the whole temperature range except where gas dynamic choking occurs. Very coarse homogeneous wicks (e. g., open arteries) are acceptable at higher temperatures. If the heat pipes are tilted, the open artery homogeneous wick will function over the entire temperature range.

Detailed performance calculations were made for several wick designs. The computations involved a numerical solution of the following pressure balance equation at different evaporator temperatures:

$$\frac{2 \sigma}{r_p} = \rho_l g h + \Delta p_l + \Delta p_v \quad (11)$$

The left side of Equation 11 represents the capillary pumping pressure developed by the wick. The first term on the right accounts for gravity. If the heat pipe is horizontal, h is equal to the diameter of the artery. Δp_l is the pressure loss in the liquid and is given by Equation 5 (after solving for Δp_l). Δp_v is the pressure loss in the vapor and includes viscous and inertial effects. No recovery of the inertial pressure drop in the condenser was assumed. The model which was described earlier and is detailed in Reference 1 was used to calculate Δp_v . After inserting the proper terms for Δp_l and Δp_v (which are both functions of q_a), Equation 11 was solved numerically for q_a . The results for two wick designs are shown in Figure 3.17 for a

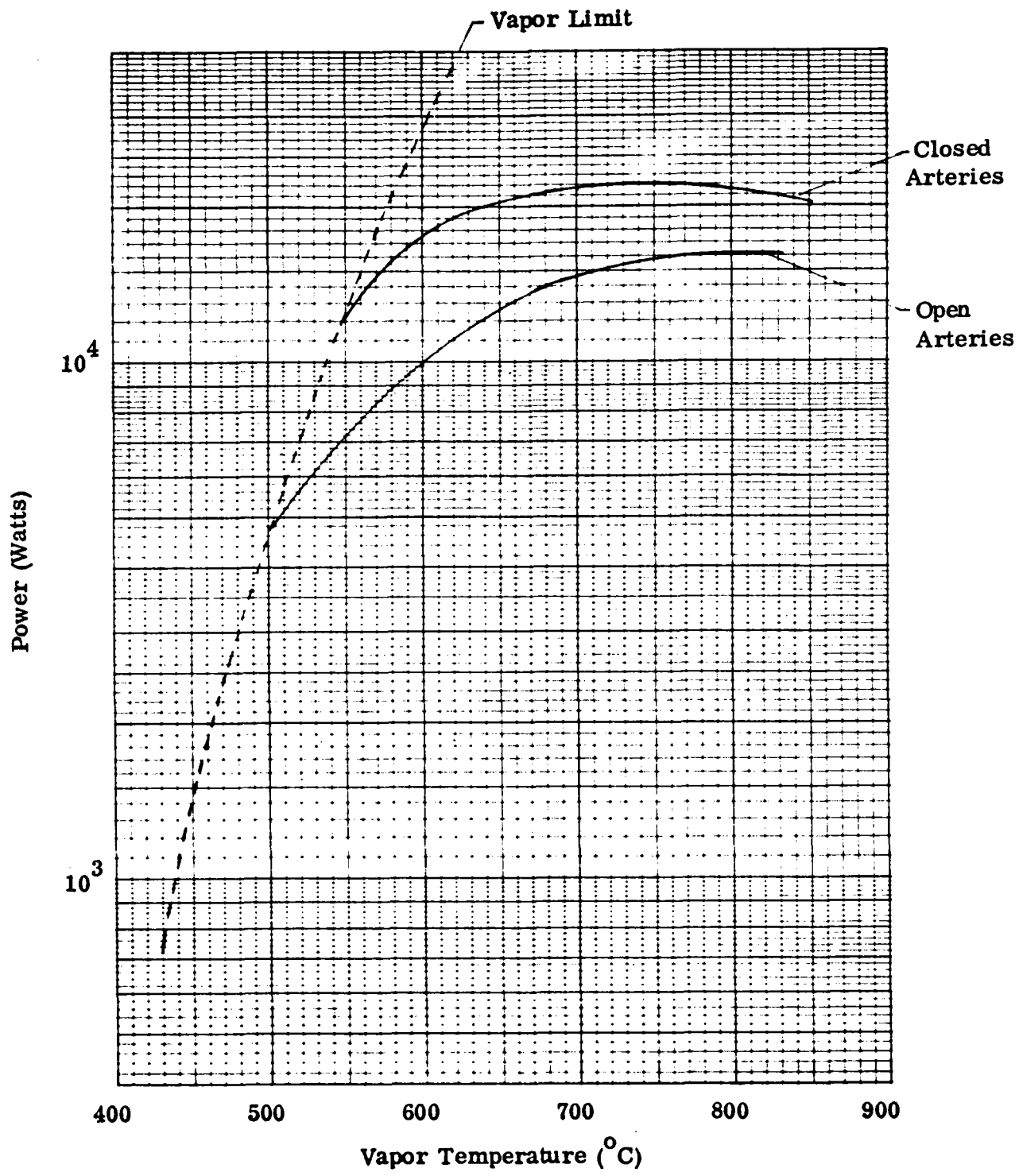


FIGURE 3.17
 THEORETICAL PERFORMANCE OF TWO WICK DESIGNS
 FOR SODIUM

sodium heat pipe.

The performance of the closed artery is insensitive to the orientation of the heat pipe (shown for horizontal orientation). This insensitivity can be predicted from Figure 3.12. Since the artery is fabricated from 100 mesh screen, its pumping capability is equivalent to a head of 25 cm and small tilts will therefore have little influence on the performance. This is not the case for the open artery wick also shown in Figure 3.17. This design requires a tilt of the heat pipe (about degrees) in order to meet the design goal of 10 MW/m^2 . Neither wick meets the goal below 580°C because of the fundamental vapor limit.

The same two wick designs were also evaluated for potassium as the working fluid. The results are shown in Figure 3.18. At the low end of the temperature range, potassium out-performs sodium because of its higher vapor limit. At all other temperatures sodium is superior because of its higher Liquid Transport and Wicking Height Factors. But it should be noted that the two wick designs were optimized for sodium and are not necessarily optimized for potassium.

3.2.2 Radial Heat Flux Limits

The preceding discussion dealt only with the axial heat transport capability of the heat pipe. The performance is also limited, however, by the radial flux; i. e., the input and output power density at evaporator and condenser. Since the condenser is much longer than the evaporator, its flux is always lower than that at the evaporator and thus poses no problem. The maximum permissible evaporator flux is limited by two effects — nucleate boiling in the wick and thermal stresses in the wall material. In the following, each limitation shall be discussed separately.

An arterial wick requires a "secondary" or "circumferential" wick to distribute the liquid from the artery over the entire evaporator. In the selected design, two layers of wire mesh screen (one each of 100 and 325 mesh) are used as the circumferential wick. Regardless of whether capillary forces in a closed artery or gravity in an open artery is used as the primary pumping mechanism, the liquid is always distributed in the secondary wick by capillary forces. Proper heat pipe design must account for the hydrodynamics within the circumferential wick.

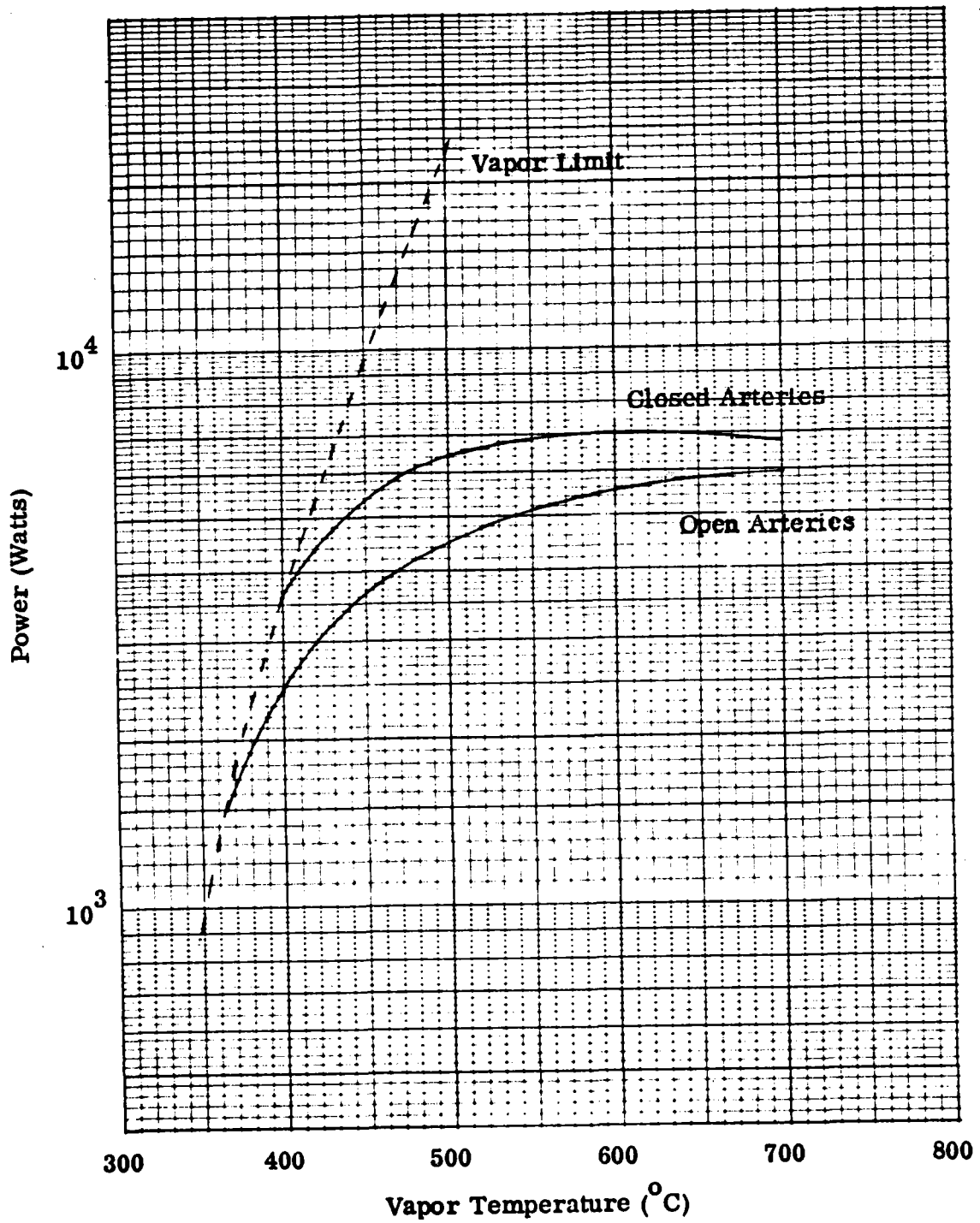


FIGURE 3.18
 THEORETICAL PERFORMANCE OF TWO WICK DESIGNS
 FOR POTASSIUM

During normal operation, the secondary wick is fully saturated and heat is conducted from the walls through the liquid/wick matrix to the vapor-liquid interface. Evaporation occurs at that interface rather than at the wall or within the liquid. However, if the radial heat flux exceeds a certain critical value, nucleation will occur within the wick. Normally, nucleation is not considered a failure mode in two phase heat transfer. Instead, it enhances the heat transfer (film) coefficient. In a wick, however, the onset of nucleate boiling will interrupt the circumferential flow of the liquid. Consequently, local dryout and subsequent evaporator failure will occur.

The onset of nucleate boiling in a wick is difficult to predict. Reference 9 gives a model which correlates the maximum flux with the pore size of the wick and its thickness. The critical ΔT which the wick can sustain is given by:

$$\Delta T_{\text{crit}} = \frac{T_{\text{sat}}}{\lambda \rho_v} \left(\frac{2 \sigma}{r_n} - (\Delta p_i) \right) \quad (12)$$

In this equation, r_n is the critical radius of nucleation cavities and Δp_i is the capillary stress on the liquid due to flow or gravity. The limiting flux which can be conducted through the wick is related to ΔT_{crit} through:

$$q_{\text{max}} = \frac{K}{t} \Delta T_{\text{crit}} \quad (13)$$

where K and t are, respectively, the thermal conductivity and thickness of the wick-liquid matrix. Combining the last two equations yields:

$$q_{\text{max}} = \frac{K T_{\text{sat}}}{t \lambda \rho_v} \left(\frac{2 \sigma}{r_n} - (\Delta p_i) \right) \quad (14)$$

The critical radius of nucleation cavities is generally not known, but an upper bound is certainly the pore size of the wick. Thus, we would expect the maximum permissible heat flux to be inversely proportional to the pore size of the secondary wick (Δp_i is usually small compared to $2 \sigma / r_n$). The other important qualitative observa-

tion from Equation 14 is that q_{\max} is inversely proportional to the vapor density ρ_v . Since ρ_v increases exponentially with temperature, the maximum flux will decrease with temperature. Thus, heat flux limits due to nucleate boiling are expected to occur mostly at the higher end of the temperature range.

The theoretical heat flux limit defined by this model is shown in Figure 3.19 for the selected circumferential wick. The graphs assume that the critical radius of nucleation cavities is either that of the 100 or the 325 mesh screen. In addition, the limit associated with a nucleation radius equal to typical imperfections in the heat pipe wall ($\sim 10^{-4}$ inches) is also plotted. The actual limits found during the test program fall between these curves and generally follow the predicted temperature dependency.

A second limit on the radial heat flux is imposed by thermal stresses within the heat pipe wall. These stresses result from the temperature gradient between the outside and the inside of the wall. At the evaporator, the outside of the wall is under compression and the inside under tension. A detailed evaluation of the permissible stresses and heat fluxes requires a complicated inelastic stress analysis which was beyond the scope of this program. Foster Wheeler conducted a simplified inelastic analysis; the results of which are shown in Table 3.2. This analysis neglected internal and external pressure stresses and axial tensile stresses resulting from the axial constraints of the heat pipes. Note that the allowable stresses in Table 3.2 are much higher than those given in the forthcoming Table 3.3. The reason for this apparent inconsistency is that thermal stresses due to temperature gradients are subject to relaxation while pressure induced stresses are not. The allowable heat fluxes calculated from thermal stress considerations are of about the same magnitude as those imposed by the wick.

3.2.3 Heat Pipe Structural Requirements

A structural analysis was conducted to determine heat pipe wall thickness requirements for thermal diffuser heat pipes operating in an environment consistent with the design conditions. Only pressure stresses are considered in this analysis. When applicable, buckling criteria were also considered. External pressure

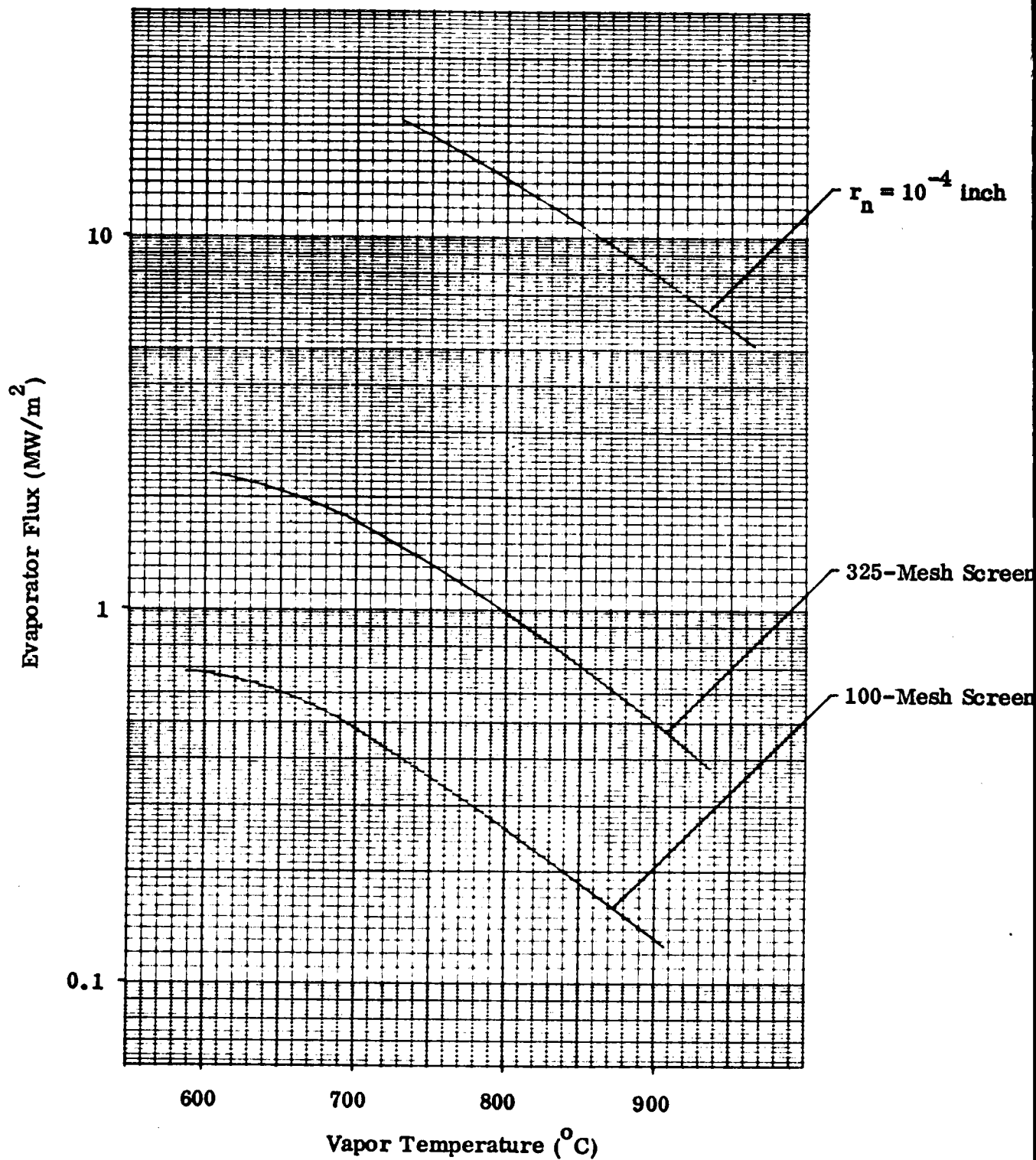


FIGURE 3.19
EVAPORATOR FLUX LIMITS

Sodium Temperature °C (°F)	Inside Tube Temperature °C (°F)	Outside Tube Temperature °C (°F)	Allowable Stress MPa (ksi)	Allowable Heat Flux MW/m ² (10 ³ Btu/h·ft ²)
482 (900)	538 (1000)	714 (1318)	345 (50)	1.47 (466.275)
543 (1010)	593 (1100)	739 (1363)	296 (43)	1.31 (416.710)
606 (1123)	649 (1200)	770 (1417)	241 (35)	1.11 (353.015)
667 (1232)	704 (1300)	813 (1494)	217 (31.5)	1.05 (332.150)
721 (1331)	760 (1400)	857 (1575)	201 (29.2)	1.02 (332.150)
777 (1431)	816 (1500)	909 (1669)	192 (27.8)	1.00 (316.235)
845 (1554)	871 (1600)	942 (1727)	143 (20.8)	0.81 (257.185)

Note: Pressure Stresses not considered

TABLE 3.2

ALLOWABLE HEAT FLUXES FOR AN AXISYMMETRICALLY HEATED
INCONEL 601 TUBE VERSUS INNER FLUID TEMPERATURE

Temperature °C (°F)	Allowable Stress	
	Inconel 601 MPa (Ksi)	Stainless Steel 304 MPa (Ksi)
649 (1200)	100.0 (14.5)	41.4 (6.0)
705 (1300)	35.9 (5.2)	25.5 (3.7)
760 (1400)	19.3 (2.8)	15.9 (2.3)
816 (1500)	12.6 (1.8)	9.7 (1.4)
871 (1600)	9.7 (1.4)	
927 (1700)	5.9 (.86)	
983 (1800)	3.3 (.48)	
1038 (1900)	2.3 (.34)	

TABLE 3.3
ALLOWABLE STRESSES FOR INCONEL 601 AND STAINLESS STEEL 304

at the evaporator end of the heat pipe is assumed to be one atmosphere. At the heat pipe's condenser, the external pressure is equal to the elevated pressure of the Brayton cycle (six atmospheres). Net pressure differentials across the heat pipe container were determined considering sodium and potassium as heat pipe working fluids. Inconel 601 and 304 stainless steel were evaluated as tentative heat pipe container materials. The assumed working stress for each material is equal to the allowable stress based on a creep rate of $1 \times 10^{-5}\%$ per hour. These stresses are presented in Table 3.3.

The required heat pipe wall thickness, normalized with respect to heat pipe radius, is shown as a function of temperature in Figure 3.20. The irregular shape of the curves is the result of different net loads at different temperatures as a consequence of the variation of the vapor pressure of the fluid. Also, the curves are a combination of the most severe requirements for either the evaporator or the condenser sections. The maximum vapor temperature of any heat pipe under design conditions is about 820°C (1508°F). Thus, Inconel 601 seems well suited for satisfying the requirements for the heat pipe wall material. For a heat pipe with an outside diameter of 6 cm, the required wall thickness is 1.7 mm. At locations within the receiver nearer the gas inlet, heat pipes (with similar dimensions) fabricated from less expensive 304 stainless steel appear to be satisfactory. From this figure, it is also evident that the utilization of potassium as the heat pipe working fluid results in reduced wall thickness requirements at all temperatures in the range of interest.

It should be emphasized that the structural analysis conducted thus far requires several refinements. First, the difference in the external pressure environments on the evaporator and condenser ends of the heat pipe suggests that different wall thicknesses may be utilized. Such a design could result in reductions in heat pipe weight and improvements in overall performance through reductions in heat pipe temperature gradients. Also, the analysis must be extended to account for the effects of stresses which may exist as a result of discontinuities in external pressures and at heat pipe supports. In addition, the end effects imposed by heat pipe end cap design must also be evaluated. Further refinement is also required

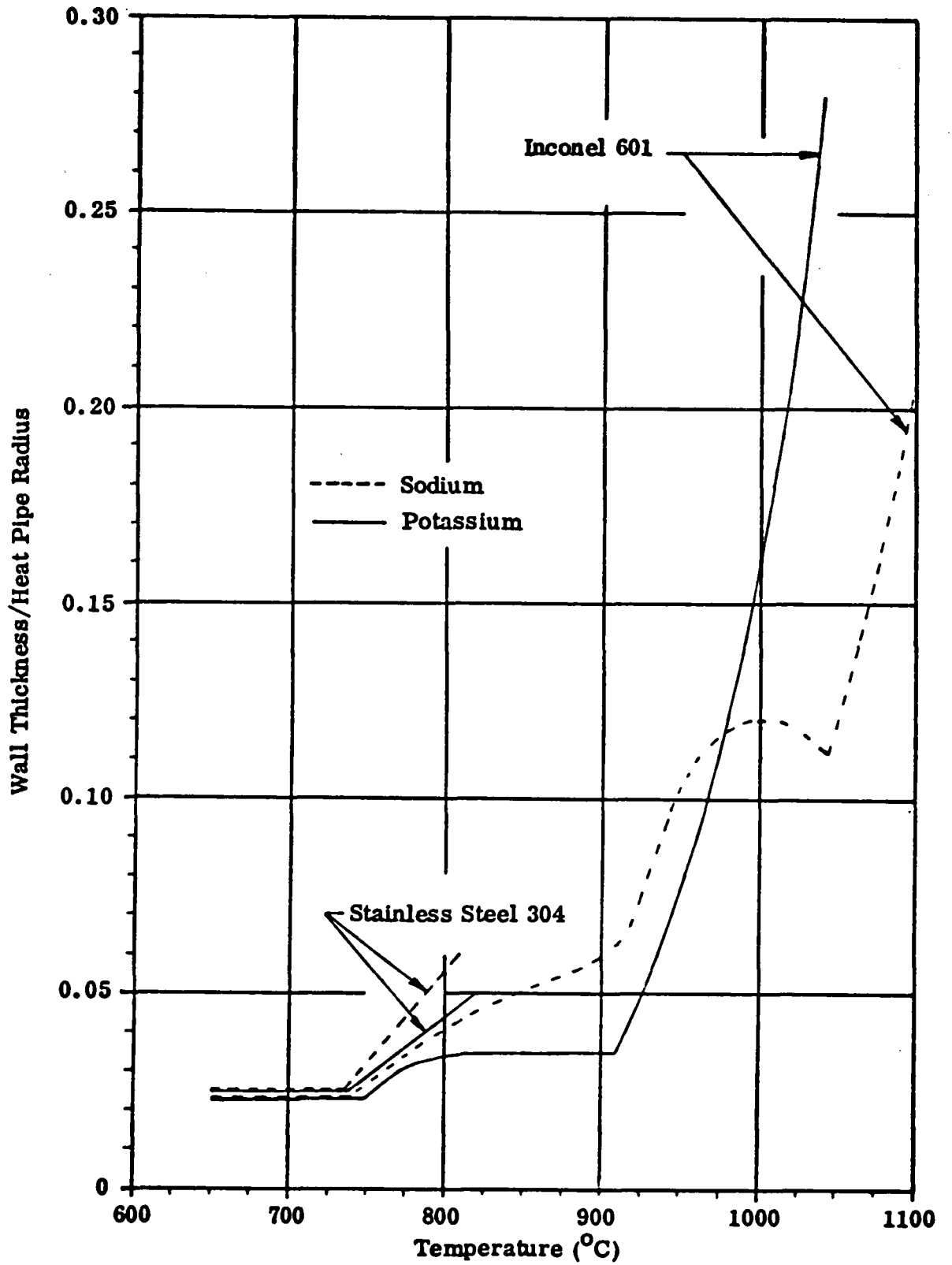


FIGURE 3.20
HEAT PIPE WALL THICKNESS REQUIREMENTS

to account for the combined effects of thermal and pressure stresses.

3.3 Experimental Heat Pipe Development

3.3.1 Objectives and Approach

During early phases of the program, the preliminary receiver design and the evaluation of heat pipe capability established the following baseline parameters for the thermal diffuser heat pipes:

- Diameter : 5 cm
- Length : 1 to 3 m
- Axial Heat Flux : 10 MW/m^2
- Radial (Evaporator Flux) : 1 MW/m^2
- Temperature Range : 450 to 900°C
- Working Fluid : Na or K
- Orientation : Horizontal to Vertical

These requirements were used as guidelines during early phases of heat pipe development. Eventually as the baseline receiver design evolved, these heat pipes operating requirements were modified as shown below:

- Diameter : 5 cm
- Length : 1.05 - 1.28 m
- Axial Heat Flux - Maximum : 6.1 MW/m^2
- Axial Heat Flux - Average : 2.5 MW/m^2
- Evaporator Flux - Maximum : 0.34 MW/m^2
- Evaporator Flux - Average : 0.04 MW/m^2
- Temperature Range : $445 - 870^\circ\text{C}$
- Working Fluid : Na or K
- Orientation : 5° Tilt (condenser above evaporator)

The distribution of the energy incident on the receiver does not experience large diurnal or seasonal variations. Certainly the magnitude of the incident energy changes,

but the incident fluxes will always be lowest at the extremities of the receiver surface and highest toward its center. In addition, the temperature distribution within the gas stream does not experience large fluctuations. It is then possible to define the heat pipe operating requirements as a function of heat pipe vapor temperature.

Figure 3.21 details the flux distribution as a function of height along one panel of the receiver. This particular panel receives the highest fluxes within the receiver. The fluxes shown were predicted by the solar flux model for the front surface of the panel and for the point on the heat pipe's circumference where the maximum fluxes occur. The variation of the air temperature and the heat pipe vapor temperature along the panel are also shown in the figure.

With the use of this figure, it is possible to define the axial and radial heat flux requirements for the heat pipes as a function of operating temperature. Curves for each flux are shown in Figure 3.22. Generally, the axial and radial flux requirements increase with temperature, except at the upper end of the operating temperature range where the required axial flux begins to decrease. These curves strictly apply for only one of the panels in the receiver. However, at the remaining panels the incident fluxes are somewhat lower; hence the curves shown represent the maximum flux requirements.

The requirements are well within the theoretical capability of liquid metal heat pipes. Sodium and potassium are both attractive heat pipe working fluids. Sodium is the more attractive of the two fluids because its liquid properties are more conducive to high heat transport. However, at the low end of the temperature range, the required axial heat flux is very near the sodium vapor limit as shown in Figure 3.22. Potassium is better suited for operation at low temperatures due to its higher vapor density and pressure. The use of potassium increases the vapor limit by nearly an order of magnitude.

The combination of the selected heat pipe diameter and the axial flux requirements converts to a total heat transfer rate of about 13 kW. This rate is high compared to most heat pipe testing in the past. It poses difficulties in applying the input to the evaporator and also in rejecting it at the condenser. The fairly large diameter of 5 cm also limits the choices of suitable wicks. The function of the wick is to trans-

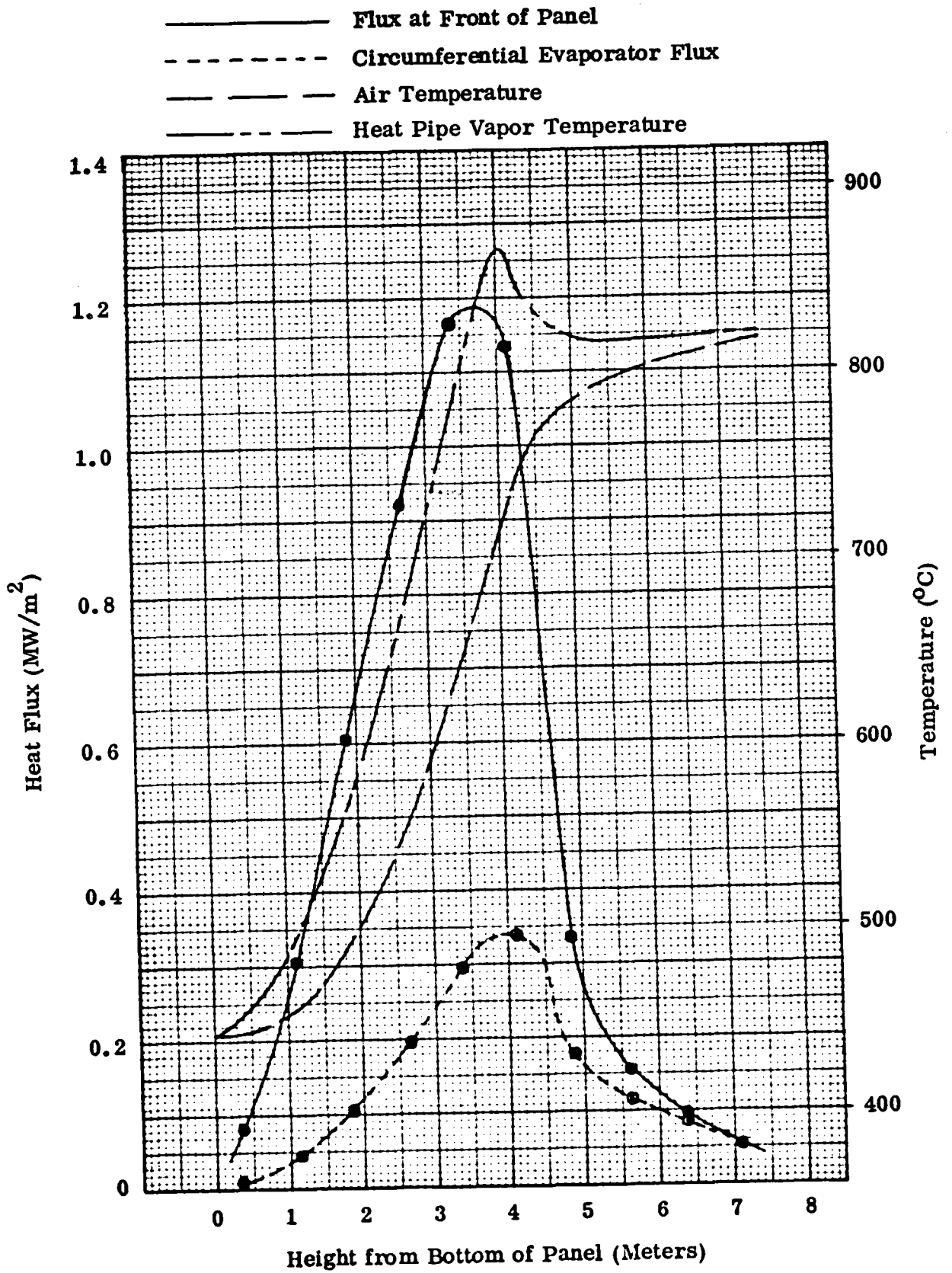


FIGURE 3.21
 FLUX DISTRIBUTION IN BASELINE RECEIVER

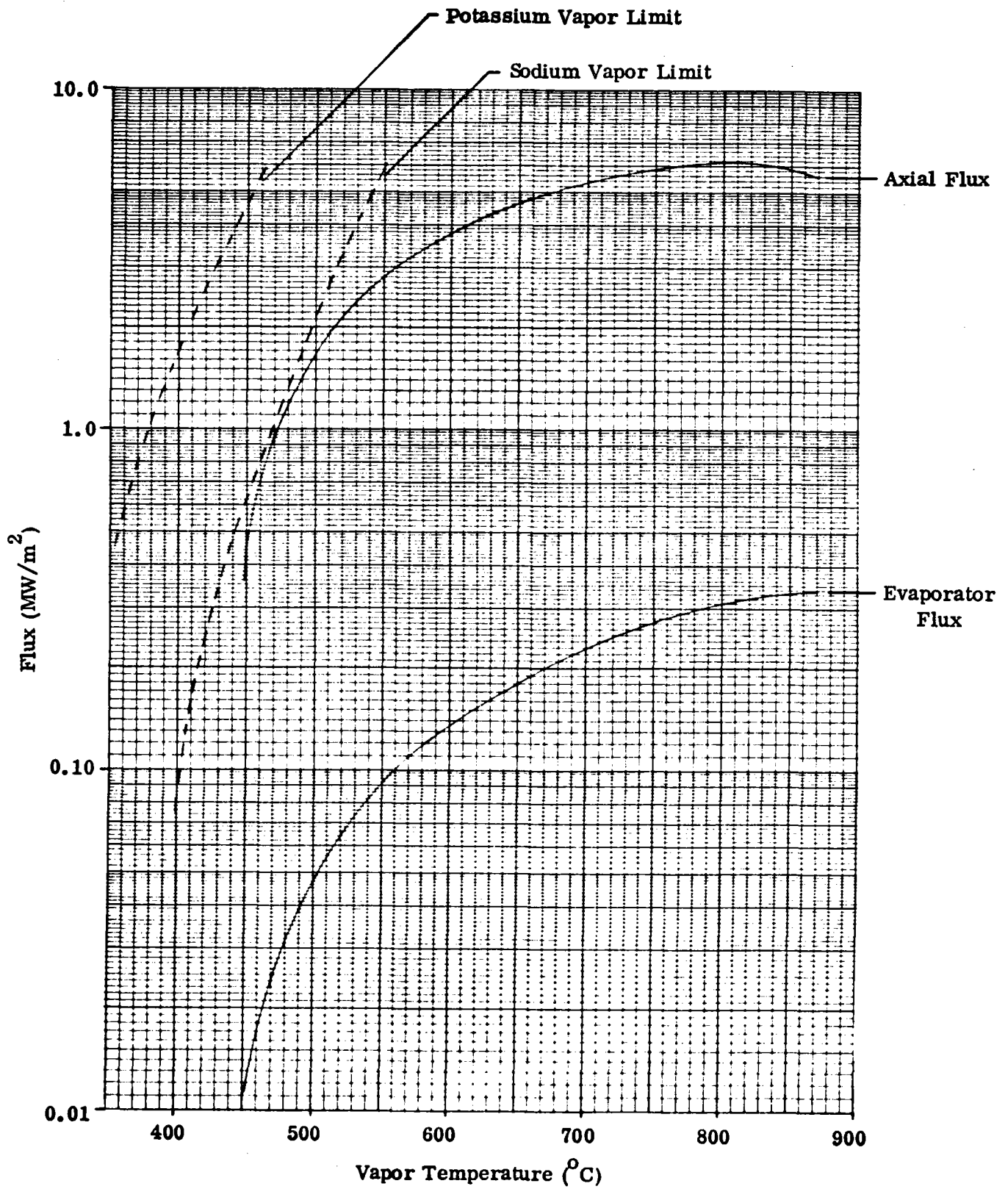


FIGURE 3.22
PEAK AXIAL AND RADIAL FLUX REQUIREMENTS

port the working fluid in the liquid state from the condenser to the evaporator and, equally important, to distribute the liquid over the evaporator surface. This latter requirement becomes difficult to meet with larger diameter heat pipes. Much development work has been done in the past concerning the axial fluid transport. Much less attention has been given to the circumferential distribution. It involves not only hydrodynamic considerations but also conductive and convective heat transfer.

The ultimate objective of the experimental portion of this program was to develop full-scale thermal diffuser heat pipes which are capable of meeting the projected requirements of the selected receiver design. To accomplish this objective, the experimental investigation began with smaller heat pipes (typically 2.5 cm in diameter). These smaller pipes were much easier and less expensive to fabricate. Also, their performance capabilities were compatible with the capabilities of the available test apparatus; hence the test results were used to validate theoretical performance models. Many wick designs were tested on a subscale basis. Once a suitable wick design was developed, the experimental effort was continued with full-scale heat pipes.

The experimental effort was directed toward the characterization of heat pipe performance under all foreseeable operating conditions. The bulk of the test program was concerned with establishing the steady-state performance capabilities of the subscale and full scale thermal diffuser heat pipes. This capability was defined in terms of the axial and radial heat flux limits as a function of heat pipe operating temperature. The influence of other parameters such as the heat pipe orientation and heat pipe working fluid was also investigated.

Another portion of the test program was devoted to establishing the transient operating characteristics of the heat pipe. Unlike the steady-state testing, transient tests were conducted only on the full-scale heat pipes. The objective of the transient tests was to establish allowable rates of heat addition for successful heat pipe start-up. These tests were conducted with sodium for several heat pipe orientations.

3.3.2 Heat Pipe Fabrication

Although there are considerable differences in the heat pipes developed during the program, all heat pipes were basically fabricated in the same manner and from

the same materials. The heat pipe envelope, including end caps and fill tube, were normally made from Inconel 601, although Inconel 600 was used for some of the earlier pipes. Wick structures were made from stainless steel wire screen for all heat pipes except one. In this one instance, the capillary structure was made from nickel screen.

The process implemented in heat pipe fabrication was basically the same for all pipes. Heat pipe components, i. e., wick structure, end caps and fill tube, and heat pipe envelopes, were thoroughly degreased. After the wick was installed in the heat pipe envelope, the subassembly was purged in nitric acid and then rinsed in de-ionized water. This step in the procedure was eliminated during the fabrication of the heat pipe whose wick was made from nickel screen instead of stainless steel screen. End caps and fill tubes were heliarc welded to the heat pipe envelope. The completed assemblies were outgassed at a vacuum of about 5×10^{-6} torr at 1000°C . The subscale heat pipes were outgassed for approximately three to four hours and the full-scale heat pipes were outgassed for eight hours. A predetermined amount of sodium was distilled into each pipe, the noncondensable gases were bled off, and the pipes were sealed by welding the fill tube.

Two of the full-scale heat pipes were also tested with potassium in addition to tests conducted with sodium. In both cases, the testing was first done with sodium. After the tests were completed, the fill tube was reopened and methanol was introduced to dissolve the oxidized sodium. The heat pipe envelope was then purged with water and finally with a nitric solution. The heat pipe was again outgassed and then filled with potassium by distillation. After the noncondensibles were bled off, the pipes were sealed by welding the fill tube.

3.3.3 Description of Test Setup

The experimental apparatus employed for heat pipe performance testing basically consisted of an RF power source, a water-cooled gas-gap calorimeter, high temperature thermocouple instrumentation, and insulation. A schematic of the test setup is shown in Figure 3.23.

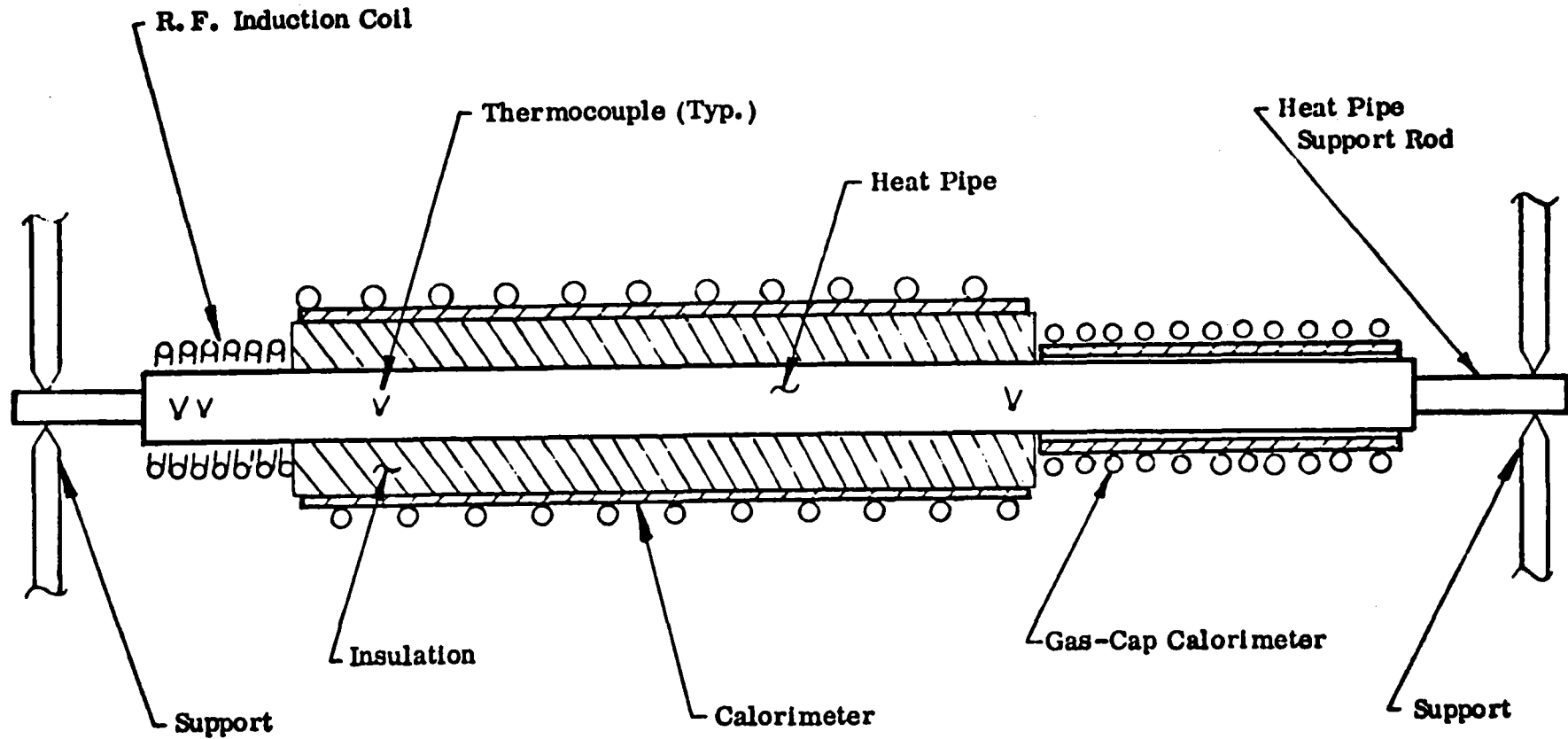


FIGURE 3.23
SCHEMATIC OF TEST SETUP

The RF power source used during the early stages of the test program was rated at 5 kW output. Later, a larger RF power source (20 kW) was acquired for testing higher performance heat pipes. A number of induction coils of various lengths were used throughout the testing program to independently vary the axial and radial heat flux. For the subscale pipes, the coils ranged in length from 5 to 16 cm; while coils 10 to 30 cm long were used for the full-scale heat pipe tests.

The heat removal rate at the heat pipe condenser was measured with a gas-gap calorimeter.⁽¹⁰⁾ The measurements consisted of the water flow rate through the calorimeter and the water temperature difference across the calorimeter. Heat transfer to the gas-gap calorimeter is accomplished chiefly by radiation and conduction across a small (typically 0.2 to 0.4 mm) gap. By filling this gap with either Argon, Helium, or a mixture of these two gases, the thermal resistance of the gap due to conduction can be changed by nearly an order of magnitude. This permits variations of the heat pipe temperature independently of the heat transfer rate.

All portions of the heat pipe between the evaporator and condenser were insulated with ceramic fiber insulation. The bulk of this insulation was enclosed by a second water-cooled calorimeter which measured the heat losses. Chromel-Alumel thermocouples were used to measure heat pipe temperature at several axial locations. At temperatures above 750°C, an optical pyrometer was also used. A mechanical fixture was used to support and orient the heat pipe and to support the calorimeters. With this fixture, it was possible to test the heat pipes horizontally, at orientations with the condenser elevated up to 86 cm above the evaporator, and vertically.

3.3.4 Testing Considerations and Data Interpretation

The use of a calorimeter with a variable conductance gap permits an independent variation of power and heat pipe temperature. This is shown schematically in Figure 3.24.a. With the gas-gap calorimeter filled with pure argon, the heat rejection capability is defined by Curve A. With helium as a filler gas, the heat rejection capability is much higher and follows Curve B. If a mixture of argon and helium is introduced, some intermediate heat rejection curve applies. Suppose the heat pipe to be tested has a performance limit at a given temperature as indicated by the sym-

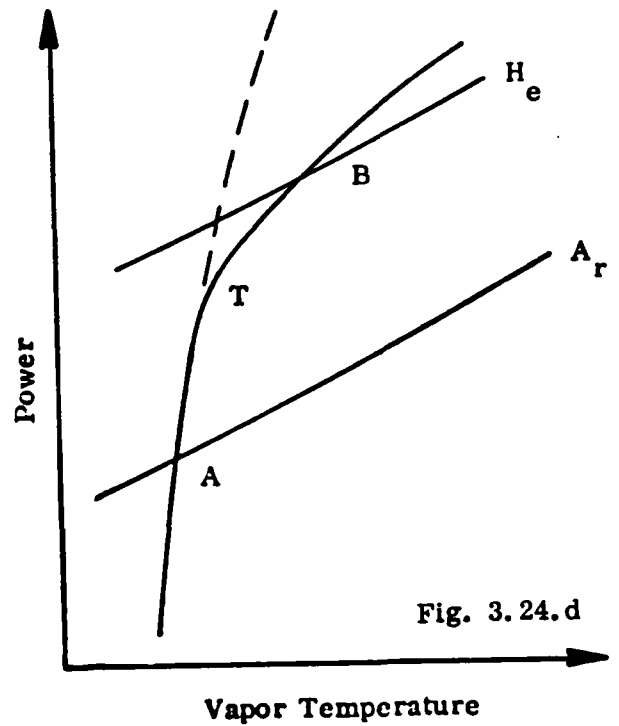
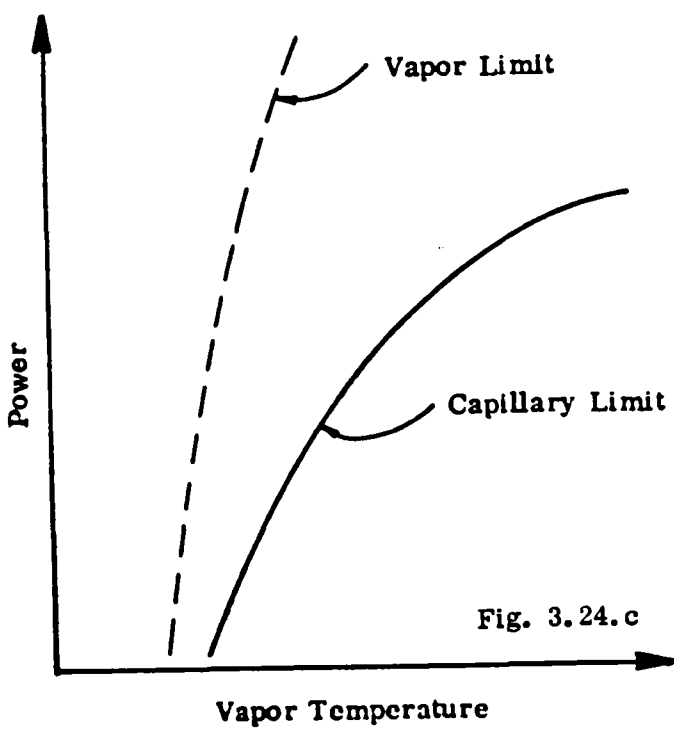
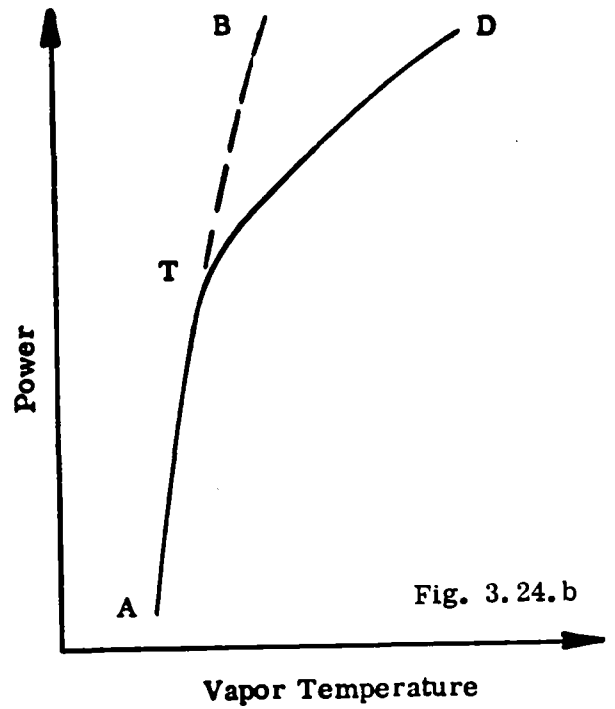
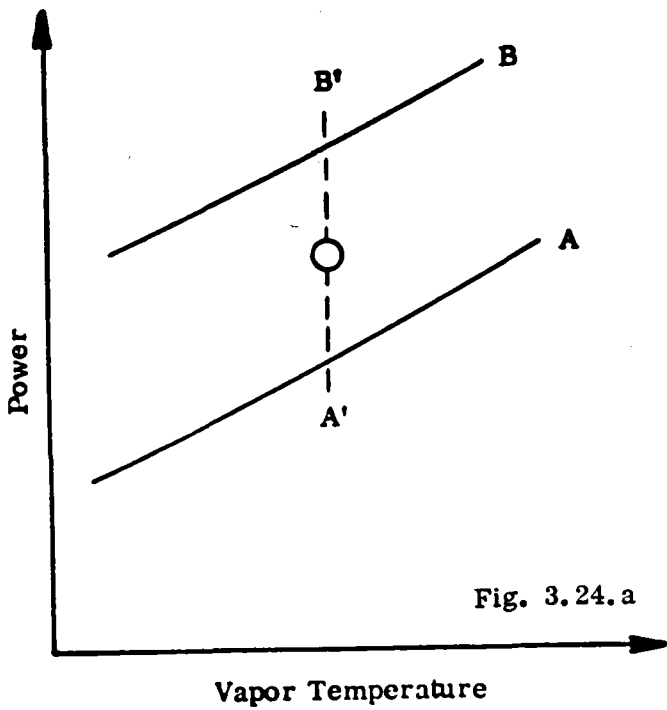


FIGURE 3.24
SCHEMATICS OF HEAT REJECTION AND PERFORMANCE LIMITS

bol (0). If argon is used in the calorimeter, the pipe cannot be tested to its full capability at this temperature since the maximum power which can be rejected corresponds to Point A'. If, on the other hand, helium is used in the calorimeter, the pipe will burn out if one attempts to test it at this particular vapor temperature. (The heat rejection required to maintain this temperature corresponds to Point B' which exceeds the capability.) However, the heat pipe can be tested to its full capability if the proper mixture of argon and helium is employed which matches the heat rejection with the capability.

Another consideration in the testing and data interpretation is the performance capability of a liquid metal heat pipe as a function of temperature. A typical capability curve is shown in Figure 3.24.b. In general, it consists of two distinct branches which are denoted as A-B and T-D, respectively. The relatively steep branch A-B represents the vapor dynamic limit. At any given vapor temperature, the dynamics of the vapor flow defines a maximum axial heat flux. This maximum may be predominantly due to inertial effects, in which case the vapor velocity becomes sonic or the restrictions may be due to viscous effects which limit the allowable vapor pressure drop to no more than the absolute vapor pressure. It is important to remember that the vapor dynamic limit is fundamental and cannot be exceeded.

The second branch T-D in Figure 3.24.b represents the capillary limit. It defines the maximum heat flux due to the limited capillary or gravity induced pumping. For each point along this curve, the available capillary pumping balances the inertial and viscous pressure losses in liquid and vapor. The location of this curve is strongly dependent on the wick design and the orientation of the heat pipe.

The temperature, corresponding to the point where the capillary limit branches off the vapor limit, is the transition temperature. It is an important parameter for every heat pipe design because different limits exist on each side of the transition temperature. In the region of the vapor dynamic limit below the transition temperature, the heat pipe cannot fail in the usual sense; i. e., a dryout of the evaporator cannot occur. Instead, upon reaching the limit, the heat pipe will increase its inertial temperature gradient until the operating temperature is consistent with the heat throughput. In the region of the capillary limit above the transition temperature a true fail-

ure of the heat pipe will occur. Upon reaching the limit, the wick will dry out in the evaporator since the pumping forces can no longer overcome the flow losses and supply sufficient liquid.

The location and shape of the capillary limit curve is design dependent. Thus, the transition temperature will also vary with the wick design. In some cases, the transition temperature may even be so low that it is outside the test range. This case is shown in Figure 3.24.c.

For the interpretation of test data, the heat rejection and the performance curves must be considered together. A typical combination is shown in Figure 3.24.d. Assume, at first, that the pipe is tested with argon in the calorimeter. As the power and temperature are increased, the performance will initially follow the vapor limit and no failure should occur. As Point A is reached, the heat rejection limit becomes dominating and the performance will follow the argon curve. Since this curve is everywhere below the capillary limit, no burnout will occur. However, the pipe has not been tested to its full capacity. Next, assume that pure helium is used in the calorimeter. Again, the pipe will follow, at first, the vapor limit curve up to the transition temperature T from whereon the capillary limits dominate. Further increases in power and temperature will cause the pipe to fail because the heat rejection capability exceeds the capillary limit. At higher temperatures, i. e., beyond Point B, the heat pipe will function again satisfactorily because the rejection capability is lower than the capillary limit. In order to obtain stable test data which represent the capillary limit between T and B, a mixture of helium and argon must be employed in the calorimeter. This mixture must be readjusted for every temperature and power within this range.

From the preceding discussion, it is obvious that pipe failures will occur most frequently near the transition temperature. In part, this is due to the specific heat rejection curve of this particular gas-gap calorimeter; but the general trend of the rejection and performance capability curves will be similar in the central receiver application.

During some of the testing, the available power source imposed an additional

limitation. But, unlike the heat rejection limit which increases with temperature, the power limit decreases slightly with temperature because of thermal radiation effects. The power limit further complicated the data interpretation and will be discussed more fully during the presentation of individual test results.

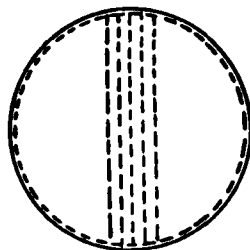
3.3.5 Heat Pipe Testing

The heat pipe development portion of the program resulted in the fabrication and testing of eight subscale heat pipes and three full-scale heat pipes. Many of these pipes were designed so that two different wick designs could be tested by alternately using opposite ends of the heat pipe for the evaporator and condenser. In this manner, two secondary (circumferential) wicks could be tested with the same axial wick, or an axial wick could be tested as both a homogeneous or an arterial wick.

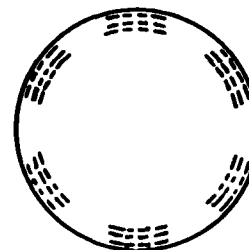
The wick designs which were tested during the subscale tests are shown in Figure 3.25. Each heat pipe is described in terms of typical dimensions and wick configuration. Primary (axial) wicks which were tested included homogeneous and arterial wicks, and segmented and communicating wicks. Some of the axial wicks required secondary (circumferential) wicks. Secondary wicks consisted of circumferential layers of screen or circumferential grooves. The numbers (1) and (2) in Figure 3.25 refer to the two opposite ends of the heat pipe. If only one wick is listed, then it applies to both ends of the pipe.

The most successful subscale heat pipe tested was SN 1-7. Its axial wicks consisted of five alternately sized tent-shaped channels. Closure at the bottom of each channel is provided by the circumferential wick. For circumferential fluid distribution, two different secondary wicks were used. One end of the pipe was circumferentially grooved. On the other end, two bias-cut screen tubes were used. One of the screen layers was used for circumferential fluid distribution, and the other was used to inhibit nucleate boiling. The term "bias-cut", as used in this context, means that a square weave screen is cut at an angle of 45 degrees to its principal axes. Thus, after installation, the weave pattern of the bias-cut screen is oriented diagonally to the long axis of the heat pipe. Circumferential wick structures employing bias-cut screen have been successfully employed by other investigator (11)

SN 1-1



SN 1-2 & 1-3



Type Inconel Material :

600

600

Diameter OD/ID (cm) :

2.5/2.2

2.5/2.2

Length (cm) :

61

61

Primary Wick :

Homogeneous Slab

Segmented Homogeneous Slab

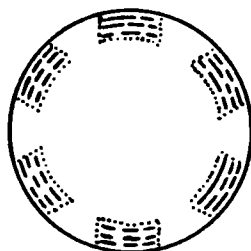
Secondary Wick :

(1) Circumferential Grooves
(2) Single Screen Layer

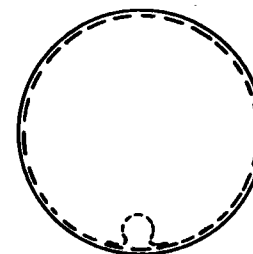
None

FIGURE 3.25
SUBSCALE HEAT PIPE WICK DESIGNS

SN 1-4



SN 1-5



Type Inconel Material :

600

600

Diameter OD/ID (cm) :

2.5/2.2

2.7/2.1

Length (cm) :

61

102

Primary Wick :

Segmented Arterial Slab

(1) Open Tent-Shaped Artery

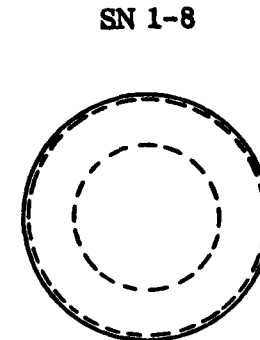
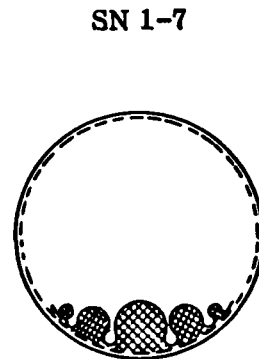
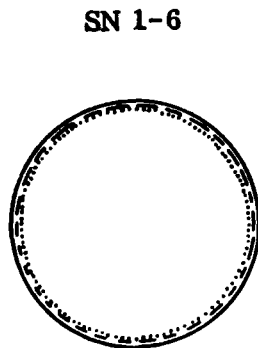
(2) Closed Tent-Shaped Artery

Secondary Wick :

None

Circumferential Grooves

FIGURE 3.25 (Continued)
SUBSCALE HEAT PIPE WICK DESIGNS



Type Inconel Material :	601	601	601
Diameter OD/ID (cm) :	2.7/2.1	2.7/2.1	2.7/2.1
Length (cm) :	102	102	102
Primary Wick :	Arterial Annular	(1) Open, Parallel Tent-Shaped Arteries (2) Closed, Parallel Tent-Shaped Arteries	Homogeneous Annulus
Secondary Wick :	None	(1) Circumferential Grooves (2) Bias-Cut Screen Tubes	Bias-Cut Screen Tubes

FIGURE 3.25 (Continued)
 SUBSCALE HEAT PIPE WICK DESIGNS

Alternately sized arteries were used to obtain the performance characteristics of an "axially graded wick structure".* The performance capabilities of such a wick is best explained with the use of Figure 3.26. At the condenser end of the heat pipe, the pressures in the liquid and vapor are equal. At this point, the stress on the liquid is zero. At points closer to the evaporator, the vapor pressure increases while the liquid pressure decreases. The liquid stress, defined as the pressure difference between the liquid and vapor, gradually increases until it is equal to the capillary pressure capability of the largest artery shown in Figure 3.26. Beyond this point, the largest artery can no longer be filled. At points closer to the evaporator, only the four smaller arteries are primed. The increased rate, at which the liquid pressure decreases in this region, reflects the change in liquid area and permeability associated with the deprimed state of the large artery. At some point within the evaporator, the liquid stress becomes equal to the capillary capability of the medium sized arteries. Beyond this point, the medium arteries are empty and the liquid transport to the end of the evaporator is accomplished entirely by the smallest arteries. The maximum heat throughput occurs when the liquid stress at the end of the evaporator equals the capillary capability of the smallest arteries.

This heat pipe was tested with both a homogeneous and an arterial axial wick structure. As a homogeneous wick, each channel is open-ended. The capillary pumping capability of each channel is a fraction of the diameter of the channel. Arterial wick behavior was accomplished by crimping and spot welding closed the end of each channel. When this is done, the pumping capability of each channel becomes a function of the pore size of the screen forming the channel.

Testing was conducted over a wide range of conditions. The maximum heat transport capability was determined at heat pipe vapor temperatures which span the operating temperature range. The heat pipe was tested horizontally, at elevations between 6 and 22 cm (condenser above the evaporator), and vertically. Throughout the tests, the length of the RF induction coil was varied between 5 and 15 cm to in-

*The term "axially graded" wick was introduced by Dynatherm in 1970 (Ref. 12) to describe a wick whose effective pore size decreases from the condenser to the evaporator. The concept was recently further investigated by TRW (Ref. 13).

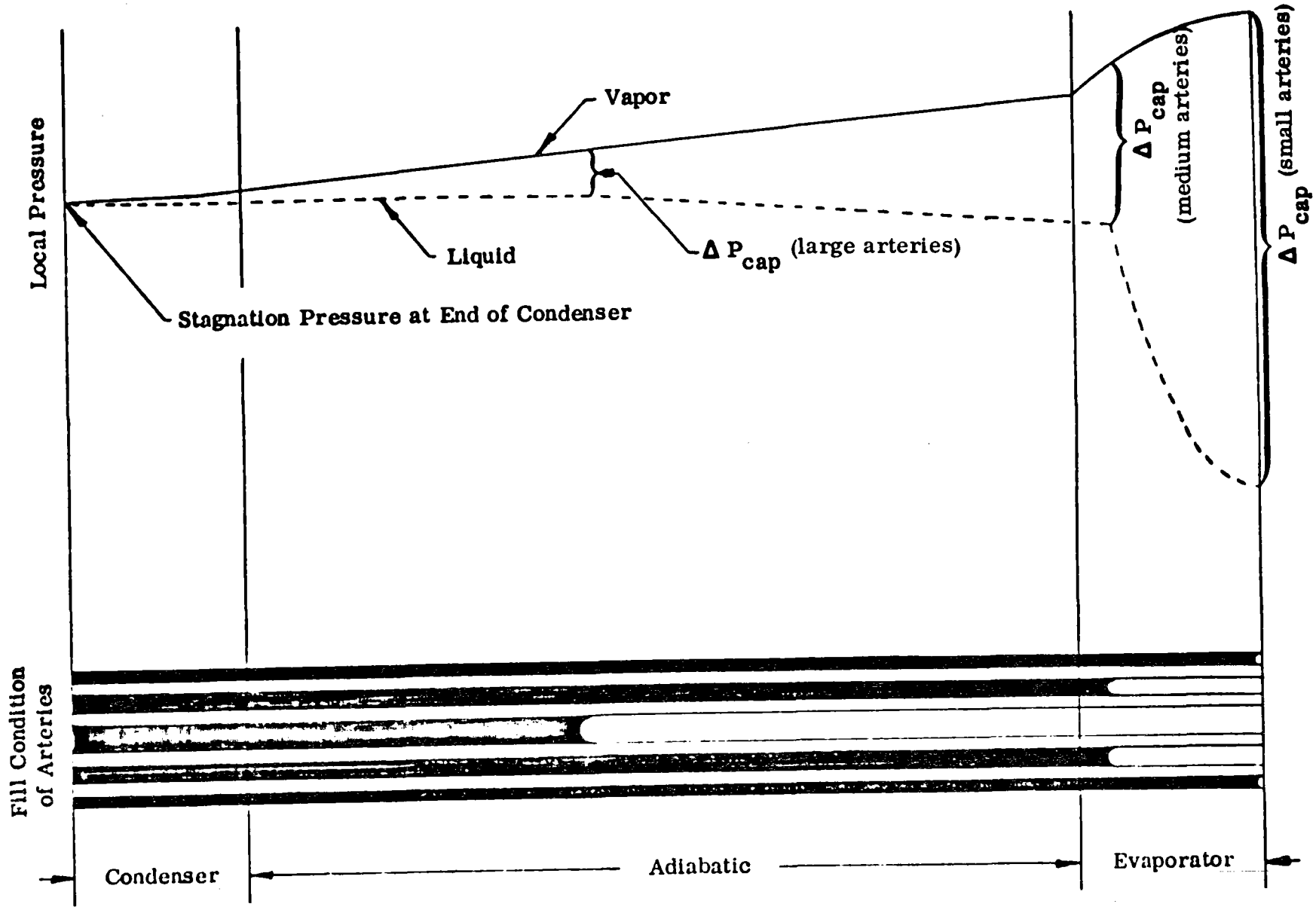


FIGURE 3.26
LIQUID FILL AND PRESSURE DISTRIBUTION
IN AXIALLY GRADED WICK

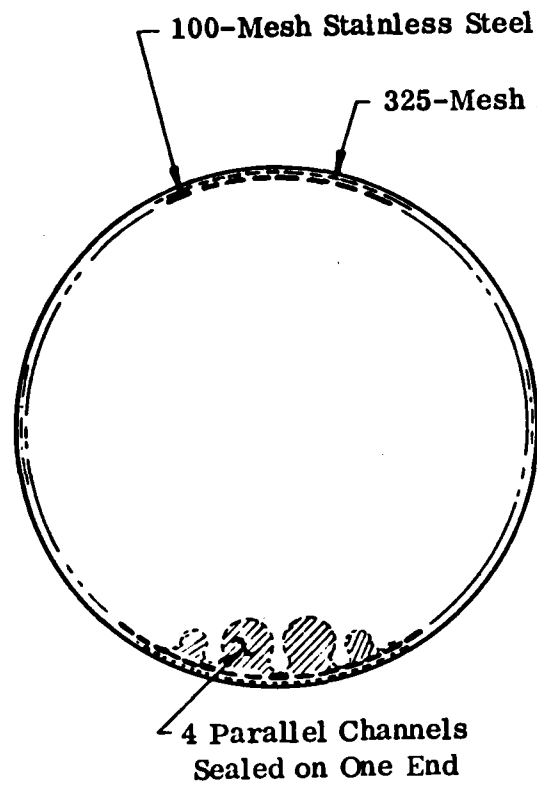
dependently vary the axial and radial heat flux. Results of these tests, as well as the results of the tests conducted on the other subscale heat pipes, are described in detail in two semiannual reports. (1, 2)

Generally, the test results achieved with SN 1-7 were quite encouraging. The performance capabilities of this heat pipe compared favorably with the projected requirements and also agreed quite well with the theoretical performance models which were developed. Axial fluxes as high as 20 MW/m^2 were obtained and radial fluxes of 1.75 MW/m^2 were measured. Other results are summarized below:

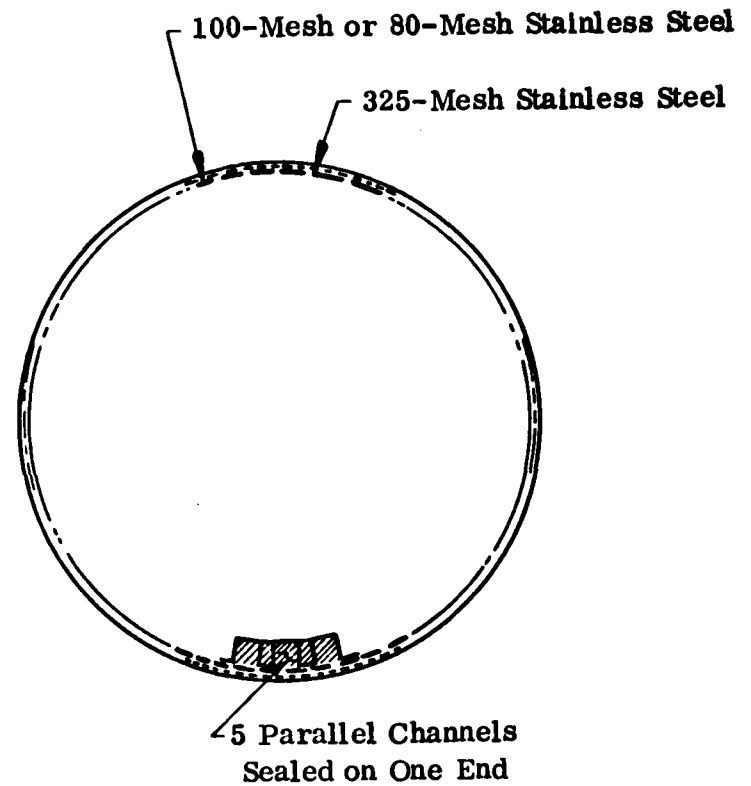
- Homogeneous axial channels provide sufficient performance at large heat pipe elevations. However, for near horizontal operation, arterial channels offer better performance.
- Bias-cut screen tubes offer considerable performance margin over circumferential grooves.
- The axial transport capability is generally limited by the capillary pumping capability of the wick structure, except at low temperatures where vapor limits are dominant.
- Nucleate boiling within the circumferential wick limits the radial flux capability at the upper end of the temperature range.

The encouraging performance of this subscale heat pipe led to the development of three full-scale heat pipes with basically the same wick design. All three heat pipes were made with Inconel 601 envelopes. The outer and inner diameter of these pipes were 6.0 cm and 5.3 cm, respectively. Two of the pipes were 183 cm long. The third heat pipe was 115 cm long and had a conical end cap.

The first two full-scale heat pipes were identical except for slight variations in the capillary wick structures, which are shown in Figure 3.27. In the first heat pipe, SN 2-1, the primary wick structure consisted of two large circular tent channels in parallel with two smaller circular tent channels. On one end of the pipe, all channels were crimped and spot welded closed to form arteries. The circumferential wicks on both ends consisted of two bias-cut screen tubes. One screen tube was made from 325-mesh stainless steel screen and the other was made from 100-mesh screen. For heat pipe SN 2-2, the primary wick consisted of three square channels



SN 2-1



SN 2-2

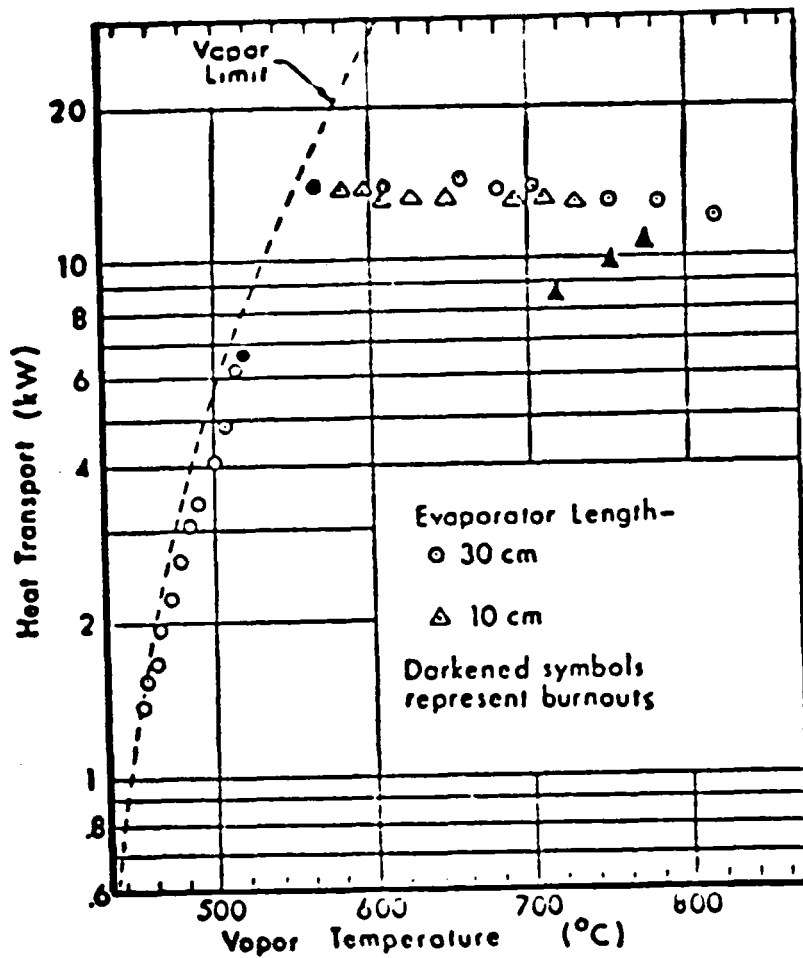
FIGURE 3.27
WICK DESIGN OF FULL-SCALE HEAT PIPES

in parallel with two smaller rectangular channels. The circumferential wick consisted of two bias-cut screen tubes. On one end of the pipe, 325-mesh and 80-mesh screens were used; and, on the other end of the pipe, 325-mesh and 100-mesh screens were used. The channels were closed on the 80-mesh end of the pipe to form arteries.

The performance capabilities of the second heat pipe were found to be somewhat better than the first, so this discussion will be limited to the second pipe. The results of the performance test conducted on the first full-scale heat pipe are discussed in the second semiannual report.⁽²⁾ The second pipe was tested over a range of conditions which included variations in heat pipe vapor temperature, heat pipe orientation, and evaporator length. The tests were conducted with both homogeneous and arterial wick structures, and with both sodium and potassium as the working fluid.

The heat pipe was first charged with sodium. Tests were performed with the closed ends of the arteries in the evaporator, the length of which was varied from 10 to 30 cm by using different induction coils. These tests were conducted with the heat pipe oriented horizontally. Typical results are shown in Figure 3.28. Two general types of test points are shown in this figure. Darkened symbols represent points which are the last stable test points prior to a dryout of the wick structure. Those points which are not darkened represent testing limitations associated with the power source or vapor limitations which do not cause wick dryout.

With the longer evaporator, wick dryout was obtained only between 520°C and 620°C; i. e., near the transition point between vapor and wick limitations. With the shorter evaporator, the pipe's performance exceeds the capability of the power source in the temperature range from 580°C to 720°C. Above 720°C dryouts did occur, although the data does show some inconsistencies. For instance, the test points near 720°C show the performance varying by at least 4 kW and possibly more. The trend established by these burnout points does not correspond to the expected trends associated with circumferential wick limits or boiling. Nonetheless, the degraded performance does occur in a temperature regime where radial flux limits do exist.



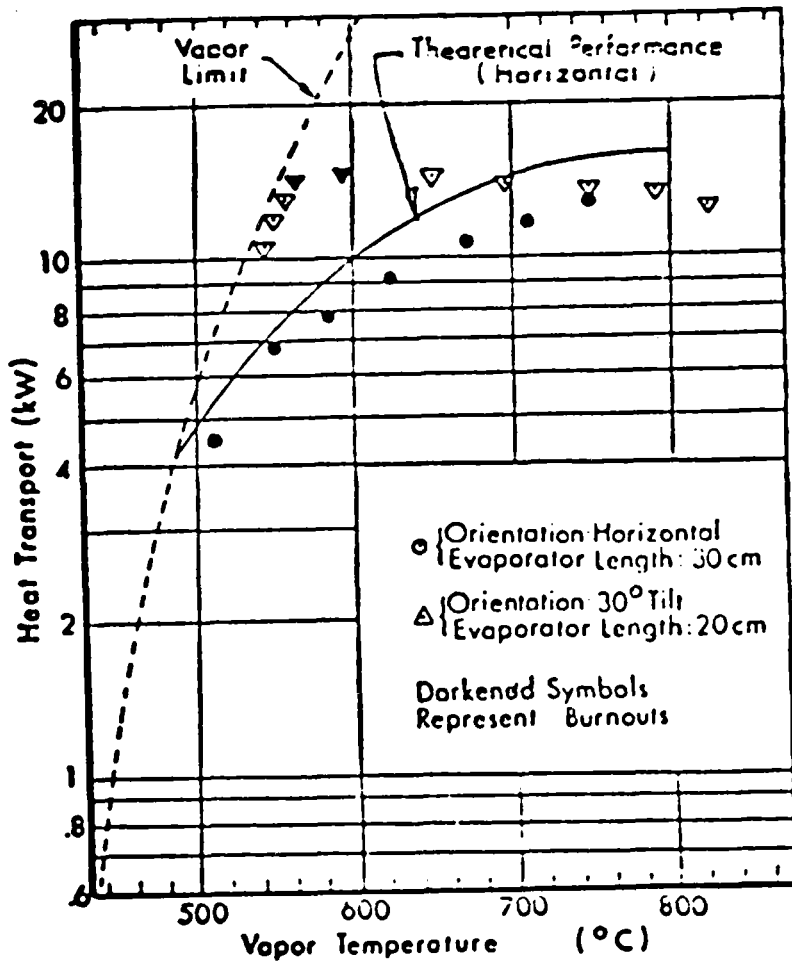
Horizontal Performance of Fullscale Heat Pipe with Closed Arteries in Evaporator

FIGURE 3.28

Tests were also conducted with the open ends of the arteries in the evaporator. Heat pipe orientations during the tests included horizontal and tilts at angles up to 30° (condenser above evaporator). Figure 3.29 shows the pipe's performance at the two extreme orientations. By comparing the horizontal test results to those obtained with the closed arteries, the superiority of the closed arteries becomes obvious. With the open arteries in the evaporator, dryouts were obtained with a 30 cm evaporator over the entire test temperature range from 500°C to 750°C . The trend established by these test points corresponds quite well with the theoretical performance capability, although the points are somewhat lower (0.5 kW to 3 kW) than anticipated. The performance of the open arteries is enhanced considerably by increasing heat pipe elevation. At a heat pipe tilt of 30° , it was only possible to measure dryouts between 560°C and 600°C . Below this temperature the data coincides with the vapor limit. At higher temperatures the performance capabilities of the heat pipe exceed the capabilities of the power source.

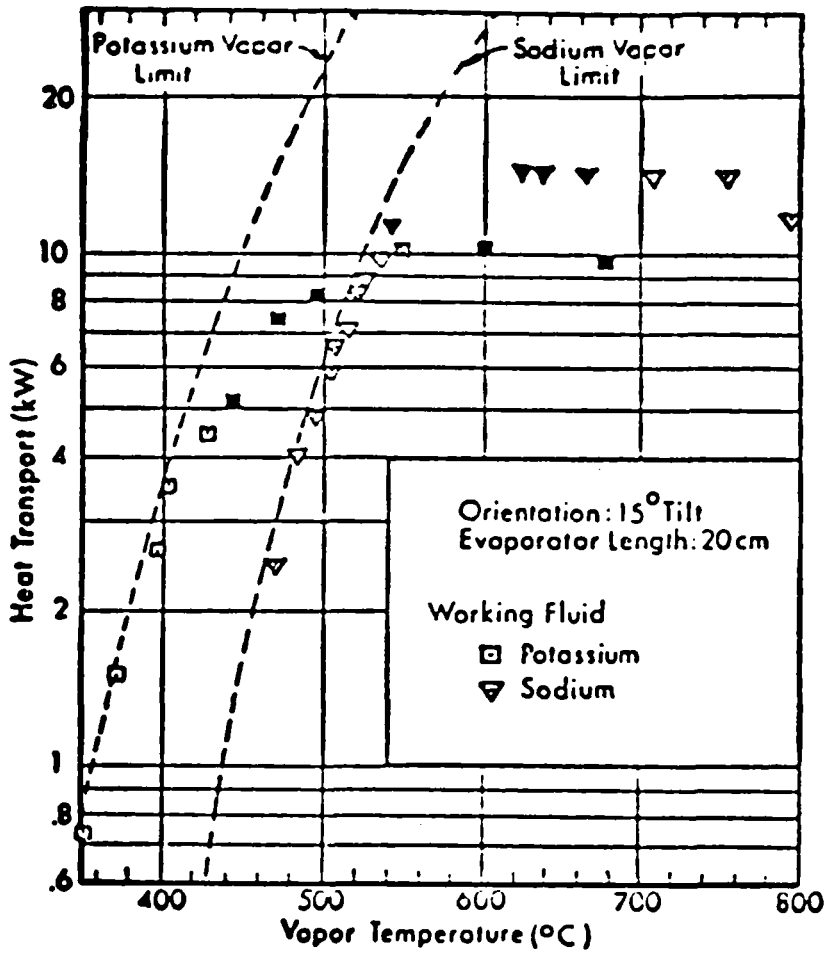
Figures 3.28 and 3.29 clearly indicate that heat pipe performance is restricted at low temperatures by the vapor limit. These restrictions can be relaxed somewhat when potassium is used instead of sodium. Figure 3.30 shows some typical test results obtained with both fluids. These tests were conducted with a 20 cm induction coil and with the heat pipe tilted at 15° . With sodium, dryouts occurred between 540°C and 620°C . Above this temperature range the pipe's performance exceeded the capability of the power source. At lower temperatures, the performance coincides with the sodium vapor limit. With potassium, dryouts were measured at all temperatures above 440°C . Below 400°C , the pipe's performance coincides with the potassium vapor limit. At all temperatures below 530°C , the pipe's performance is better with potassium than with sodium. It should be noted that the performance margin realized with potassium is a function of wick configuration. Since this heat pipe was originally designed for operation with sodium, another pipe specifically designed for use with potassium could offer even more incentive to use potassium at low temperatures.

In addition to these steady-state tests, a considerable amount of testing was conducted to characterize the transient behavior of the second full-scale heat pipe.



Full Scale Heat Pipe Performance
with Open Arteries in Evaporator

FIGURE 3.29



Full Scale Heat Pipe Performance with Sodium and Potassium (Open Arteries in Evaporator)

FIGURE 3.30

During these tests, heat pipe behavior was observed during start-up when power was applied instantaneously and at various rates. All tests were conducted with sodium. The open ends of the arteries were located at the heat pipe evaporator which was 20 cm long. Heat pipe orientations during the tests included inclinations of 15° and 30° . At 30° with the heat pipe initially at room temperature, the heat pipe started successfully when subjected to an instantaneous power input of 10 kW. With the heat pipe tilted at 15° , successful heat pipe start-up was possible only for instantaneous power inputs less than 7.7 kW. In order to increase the power at which start-up was possible, it was necessary to apply power at a finite rate. The greatest rate for successful heat pipe start-up at an inclination of 15° was determined to be 1 kW/minute.

The third full-scale heat pipe, SN 2-3, was quite similar to a full-scale thermal diffuser heat pipe. Its outer diameter was 6.0 cm and its overall length was 115 cm. The end cap on the evaporator end of the pipe was cone shaped. The wick structure in this heat pipe is quite similar to the wick used in SN 2-2. The primary wick consists of three square channels in parallel with two rectangular channels. These channels extend over the entire length of the heat pipe up to but not including the conical end cap. At the junction of the cylindrical portion of the heat pipe and the conical end cap, the channels are butted into a slab wick. This slab was made from 80-mesh screen and has the same cross section as formed by the five channels. The secondary wick consists of two bias-cut screen tubes; one made from 325-mesh screen and the other made from 80-mesh screen. The conical end cap is also lined with the same secondary wick.

The heat pipe was tested with both sodium and potassium. Tests were conducted with the heat pipe horizontal and tilted at 5° . The induction coil used during the tests was shaped to heat the pipe in approximately the same manner expected in the baseline receiver. This requires that nearly one-third of the heat input to the pipe occurs on its conical end cap. Temperature measurements made during the tests indicate that actually 37% of the energy induced by the heating coil occurs at the conical end cap.

Figure 3.31 shows typical test results obtained with both heat pipe fluids at the design tilt of 5° . The figure also shows the required axial heat transport taken from Figure 3.22. With sodium, dryouts were obtained between 500°C and 600°C . Below this temperature range, the heat pipe's performance is limited by the vapor limit. At higher temperatures, the performance capabilities of the pipe exceed the performance capabilities of the power source. Comparing the test results with the required performance, the heat pipe appears to be capable of meeting the requirements over the entire temperature range with sodium. At low temperatures, however, very little design margin exists. At these temperatures, potassium offers better performance. Note that some of the test points with potassium are partially shaded. These points are characterized by stable hotspots existing on the conical end cap. These hotspots were noticed over a considerable portion of the test range with potassium and were usually followed by dryouts with slight power increases.

Transient tests were conducted to determine the start-up capabilities of SN 2-3 at the design orientation of 5° tilt. The tests were performed only with sodium as the working fluid. Throughout the tests, argon filled the gas-gap in the calorimeter. Under these conditions, it was determined that the highest instantaneous power input which the pipe could withstand was 6 kW. At higher inputs dryouts occurred. In order to achieve start-up at higher powers, the maximum rate of heat input was found to be 1.8 kW/minute.

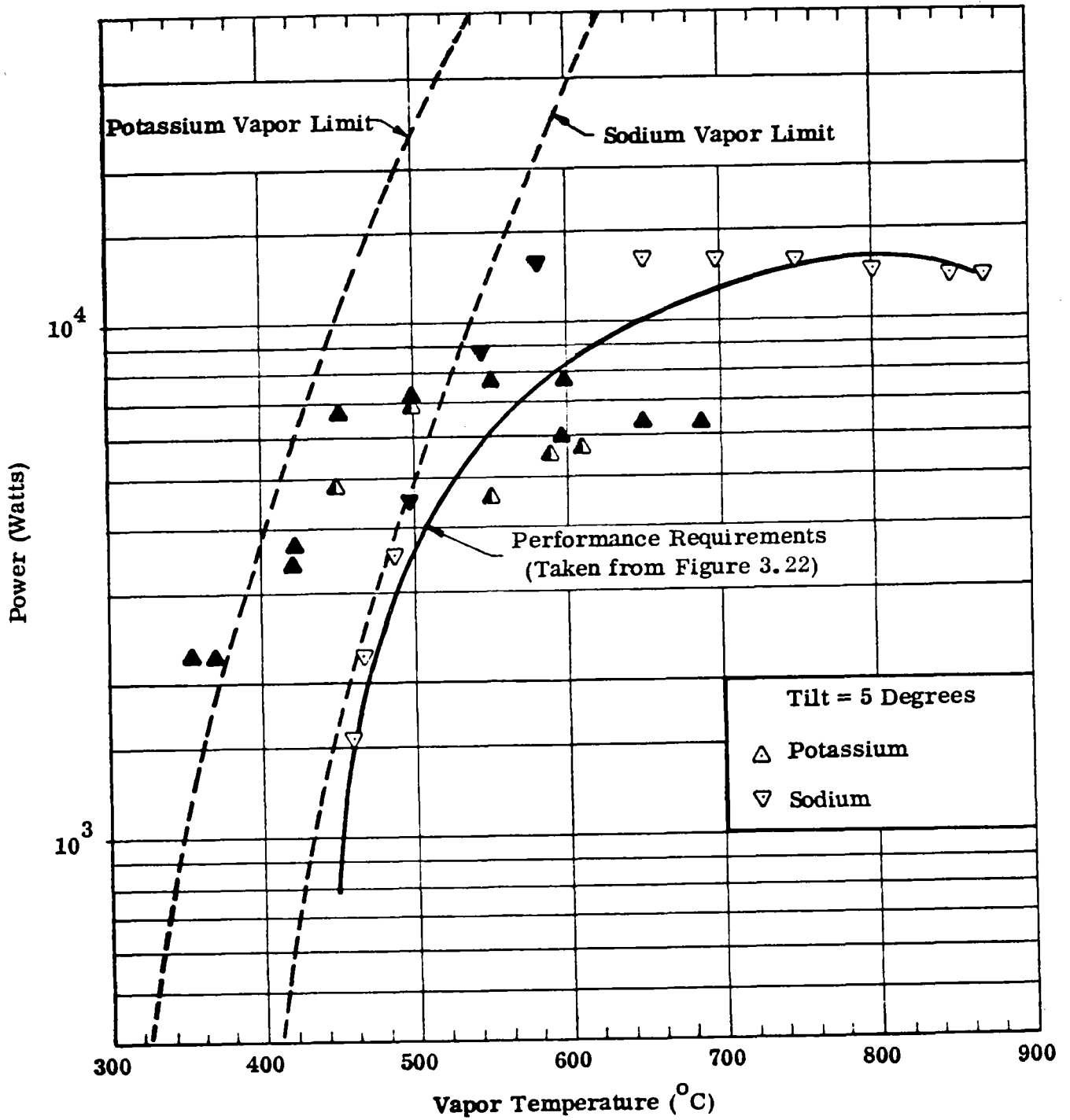


FIGURE 3.31
FULL-SCALE HEAT PIPE PERFORMANCE
WITH CONICAL END CAP

4. HEAT PIPE TECHNOLOGY ASSESSMENT

The technology of heat pipes is about 16 years old. Heat pipes were first developed at Los Alamos and from there the interest has quickly spread to many industrial, government, and university laboratories. During the past five years, three international conferences have been devoted exclusively to this technology. As a result of these past and present activities, the technology is now well established and applications are rapidly emerging.

The successful operation and long-term performance of any heat pipe is determined by three parameters:

- (1) The hydrodynamics of the working fluid
- (2) Compatibility between fluid and heat pipe envelope
- (3) The structural integrity of the container

Most of the past research and development has been devoted to a better understanding and optimization of the internal hydrodynamics. A large array of wick structures has been developed which permits the transport of large amounts of thermal energy with small losses in temperature. The problem of compatibility and structural integrity has been addressed primarily by conducting real time and accelerated life tests. The majority of these life tests has been restricted, however, to the low and medium temperature range ($< 300^{\circ}\text{C}$).

In any high temperature system, materials problems are always of concern. Examples of potential problems are corrosion resistance, compatibility with the working fluid, hydrogen embrittlement, stress corrosion, long-term creep and rupture strength, and low cycle fatigue. A heat pipe, which is a sealed system with small internal volume and which contains a wick, may conceivably pose some additional problems. Among them are generation of noncondensable gas which is trapped within the pipe, the unusually large surface area exposed by the wick, and mass transport phenomena within the wick. These potential problems with high performance liquid metal heat pipes have been of some concern and may have been responsible for the slow acceptance of these devices. A systematic study of the various effects

which might influence the reliability of liquid metal heat pipes was recently undertaken by GE for JPL. * The study showed that the applicable materials and liquid metal technology is well founded and that liquid metal heat pipes can be highly reliable devices. Also, the vast amount of liquid metal technology which has been developed during various reactor programs is directly applicable to the material problems in heat pipes. Highlights of the liquid metal and heat pipe background are:

- 800,000 hours cumulative testing of liquid metal systems during reactor programs at 800-2000^oF (austenitic SS, cobalt, and nickel based alloys).
- 100,000 hours cumulative testing of sodium heat pipes reported in the literature through 1972 (1300-1500^oF).
- 1,000,000 hours cumulative industrial use of Dynatherm's Isothermal Furnace Liners with 40,000 MTBF (900-2000^oF).

Early applications were mostly restricted to aerospace systems and the production quantities and concomitantly the hardware experience was rather limited. The aerospace experience did result, however, in valuable process development and quality control standards. During the last few years, several commercial and industrial applications have been developed; and today, perhaps, one quarter of a million heat pipes are in use. Most of these heat pipes are of the low temperature type and fabricated from aluminum, copper, or carbon steel. The preferred working fluids are ammonia, water, and various refrigerants.

In the high temperature field, much less hardware experience is available, in spite of the fact that high temperature liquid metal heat pipes were historically among the first to be developed. One notable exception is Dynatherm's product line of Isothermal Furnace Liners. These are annular potassium or sodium heat pipes which are widely used for isothermalizing tubular diffusion furnaces. More than 600 of these liquid metal heat pipes are currently in use.

* Heat Pipe Operating Reliability for the Dish-Stirling Solar Receiver," by W. F. Zimmerman, General Electric Company, and J. W. Stearns, JPL. November 15, 1978.

The technology of the heat pipes for the solar receiver has many similarities with that of the Isothermal Furnace Liners (IFL). Firstly, their geometries are comparable -- the receiver heat pipes being 5 cm in diameter and 1 to 2 m long, while the IFL's range from 3 to 15 cm in diameter and in length from 0.15 to 1.5 m. Both are fabricated from Inconel 600 and use sodium or potassium as the working fluid. Both heat pipes are heated by radiation and are required to operate in air. Finally, most IFL's which are in industrial use are cycled at least daily which exposes them to similar low cycle fatigue loading as the solar receiver heat pipes will experience. In some respects, however, the solar receiver heat pipes will be subjected to more severe conditions. The radial heat fluxes at the evaporator will be higher and more non-uniform than those experienced by most IFL's. Also, the cycling rate due to changes in the solar flux could be much faster. Development heat pipes have been tested to these requirements and they have passed the tests. Also, available material data indicate that long-term performance under these conditions can be expected. However, real time life tests are urgently needed to verify these predictions and to establish the necessary technology base.

One concern which is frequently expressed about liquid metal heat pipes is their safety. Alkali metals are, of course, highly reactive with oxygen and with water. Unlike pumped liquid metal transport systems which contain large quantities of it, heat pipes usually contain only a very small amount of fluid. A typical sodium heat pipe, such as the ones designed for the solar receiver, has a fluid inventory of only 100 g. Laboratory experiments at Dynatherm during which sodium and potassium heat pipes were made to fail at high temperatures have never lead to any violent reaction but always to a slow oxidation of the working fluid. The same observation was made by users of Isothermal Furnace Liners who exceeded the specified temperature limit due to a failure of the furnace control mechanism.

5. POWER CONVERSION CYCLES FOR THE HEAT PIPE CENTRAL SOLAR RECEIVER

Gas turbine plants are based on the thermodynamic Brayton cycle and can be either of the open or the closed cycle type. Early in the program, the open cycle was selected as the prime candidate for a solar plant. Material considerations of the heat pipes suggest a top cycle temperature of about 850°C (1550°F) which is very compatible with modern gas turbines. The simplest gas turbine plant would consist only of a compressor, the solar air heater, and the turbine-generator set. But the thermodynamic cycle efficiency of this simple plant is only about 25% which represents a poor utilization of the expensive heliostats. The addition of a recuperator increases the efficiency to about 35 to 39%. A flow diagram of such a recuperative system is shown in Figure 5.1. Also shown are typical temperatures, pressures, and input and output powers which were used for a preliminary system study. The calculations were based on a turbine efficiency of 90%, compressor efficiency of 85%, and a recuperator effectiveness of 85%. Gas turbine plants of this type are commercially available. They are relatively inexpensive and lightweight, thus the whole plant could conceivably be located on top of the receiver tower. This simple type of plant rejects a large amount of thermal energy (19 MW for a 10 MW electrical plant) at a relatively high temperature ($290^{\circ}\text{C}/552^{\circ}\text{F}$). If the wasted energy could be utilized, the overall conversion efficiency could be considerably improved. It should be noted that a steam plant of comparable efficiency does not offer the same growth potential. Condenser temperatures of steam plants are typically 40 to 60°C (100 to 140°F), thus the availability of the rejected heat is negligible.

Several approaches have been considered which make use of the high temperature exhaust of the basic Brayton system shown in Figure 5.1. Two of them are discussed here because they show the diversity of available approaches. The first system utilizes an Organic Rankine Cycle System (ORC) as bottoming cycle. A flow diagram of this gas turbine-ORC plant is shown in Figure 5.2. The temperatures, pressures, and flow rates remain the same as in the simple, recuperated cycle. The exhaust air from the recuperator, however, is used as the heat source in the vaporizer of an ORC. The performance estimates were based on a packaged ORC which uses

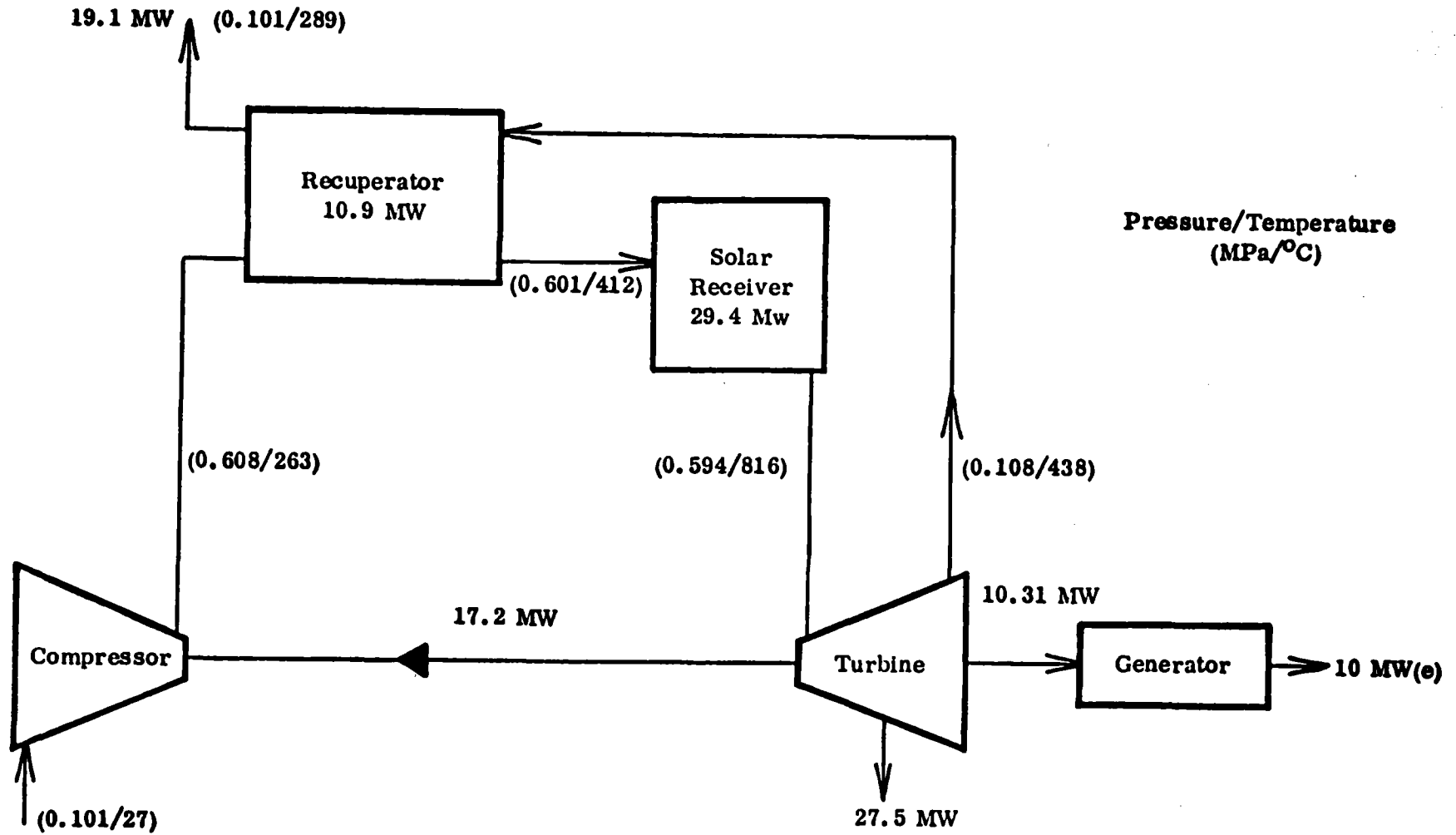


FIGURE 5.1
FLOW SHEET OF RECUPERATIVE OPEN GAS CYCLE ($\eta = 0.35$)

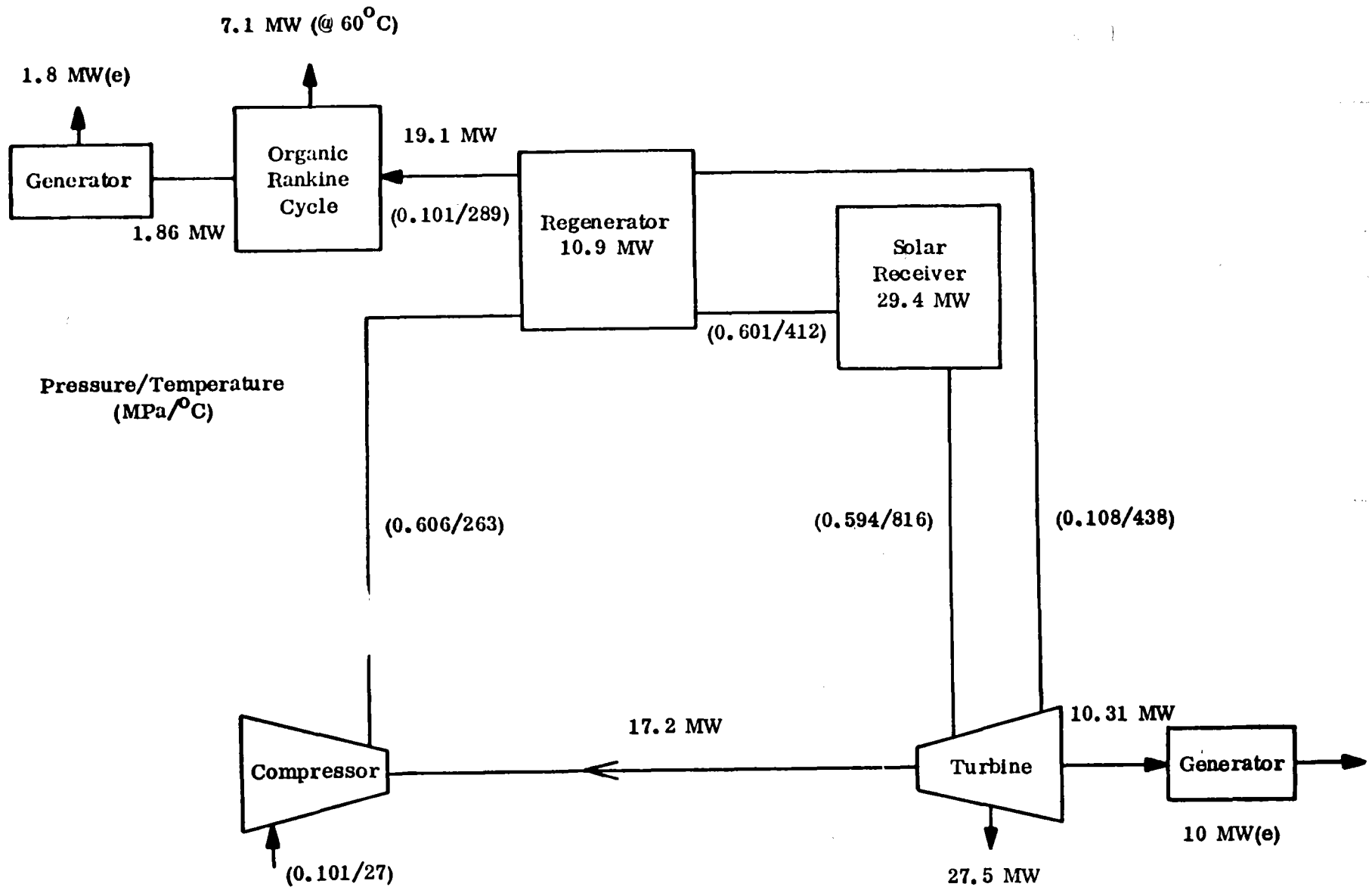


FIGURE 5.2

FLOW SHEET OF RECUPERATIVE OPEN GAS CYCLE WITH ORGANIC RANKINE BOTTOMING CYCLE ($\eta = 0.41$)

toluene as the working fluid. It has been developed by Sundstrand Energy Systems, Rockford, Illinois. *

A typical ORC unit delivers 600 kW(e) with a conversion efficiency of approximately 20%. Heat is removed by the vaporizer of the ORC from the waste heat airstream which should be 316°C (600°F) or higher and which is cooled to 166°C (330°F). The waste airstream from the recuperator of the selected Brayton cycle is only 289°C (552°F) and its flow rate 72.8 kg/sec (5.77×10^5 lb/hr). Assuming that the same output can be maintained with the lower temperature air, the thermal energy that can be withdrawn for the waste air is 9.0 MW(th) (by cooling it from 289 to 166°C) and the electrical output from the ORC is 1.8 MW(e). Thus the overall output is 11.8 MW(e) and the combined thermal efficiency is 40.1%. The addition of the ORC bottoming system complicates the plant somewhat. Firstly, water cooling of the ORC is required since about 7 MW must be rejected at 60°C (140°F). Secondly, at least the ORC must be located at ground level. There is no real objection to that since the pressure losses in the piping can be held to 6.8 kPa (1 psi). The preferred location of the conversion equipment requires, in any case, a much more detailed system study.

A second high efficiency system is shown in Figure 5.3. It employs compressor intercooling and reheat between two turbine stages to achieve a conversion efficiency of 44%. The same component efficiencies for compressor and turbine were assumed as in the basic cycle. A three stage compressor is used with intercooling between stages. The intercooling could be done effectively and with minimal pressure loss with a heat pipe air-to-air heat exchanger. The use of intercooling reduces the compressor work considerably. At the high temperature side of the cycle, reheat between two turbine stages is employed to raise the average temperature at which heat is added to the gas. The results of these modifications to the basic Brayton cycle is an effective conversion efficiency of 44%.

Interstage cooling complicates the compressor design and may require the development of a new compressor. Reheat between turbine stages requires that at

* Power Generation through Waste Heat Recovery, Data Sheet 9014824

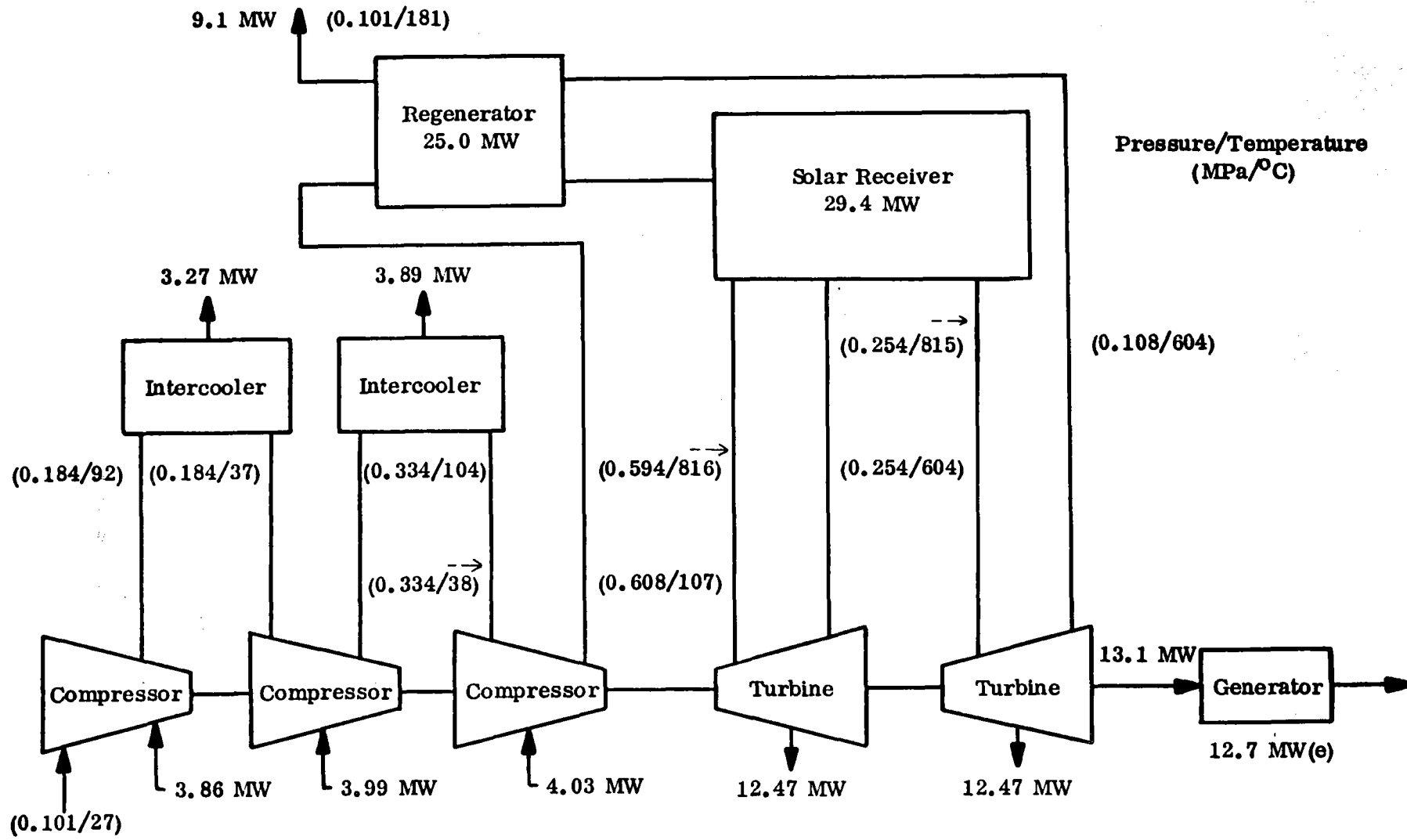


FIGURE 5.3
FLOW SHEET OF RECUPERATIVE OPEN GAS CYCLE WITH
INTERCOOLING AND REHEAT ($\eta = 0.44$)

least the high pressure stage be located near the receiver and therefore on top of the tower. However, a solar gas turbine plant will probably require a two shaft system just to accommodate the varying thermal input. The high pressure turbine and the generator could be located near the receiver, while the compressor with its heat exchangers and a low pressure turbine stage could be located at ground level. Table 5.1 summarizes the pertinent parameters of the three candidate conversion cycles. An estimate of the relative capital cost is given in Section 6.

Parameter	Baseline Cycle	Baseline Cycle with ORC Bottoming System	Baseline Cycle with Compressor Intercooling and Turbine Reheat
Turbine Inlet Temp. (°C)	816	816	816
Pressure Ratio	6	6	6
Output (MW(e))	10.0	11.8	12.7
Thermal Input (MW)	29.4	29.4	29.4
Turbine Output (MW)	27.5	27.5 ⁽¹⁾	24.9 ⁽²⁾
Compressor Work (MW)	17.2	17.2	11.9
Heat Exchangers (MW)	10.9	22.9 ⁽³⁾	32.2
Exhaust Temp. (°C)	289	166 and 60 ⁽⁴⁾	181 and 68 ⁽⁵⁾
Gas Flow Rate (Kg/sec)	72.6	72.6	58.8
Thermodynamic Efficiency	35	41	44

- (1) Not including output from ORC.
- (2) Combined turbine work from both stages.
- (3) Of the 22.9 MW, 10.9 MW are exchanged in the recuperator and the remaining 12.0 MW are transferred from the exhaust gas to the ORC.
- (4) Heat rejection from the ORC occurs at 60°C.
- (5) The average heat rejection temperature from the intercoolers is 68°C.

TABLE 5.1
COMPARISON OF THREE GAS TURBINE SYSTEMS

6. COMPARATIVE COST ANALYSIS

An estimate of the capital cost of a solar gas turbine plant with a heat pipe central receiver was made. Since the scope of this program covered only the heat pipe receiver, detailed estimates could only be made for this one component. In order to arrive at an overall plant cost, the estimates for the solar steam plant⁽¹⁾ were used for all other components. Some of those estimates were adjusted, however, in order to account for the higher efficiency and the simpler design of a high temperature gas turbine plant. This approach is discussed more fully in the following subsections.

The basic ground rules and assumptions for all estimates were:

- No interest during construction
- Cost in mid-1978 dollars
- Free land and land rights as in the water/steam pilot plant
- No cost for development, operation, maintenance, and testing during start-up, and spare parts are included
- The cost for the collector field is $\$65/m^2$
- Plant site at Barstow, California

Table 6.1 shows the estimate for the capital cost of the solar plant which was generated by our subcontractor, Foster Wheeler. It is a fairly independent estimate and is based primarily on Foster Wheeler's experience with power plants of similar nature. Dynatherm provided the costs for the heat pipes and the only component costs which were copied from the water/steam plant are those of the collector field and the master control. The table shows two cost figures for the collector field; they correspond to cycle efficiencies of 33 and 38%, respectively. This is the range of efficiencies predicted for the baseline solar gas turbine plant.

(1) Central Receiver Solar Thermal Power System, Phase 1, Volume VII, Book 1, McDonnell Douglas Report MDCG6776, May 1977

TABLE 6.1
CAPITAL COST ESTIMATES

<u>Item</u>	<u>\$ Million</u>
Receiver and Platform	3.51
Transportation and Installation	0.88
Tower Assembly	1.50
Tower Foundation and Site Preparation	0.54
Collector Field (Heliostats)	3.10 - 3.58
Buildings and Facilities	0.50
Turbine-Generator Unit	2.97
Master Control	2.24
Miscellaneous	<u>1.69</u>
 Total Direct Costs	 16.93 - 17.41
Contingency Allowance and Indirect Costs (15%)	<u>2.54 - 2.61</u>
 TOTAL CAPITAL COSTS	 19.47 - 20.02

An item-by-item discussion of the cost items is provided below:

- Receiver and Platform - This cost item covers the receiver unit, the platform, and all interconnecting piping with the turbine-generator set. It includes the labor and material required to design, fabricate, and support an acceptance test for up to six months. Material costs were based on actual vendor quotations and up-to-date catalog prices, heat pipe costs (\$2.4 million) were provided by Dynatherm, and receiver design and manufacture costs are based on Foster Wheeler experience. We assumed the receiver panels to be factory-assembled with on-site final receiver assembly.
- Transportation and Installation - This cost item includes packing, transportation, and site-labor assembly and installation costs for the receiver, platform, and turbine-generator unit on top of the tower. Site labor costs are based on today's prevailing rates for the Barstow area.
- Tower Assembly, Foundation, and Site Preparation - These costs are based on the costs developed for the water/steam system. The costs were adjusted to account for differences in tower height, weight on top of the tower, and inflation.
- Collector Field - This cost of the collector field was assumed to be \$65/m².
- Buildings and Facilities - This cost item includes all structures and facilities required for the plant, such as maintenance buildings and administrative buildings. It does not include a turbine-generator building, since these components will be located on top of the tower.
- Turbine-Generator Unit - This cost item includes the turbine, compressor, electric generator, regenerator, and instrumentation and control normally associated with a gas-turbine plant. It does not include the master control system of the plant.
- Master Control - The details of the control system have not been developed. We assume that the cost will be the same as for the water/steam plant. This is a conservative assumption, since the master control system for the gas-solar plant is expected to be somewhat simpler.
- Miscellaneous - This cost item includes field communication, transportation and handling equipment, furnishing and fixtures, and maintenance and service equipment.

As shown in Table 6.1, the projected cost, in mid-1978 dollars, of the heat pipe central solar receiver gas-turbine plant ranges from \$1,947 to \$2,002/kW, depending on the assumed cycle efficiency.

The cost of the heat pipes was estimated at 2.4 M\$. This estimate was based on actual quotes for materials and an extrapolation of Dynatherm's experience of labor cost for commercial liquid metal heat pipes. Based on 5733 heat pipes per receiver, the unit cost of a single heat pipe is \$420. This cost breaks down as follows:

Materials:

Tubing	\$ 85
Fin Material	98
End Caps, Fill Tube, etc.	14
Wick, Sodium	45

Fabrication:

Fin Attachment (Subcontract)	24
Heat Pipe Fabrication (7.7 hours @ \$20/hr)	154
	——

TOTAL	\$420
--------------	--------------

The above labor cost is not based on automated fabrication techniques. Instead, it assumes that the same process is used which was developed by Dynatherm for commercial liquid metal heat pipes. The only improvement which was incorporated is processing of up to 20 heat pipes simultaneously in batches. It is estimated that true automation could reduce the labor input to perhaps less than one hour per heat pipe.

A second estimate for the capital cost of the solar plant was generated by Dynatherm. The same cost basis as in Table 6.1 was used for the receiver, the tower, and the turbine generator unit. The remaining cost items of the plant were scaled on an item-by-item basis from the McDonnell Douglas estimate for the steam plant.⁽¹⁾ Adjustments were made to account for the technical differences between the two plants, and all costs pertaining to thermal storage were eliminated. No

(1) loc. cit.

judgment as to the accuracy of the steam plant estimates was attempted, however. This second estimate for the solar gas turbine plant is mostly of comparative value. The results are shown in Table 6.2 and the supporting item-by-item discussion is given below:

- Receiver, Tower, and Foundation - The estimate for the gas turbine plant is the same as in Table 6.1. For the steam plant, CBS Items 4190.21, .23, .24, .25, .26, and .27 were escalated by 7% in order to account for the difference between 1977 and 1978 dollars.
- Collectors - The cost of the collectors was assumed to be $\$65/\text{m}^2$. The gas turbine plant requires 1363 heliostats of 41 m^2 each while the reference steam plant uses 1760 heliostats with a unit area of 38 m^2 .
- Turbine Equipment - For the gas turbine plant, the Foster Wheeler estimate which is based on a vendor quote was used. For the steam plant, the sum of CBS Items 4300.1, .2, .3, .4, and .5 was escalated by 7%. These include the turbine generator unit, the heat rejection equipment, the condensing system, the feedwater heating system, and the water circulation/treatment equipment.
- Buildings - The total cost of all buildings is given as 2.44 M\$. For the solar steam plant, the cost of the thermal storage building (0.13 M\$) was subtracted and the remainder escalated by 7%. For the gas turbine plant, the cost of the turbine building and the water treatment equipment building was also eliminated to arrive at a cost of 1.10 M\$.
- Miscellaneous Electric Equipment, Master Control, Distributables, and Yard Work - These items were assumed to be identical for both plants and escalated by 7%.
- Miscellaneous Plant Equipment - The cost for the steam plant is given as 2.66 M\$ which becomes 2.85 M\$ after escalation. For the gas turbine plant, several items were subtracted as not applicable or covered in other cost items. Among the eliminated items are: cranes and hoists and receiver equipment (CBS Items 4500.11 and 4500.14) and auxiliaries for the water cooling system (4500.221 and 4500.223).
- Contingency Allowance and Indirect Costs - These were assumed to be 15% of the total direct cost for both types of plants.

TABLE 6.2
COST COMPARISON OF HEAT PIPE AIR BRAYTON
AND STEAM RANKINE 10 MW(e) POWER PLANT

<u>Cost Item</u>	<u>Heat Pipe Gas Turbine Plant</u> \$ Millions	<u>Steam Rankine Plant</u> \$ Millions
Receiver	4.39	10.74
Tower & Foundation	2.04	0.67
Collectors ⁽¹⁾	3.63	4.35
Turbine Equipment	2.97	5.40
Buildings ⁽²⁾	1.10	2.47
Misc. Electric Equipment ⁽³⁾	1.13	1.13
Misc. Plant Equipment ⁽²⁾	1.24	2.85
Master Control ⁽³⁾	2.26	2.26
Distributables ⁽³⁾	3.05	3.05
Yard Work	<u>0.70</u>	<u>0.70</u>
Total Direct Cost	22.51	33.62
Contingency Allowance and Indirect Costs (15%)	<u>3.38</u>	<u>5.04</u>
Total Capital Costs	25.89	38.66

(1) Based on \$65/m²

(2) Adjusted to reflect savings in gas turbine plant

(3) Assumed identical in gas turbine and steam plant

Note: Costs based on mid-1978 dollars

Percentage Cost of Heat Pipe Gas Turbine Plant: 67%

Based on the above analysis, the capital cost of a solar gas turbine plant is 33% lower than that of an equivalent solar steam plant. This comparison applied only to the 10 MW pilot plant. At this time, it is not known how the costs of the gas turbine plant scale for commercial plant sizes.

The critical components of a solar gas turbine plant with a heat pipe receiver are the heat pipe themselves. Although developed successfully in the laboratory, they have not been manufactured in sufficient quantity to allow an accurate projection of their future cost. In the pilot plant design, the average thermal load per heat pipe is 5000 Watts. Thus, for a plant efficiency of 33%, each heat pipe transports the electric equivalent of 1.65 kW. For the pilot plant, the cost per heat pipe assembly was previously given as \$420. This would convert to 254 \$/kW(e) as the contribution of the heat pipes to the overall plant cost. This cost is probably not acceptable for commercial plants.

One projection of future cost can be derived from the experience with commercial heat pipe air-to-air heat exchangers. These devices are currently produced in fairly large quantities and the cost per individual heat pipe is about 50 dollars. If this figure was to be applied to the solar receiver, the cost contribution of the heat pipes would be 30 \$/kW(e). A different estimate can be obtained from the material cost. Each heat pipe (including fins) weighs about 22.5 pounds. The current price for Inconel 601 (the preferred material) is \$5.50/lb. As a rule of thumb, the fabrication cost of mass produced goods is about \$2.00/lb. Thus the fabricated cost per heat pipe would be \$169 which converts to 102 \$/kW(e). The lower number of 30 \$/kW(e) is probably optimistic and the higher number of 102 \$/kW(e) pessimistic. Less expensive materials than Inconel, such as stainless steel 310, can be considered. A realistic estimate would place the contribution of the heat pipes to the cost of the solar plant in the neighborhood of 75 \$/kW(e).

Finally, a first estimate was made of the cost benefits resulting from a bottoming conversion system. The installed cost of packaged Organic Rankine Cycle (ORC) is listed as 700-800 \$/kW(e).⁽¹⁾ In the combined cycle which was discussed

(1) Power Generation Through Waste Heat Recovery, Sundstrand Energy Systems Data Sheet 9014824

in Section 5, 1.8 MW(e) were generated by the ORC increasing the total output of the pilot plant to 11.8 MW(e). Since all other components of the combined plant would remain unchanged, the overall plant cost must be incremented by the cost of the ORC. Assuming a base cost of 20.02 M\$ for the 33% solar plant (see Table 6.1), the total cost of the combined plant then becomes 21.28 to 21.46 M\$ with an output of 11.8 MW(e). Thus the specific cost of the combined plant is 1800 to 1820 \$/kW(e) which represents a savings of 200 \$/kW(e) over the simple solar plant.

An Organic Rankine Cycle may not be the optimum bottoming system for the solar gas turbine plant. It was chosen because data were readily available and because a packaged system would have the least effect on other components. Nevertheless, this simple analysis shows the potential for cost reduction in a solar gas turbine plant.

7. RECOMMENDED FUTURE WORK

During the present program, the basic technology of high temperature liquid metal heat pipes as applied to an air solar receiver was developed. The primary function of the heat pipes is that of "thermal diffusers". The heat pipes absorb the very high solar flux and then diffuse it nearly loss free to a gas stream. A conceptual design of a 30 MW(th) receiver with a gas outlet temperature of 816^oC (1500^oF) was generated as part of the program. A preliminary economic analysis has shown that a solar gas turbine plant with a heat pipe receiver is less expensive than a similar solar steam plant.

Several areas can be identified in which development is required in order to reduce the concept of a heat pipe receiver to practice. This needed development can be grouped into three tasks:

- (1) Life testing of full-scale solar receiver heat pipes
- (2) Additional component testing to verify compliance with specific receiver requirements
- (3) Development, design, and fabrication of a representative receiver module and testing it in a solar concentrator

Heat pipes are pressure vessels partly filled with a working fluid and must operate for a long time at high temperatures. The pressure of the working fluid stresses the container material, and additional stresses result from the large thermal gradients within the walls. Furthermore, the daily cycles in a solar receiver raise the possibility of failure due to fatigue. This scenario indicates the undisputable need for long-term endurance testing. Life tests with liquid metal heat pipes have been conducted in the past, and the basic compatibility between alkali metals and some standard container materials (e. g. , stainless steel and Inconel) has been established. However, all previous life tests were done with small heat pipe samples and at low power levels. The objective of the first task is to start a life test program which simulates the condition in a solar receiver.

Extensive component testing of individual heat pipes was already done during the current program. However, recent receiver designs⁽¹⁴⁾ require lower gas inlet temperatures than previously considered; thus additional performance mapping, in particular of potassium heat pipes, is needed. Also, the response of the heat pipes to rapid changes of the input power (solar flux) has not yet been studied sufficiently. Another objective of the component testing is to induce intentionally a failure of a heat pipe. The safety of liquid metal heat pipes has been of some concern to potential users. It is therefore important that the effects of a failure be studied under controlled laboratory conditions.

The major task of the recommended follow-on work is the development and testing of a representative receiver module. This module would typically contain about 27 heat pipes and collect 250 kW of thermal energy. With a properly structured test program, a module of this size can be made to simulate the operating conditions of every segment of a panel of a full scale receiver. The main two test variables are air inlet temperature and solar flux. For example, low gas inlet temperature and low flux will simulate the bottom of a panel, medium gas temperature and high flux will simulate the center, and high gas inlet temperature and low flux will simulate the top of a panel.

A conceptual design of the recommended demonstration module is shown in Figure 7.1. In addition to serving as a demonstration of its feasibility, the testing of such a module will accomplish several important specific objectives.

- Test the performance of the heat pipes under actual solar flux distribution
- Determine the effects of reradiation and reflection by a cluster of heat pipes
- Verify the redundancy of a heat pipe receiver; i. e., that it can tolerate a single heat pipe failure

These objectives cannot be achieved with individual heat pipes and through laboratory testing. On the other hand, it is not advisable to proceed with the development of a full-scale heat pipe receiver without extensive testing on the sub-

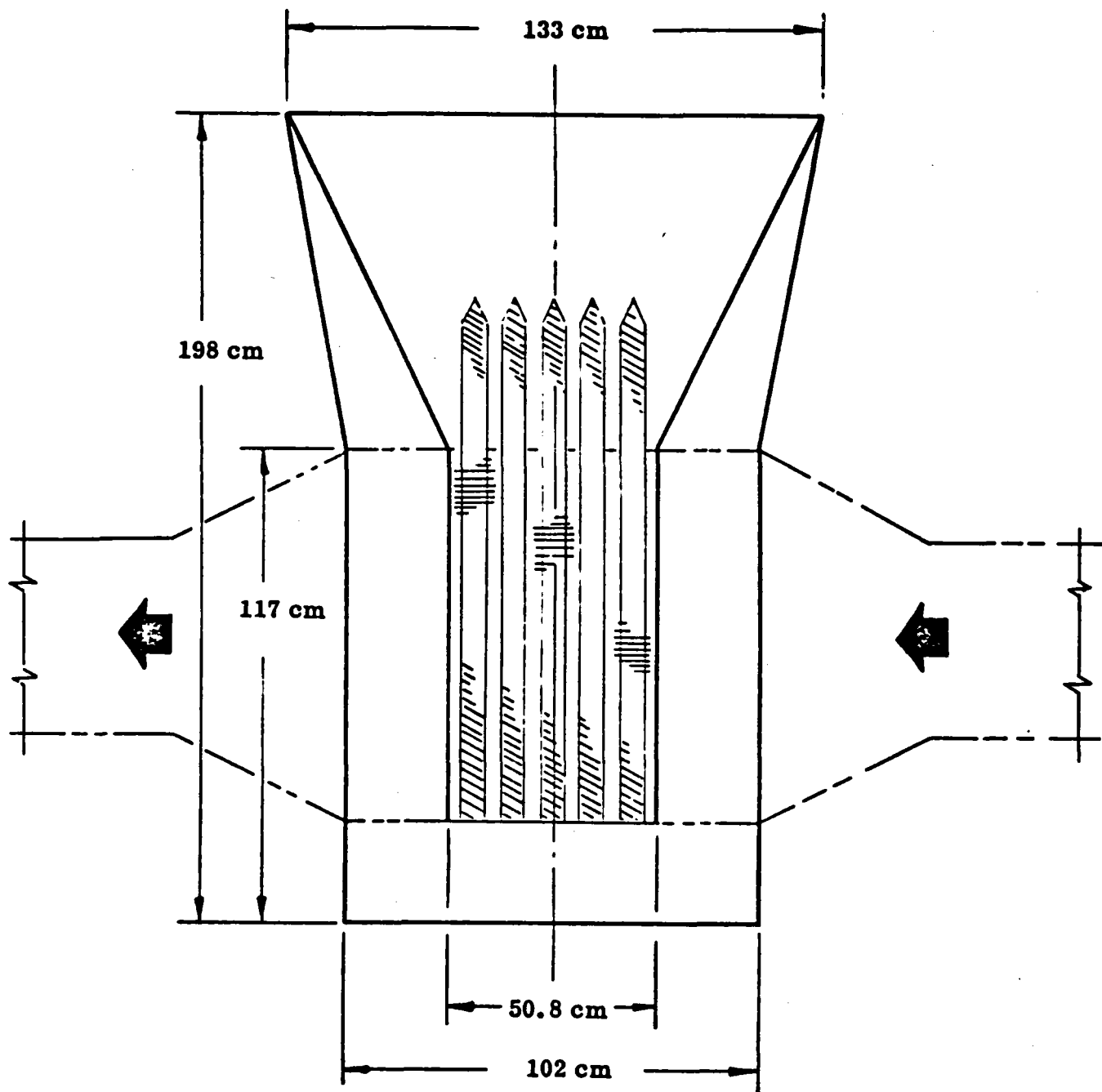


FIGURE 7.1
 CONCEPTUAL DESIGN OF
 DEMONSTRATION RECEIVER

system level. The recommended module containing approximately 27 heat pipes and handling a thermal input of about 250 kW appears to be of optimum size to demonstrate the feasibility of the concept with minimum risk.

8. REFERENCES

1. Bienert, W. B., Wolf, D. A., "Heat Pipe Central Solar Receiver," Semiannual Progress Report under DOE Contract No. EY-76-C-02-2839. *000, November 1976
2. Bienert, W. B., Wolf, D. A., "Heat Pipes Central Receiver," Semiannual Progress Report under DOE Contract No. EY-76-C-02-2839. *000, September 1977
3. Dunn, P. D. and Reay, D. A., "Heat Pipes," Pergamon, 1976
4. Busse, C. A., "Theory of Ultimate Heat Transfer Limit of Cylindrical Heat Pipes," International Journal Heat Mass Transfer, Volume 16, 1973
5. Levy, E. K., "Effects of Friction on the Sonic Velocity Limit in Sodium Heat Pipes," ASME Paper HPT-71-022
6. Deverall, J. E., Kemme, J. E., and Florschuetz, L. W., "Sonic Limitations and Startup Problems of Heat Pipes," Los Alamos Scientific Laboratories, Report No. LA-4518, November 1970
7. Kemme, J. E., "Heat Pipe Design Considerations," Los Alamos Scientific Laboratories, Report No. LA-4221-M5, August 1969
8. "Heat Pipe Design Handbook," Dynatherm Corporation, N74-22569, August 1972
9. Chapman, A. J., "Heat Transfer," 3rd Edition, Macmillan Publishing Co., Inc., New York, 1974
10. Kemme, J. E., "Heat Pipe Capability Experiments," Los Alamos Scientific Laboratories, Report No. LA-3585-M5
11. Uhlemann, H., Marks, D. J., Spigt, C. L., "Design and Construction of Wick Structures," Proceedings of the First International Heat Pipe Conference, Stuttgart, Germany, October 1973
12. Proposal to Design, Build and Qualify Heat Pipes for the ATS-F&G, DTM-COM-148A, March 1971
13. Groll, M., Pittman, R. B., and Eninger, J. E., "Parametric Performance of Circumferentially Grooved Heat Pipes with Homogeneous and Graded-Porosity Slab Wicks at Cryogenic Temperatures," Second International Heat Pipe Conference, Bologna, Italy, March 1976
14. Solar Central Hybrid Power System Study, Contract No. ET-78-C-03-2051, performed by Bechtel National, Inc., for DOE/SAN